秋田県立大学大学院博士学位論文

Development of Tough Poly(vinyl alcohol) Hydrogels and their Applications

(強靱な PVA ハイドロゲルの創製および その応用に関する研究)

孫　曼兮

Manxi Sun

2021 年 3 月

Abstract

Hydrogels, as soft and wet materials, have attracted great attention in the field of functional materials. It has been used in the field of drug delivery system, superabsorbent, biosensor, tissue engineering, wound dressing, conductive device, and others. Conventional hydrogels show weak mechanical properties which greatly limits the application of hydrogel. Most recently, the designed hydrogels, according to the energy dissipation principle, overcome the low mechanical strength, poor toughness, and limited recoverability of common hydrogels and show excellent mechanical properties. In this work, the prepared hydrogels based on Poly(vinyl alcohol)(PVA) possess thermal stability, instantaneous recovery, anti-fatigue, and high toughness.

In chapter 1, the research background of hydrogel was introduced, including hydrogel types, hydrogel applications, research status of tough hydrogel and the purpose of this study.

In chapter 2, the properties of experiment materials, as well as experimental methods and characterizations are presented.

In chapter 3, a biobased monomer, i.e., epoxidized soybean oil (ESO), was used to modify PVA to formulate a series of ESO-crosslinked PVA (PVA-ESO) hydrogels. Infrared spectroscopy (FT-IR), X-ray diffraction (XRD), and thermogravimetric analyses (TGA) were used to confirm the formation of PVA-ESO copolymer. Scanning electron microscope (SEM) revealed that the formed PVA-ESO hydrogels presented a distinct porous structure while no obvious pores were observed on pure PVA hydrogel. The tensile strength of PVA-ESO hydrogels increased up to 2.4 times when compared to that of pure PVA hydrogel. Dynamic mechanical analysis (DMA) indicated that the elastic properties of PVA-ESO hydrogels are better than that of pure PVA hydrogel, which are similar to that of natural cartilage. In summary, the modification of PVA with ESO can improve the thermal stability and mechanical properties of the hydrogels due to the improved cross-linking degree and the formed hydrophobic association.

In chapter 4, a tough double crosslinked hydrogel (DC-Gel) was obtained from polyvinyl alcohol/poly (acrylic acid) (PVA/PAA) by facilely visible light triggered polymerization and subsequent salt impregnation. The ionic DC-Gels have been proofed with a high toughness (up to 19 MJ/m^3), recovery property, self-healing ability and conductivity. The rubber-like flexible network and homogeneous interconnected phase of the ionic DC-Gels were certificated by scanning electron microscope and thermodynamics analysis. The tensile strengths and stretches at break of the ionic DC-Gels closely depended on the acrylic acid (AA) content. Cyclic tensile test results showed that the ionic DC-Gels with the optimized AA content (PVA: AA=1:5) afforded a good comprehensive mechanical properties and recoverable energy dissipation; the resilience and stress of the hydrogel at a strain of 150% maintained over 85% and 1.8 MPa, respectively. When the ionic DC hydrogel was applied to assemble a strain sensor, the excellent resilience is beneficial for precisely and quickly distinguishing the deformation of hydrogel-based sensor. This part provides a potential approach for the development of ion hydrogels with stretchable, self-healing, high resilience and strain-sensitive properties.

In chapter 5, a composite double network ionic hydrogel (CDN-gel) was obtained by the facile visible light triggered polymerization of acrylic acid (AA), PVA, and hydrolyzed triethoxyvinylsilane (TEVS) and subsequent salt impregnation. The resulting CDN-gels exhibited high toughness, recovery ability, and notch-insensitivity. The tensile strength, fracture elongation, Young's modulus, and toughness of the CDN-gels reached up to ~21 MPa, ~700%, ~3.5 MPa, and ~49 MJ/m^3, respectively. The residual strain at a strain of 200% was only ~25% after stretch-release of 1000 cycles. These properties will enable greater application of these hydrogel materials, especially for the fatigue resistance of tough hydrogels, as well as broaden their applications in damping.

In chapter 6, the present study is summarized.

Content

Chapter 1 Introduction

1.1 Background

A Hydrogel is a kind of material with a three-dimensional network structure [1]. The hydrophilic structure of which renders them capable of holding large amounts of water in their three-dimensional networks [2]. Hydrogel is also being used for everyday applications, such as tofu, pectin, contact lens. Moreover, there are many living things that possess supporting tissues in nature, supporting tissues play an essential role in the body, and include both hard tissues (bone) and soft tissues (tendon, ligament, skin, fascia etc.) [3]. Hydrogels have been used as one of the most common tissue engineering scaffolds over the past two decades due to their ability to maintain a distinct 3D structure, to provide mechanical support for the cells in the engineered tissues, and to simulate the native extracellular matrix. Nowadays, there are many investigations of hydrogels on many fields, e.g., biology technology [4], environmental science [5], and sensor [6]. Literature on this material was found to be expanding, especially in the scientific areas of research.

1.1.1 Definition

For the hydrogel, experts of different knowledge and understanding in this academic area, have different emphasis point on the definition of the hydrogel. The word “hydrogel”, according to Lee, Kwon and Park, dates back to an article published in 1894 [7]. Flory [8] believes that a material must meet the following two conditions before it can be called hydrogel: (1) the material has a continuous three-dimensional structure on a macroscopic scale and remains unchanged during the research period; (2) It has a similar the rheological properties of solids. Hoffman [9] believes that hydrogel is a three-dimensional network structure of hydrophilic polymers, which can absorb from 10-20% (an arbitrary lower limit) up to thousands of times their dry weight in

water. It is chemically stable or degradable. Manjun He defined a defined a hydrogel as a three-dimensional structure cross-linked by chemical bonds between polymer chains and the cross-linked polymer chains can penetrate or diffuse of small molecules through the three-dimensional network, which is absorbable but don't dissolve (in the short term) in water [10].

Hydrogel is a kind of soft insoluble materials with a three-dimensional network structure that can absorb and retain a large amount of moisture. From a macroscopic point of view, it is similar to the solid state. While in molecular aspect, it is similar to liquid on the microscopic scale, hydrogels are both elastomer and concentrated polymer solution [11]. In a word in brief, hydrogel is a semi-solid substance material, which can maintain a fixed geometry. Compared with colloids, hydrogels tend to have characteristics such as elasticity and toughness [12]. That is, the hydrogel can partially or complete recovery after removing the external force which deformed the hydrogel. Compared with water-absorbent sponge, water can be squeezed out under the press of external force, while the hydrogel can withstand certain extrusion deformation and maintain the moisture [13]. The hydrogel can withstand certain extrusion deformation and maintain the water content which is contributed to the hydrophilic polymer network structure of the hydrogel [14-16]. It forms hydrogen bonds with water, and a large number of water molecules are fixed, forming bound moisture [17].

Due to the water content, porosity and soft consistency of hydrogels, they closely simulate natural living tissue [18], more so than any other class of synthetic biomaterials, and the diffusion coefficient of water-soluble molecules in the hydrogel is close to the diffusion coefficient in water, thus can be penetrated by metabolites [19-21]. Simultaneously, the high water content of hydrogels can provide an ideal environment for cell survival, and structure which mimics the native tissues [3]. In a broad sense, living organisms are also hydrogels, such as jellyfish in the ocean, ligaments and tendons in the human body. During last two decades, natural Hydrogels were gradually replaced by synthetic hydrogels which has long service life, high capacity of water absorption, and high hydrogel strength [10, 11, 22].

1.1.2 Types of hydrogels

Recently, the hydrogel products can be classified on different bases as source, structure, composition, and crosslinking method. Natural matirials used to develop hydrogels include collagen/gelatin, hyaluronic acid, fibrin, alginic acid, cellulose, agarose and chitosan [19, 23, 24]. Synthetic matirials used to prepare hydrogels include polyethylene glycol, polyvinyl alcohol, polyhydroxyethyl methacrylate, polyacrylic acid, polymethacrylic acid, and polyacrylamide [1].

According to origins, it can be divided into two types, including synthetic hydrogels and natural hydrogels. Natural hydrogels include sugar hydrogels (chitosan hydrogel [25], agarose hydrogel [26], alginate hydrogel [27], cellulose hydrogel[19], starch hydrogel [9], etc.), DNA hydrogel [28], silk Protein hydrogel[29], etc. The most common systems used to form synthetic hydrogels are water-soluble polymers such as poly(acrylic acid) [30], poly(vinyl alcohol) [31], poly(vinyl pyrrolidone) [32], poly(ethylene glycol) [33], polyacrylamide[34] and so on. Chemical hydrogels are commonly prepared in two different ways: 'three-dimensional polymerization' (Fig. 1.1), in which a hydrophilic monomer is polymerized in the presence of a polyfunctional cross-linking agent, or by direct cross-linking of water-soluble polymers (Fig. 1.2). Polymerization is usually initiated by free-radical generating compounds such as benzoyl peroxide, 2,2-azo-isobutyronitrile (AIBN), and ammonium peroxodisulphate or by using UV-, gamma- or electron beam-radiation.

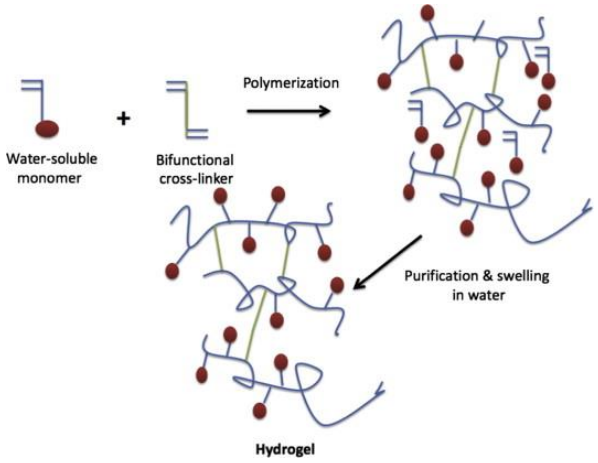

Fig. 1.1 Synthesis of hydrogels by three-dimensional polymerization [11]

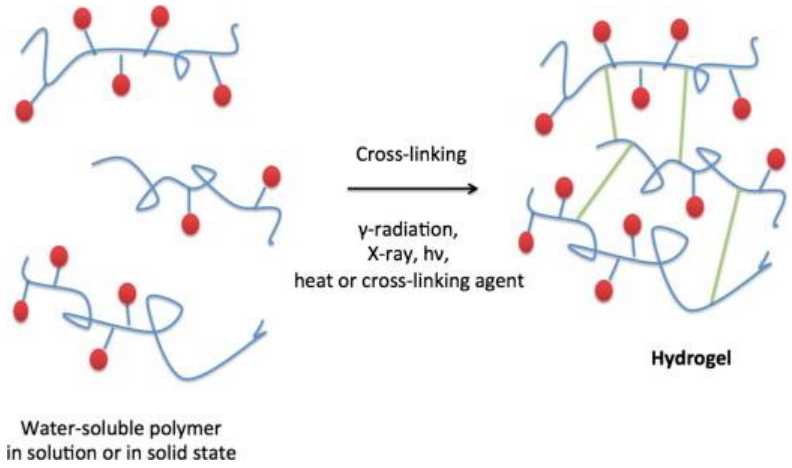

Fig. 1.2 Synthesis of hydrogels by cross-linking of ready-made water-soluble polymers [11]

The method of preparation leads to formations of some important classes of hydrogels. These can be exemplified by the following: (a) Homopolymeric hydrogels are referred to polymer network derived from a single species of monomer, which is a basic structural unit comprising of any polymer network. Homopolymers may have cross-linked skeletal structure depending on the nature of the monomer and polymerization technique. (b) Copolymeric hydrogels are comprised of two or more different monomer species with at least one hydrophilic component, arranged in a random, block or alternating configuration along the chain of the polymer network. (c) Multipolymer interpenetrating polymeric hydrogel (IPN), an important class of hydrogels, is made of two independent cross-linked synthetic and/or natural polymer component, contained in a network form. In semi-IPN hydrogel, one component is a cross-linked polymer and other component is a non-cross-linked polymer [1, 35-37].

The classification of hydrogels depends on their physical structure and chemical composition can be classified as follows: (a) Amorphous (non-crystalline). (b) Semi-crystalline: A complex mixture of amorphous and crystalline phases. (c) Crystalline [21, 31].

Hydrogels can be divided into two categories based on the chemical or physical nature of the cross-link junctions. Chemically cross-linked networks have permanent

junctions, while physical networks have transient junctions that arise from either polymer chain entanglements or physical interactions such as ionic interactions, hydrogen bonds, or hydrophobic interactions. Hydrogels appearance as matrix, film, or microsphere depends on the technique of polymerization involved in the preparation process [15, 38-40].

Hydrogels may be categorized into four groups on the basis of presence or absence of electrical charge located on the crosslinked chains: (a) Nonionic (neutral). (b) Ionic (including anionic or cationic). (c) Amphoteric electrolyte (ampholytic) containing both acidic and basic groups. (d) Zwitterionic (polybetaines) containing both anionic and cationic groups in each structural repeating unit [28, 33, 41-43].

1.1.3 The applications of hydrogels

To develop the application of hydrogels, such as introducing different functional groups into the main chain of polymer hydrogels to prepare functional hydrogels, or composite and assemble with other materials, which can be used for drug delivery[44] and actuators [20], supercapacitors [40], sensors [45], and displays [46]. The applications of hydrogels are discussed in detail further below.

The principle of slow release has been utilized since 1950 in the pharmaceutical industry but it was not until the mid-1960's that polymers were used for slow release of molecules [47]. Folkman and Long first reported sustained drug release from polymers in 1964 [48]. However, it was not until the 1970's when polymeric hydrogels were considered as drug delivery devices[49]. In recent years major emphasis has been put on the studying of polymeric hydrogels in biomedical research related to drug delivery due to their dynamic properties. For example, a complex between Polyethylene Glycol (PEG) and α-cyclodextrins can produce a supramolecular hydrogel that can be tailored to respond to numerous specific stimuli, from temperature and pH to electrical fields [50]. This third stage of hydrogel development gave rise to the development of so-called "smart hydrogels": these are hydrogels with a vast array of tunable properties and possible applications as drug delivery (Fig. 1.3). Polo Fonseca et al. [51] found in

an oral administration simulation that a polyurethane hydrogel was able to deliver the hydrophobic acidic NSAID sodium diclofenac in a sustained fashion for up to 40 h in a neutral solution and to achieve 80% of cumulative release.

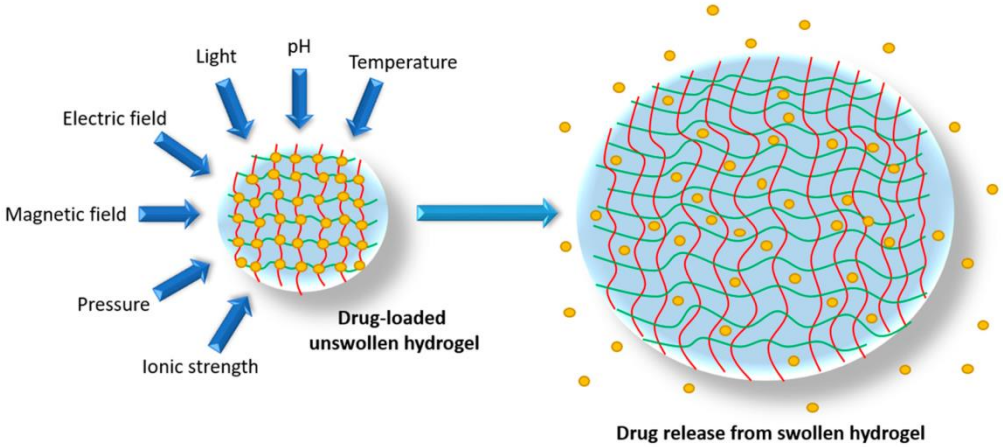

Fig. 1.3 Swelling of a drug delivery hydrogel in response to various chemical and physical stimuli. Red and yellow lines indicate the interwoven matrix structure of a hydrogel, with the yellow dots representing drug molecules [44]

Stimuli-responsive hydrogels are particularly relevant to robotic implementations targeted for physiological environments. Thermal transitions are the most widely employed transformation mechanism in generating mechanical responses in hydrogel actuators. More than that deformation of hydrogels can also be triggered by changes in ion concentration, pH, light exposure, and electric field [20, 52-54]. A recent example of a composite bilayer actuator was presented by Chen and co-workers who prepared a hydrogel containing a poly(acrylic acid-co-acrylamide) (p(AAc-co-AAm)) layer and a poly(N-isopropylacrylamide) (PNIPAm) layer, which can be used to prepare hydrogel actuators that function in open air and can grasp a heated object (Fig. 1.4).

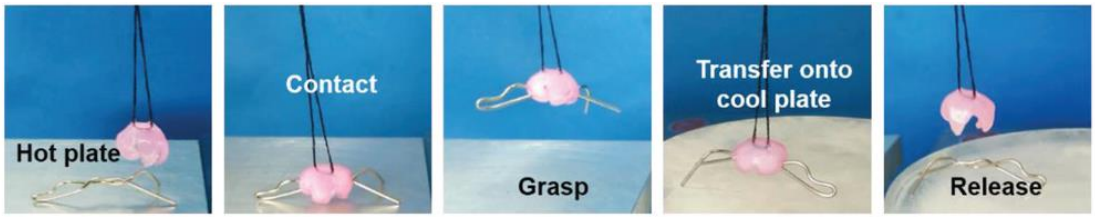

Fig. 1.4 The hydrogel gripper grasps a heated metal wire, lifts it up, and releases it when brought in contact with an ice-cold surface [55]

The inception of flexible supercapacitors that can work steadily under large deformation has been a research hotspot in recent years. These hydrogel-based supercapacitors can be immune to the harm caused by external forces and maintain good mechanical integrity and electrochemical stability [4, 56, 57]. Developing the hydrogel-based supercapacitors can provide a fresh perspective on multifunction applications and herald a new territory for flexible energy storage devices (Fig. 1.5). Peng et al. [41] report a zwitterionic gel electrolyte that successfully brings the synergic advantages of robust water retention ability and ion migration channels, manifesting in superior electrochemical performance. When applying the zwitterionic gel electrolyte, the hydrogel supercapacitor reaches a volume capacitance of 300.8 F cm-3 at 0.8 A cm-3 with a rate capacity of only 14.9% capacitance loss as the current density increases from 0.8 to 20 A cm-3, which is better than most among the previously reported graphene-based solid-state supercapacitors.

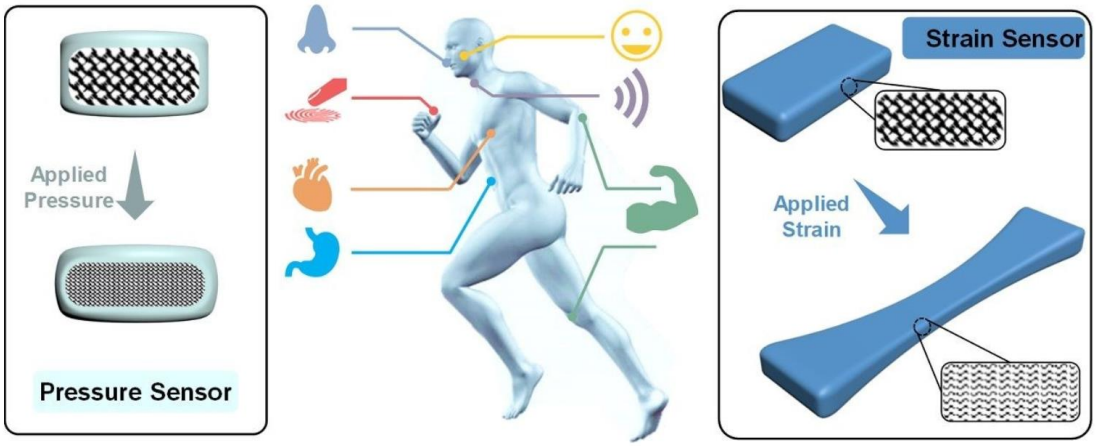

Fig. 1.5 Schematic illustration to potential applications of flexible pressure and strain sensors for implantable and wearable devices [58]

The flexible and stretchable hydrogel is enabled to fabricate slender, lightweight, stretchable, and foldable sensors (Fig. 1.5). Keplinger et al. [59] have synthesized polyacrylamide (PAAm) based ionic, highly stretchable, fully transparent hydrogel by varying the concentration of NaCl for actuators, which can be used as ion wire, speaker, etc. Yue et al. [60] synthesised hydrogel which composed of alternating hard layers of a polymeric surfactant (PDGI) and soft layers of interpenetrating networks of

poly(acrylamide)–poly(acrylic acid). Reversible, wide range switching of the stop-band position was achieved using different external stimuli of temperature, pH, and stress/strain.

The landmark paper by Wichterle and Lim on the biomedical usage of PHEMA hydrogel as contact lenses captivated the interest of biomaterial researchers around the globe [14]. Smeds et al. [61] used two methacrylate modified polysaccharides, alginate and hyaluronan to synthesis a viscoelastic hydrogel, which had mechanical properties similar to those of nucleus pulposus and meniscus. Myung et al. [62] reported an in situ-forming hydrogel of collagen type I crosslinked via multi-functional polyethylene glycol (PEG)-N-hydroxysuccinimide (NHS), which exhibited physical and biological properties desirable for a corneal stromal defect wound repair matrix that could be applied without the need for sutures or an external trigger such as a catalyst or light energy.

The application of high-strength hydrogels produced by imitating organisms in fields such as flexible devices and tissue replacement is the current hot research domain. However, most hydrogels still have the defects of inhomogeneous structure and poor mechanical properties. It is urgent to development hydrogel with high strength and versatility by sorting out the classification of hydrogels, the interaction between polymer chains and the spatial structure, so as to better broaden the application area.

1.2 Interaction between polymer chains in hydrogels

The mechanical properties of hydrogel can be enhanced by the multiple aggregation structure and the interaction between macromolecules. This provides important ideas for the design and preparation of high-strength hydrogels [63]. The interactions between macromolecules in hydrogel preparation are including hydrogen bond, ionic bond, coordinate bond, hydrophobic interaction, dipole interaction, host-guest interaction, and π-π stacking interaction, etc. Above all, the mechanical properties of hydrogels usually can be improved by multiple dynamic bonds/interactions (hydrogen bonding, dipolar-dopolar interaction, hydrophobic associations, and ionic

bonds/coordination bonds). This part will focus on how the four types of multiple dynamic bonds/interactions enhance hydrogels [64].

1.2.1 The enhancement of hydrogen bond

The hydrogen bond (H-bond) represents a fundamental interaction widely existing in nature, which plays a key role in chemical, physical and biochemical processes. Hydrogen bonds are generally formed between H atoms and other highly electronegative atoms (such as O, N) [65].

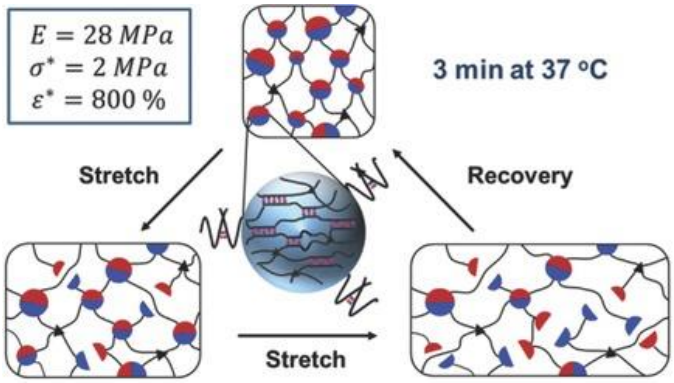

Fig. 1.6 H-bond crosslinking high strength hydrogel [68]

H-bonds can be divided into singlet hydrogen bonds and multiple hydrogen bonds. Singlet H-bond in hydrogel is prone to easy breakage during deformation, slippage, and dislocation, while the multiple H-bonds can easily increase the mechanical properties of hydrogels without sacrificing the extensibility and toughness because of its directionality, versatility and reversibility. Hydrogen bonding is ubiquitous in natural systems and has been widely used to impart various properties into polymer systems such as injectable self-healing [45], high toughness [66], and shape memory [67]. Sergei S. Sheiko et al. [68] designed a hybrid hydrogel composed of a loose chemical network and dense clusters of sacrificial hydrogen bonds to achieve high stiffness (28 MPa), high strength (2 MPa), and high toughness (9300 J/m^{-2}), along with complete and fast recovery of strain and mechanical properties (100% recovery in 3 min at 37 ℃). At the same time, the hydrogel also has some problems. For example, the Young's modulus is extremely dependent on the pH of the environment. Under weakly alkaline

and neutral pH conditions, the Young's modulus drops sharply (Fig. 1.6).

Chen et al. [69] reported a tannic acid (TA) as a molecular coupling bridge between cellulose nanocrystals (CNC) and poly(vinyl alcohol) (PVA) chains for the fabrication of a bio-based advanced physical hydrogel via strong multiple H-bonds. This hydrogel has ultrahigh tensile strength (~8.7 MPa), large elongation (~1107.6%), and remarkable toughness (~58.2 MJ/m^{-3}). However, the resilience of TA-PVA/CNC is relatively weak (Fig. 1.7).

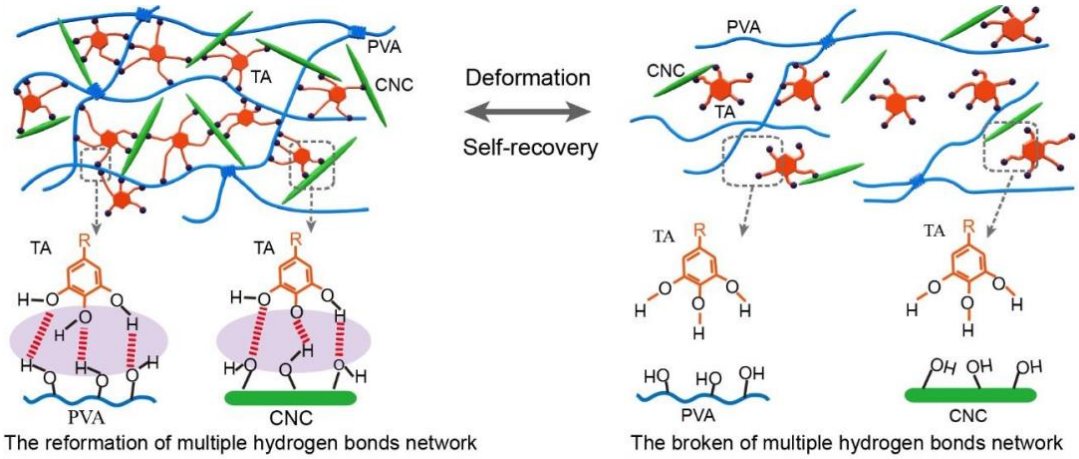

Fig. 1.7 Schematic for the reversible hydrogen bonds [69]

1.2.2 The enhancement of hydrophobic association

Hydrophobic association (HA) can be used as a mechanical dissipation mechanism of hydrogels. Some studies have reported that elastin contains alternating hydrophobic and crosslinking domains [70]. Hydrophobic interactions play a dominant role in the formation of large biological systems [71]. These interactions can occur in synthetic hydrogels via incorporating of hydrophobic sequences within the hydrophilic polymer network chains [72]. The hydrophilic monomer is copolymerized with hydrophobic monomer. When the reaction starts, the hydrophobic micro domain acts as physical cross-linking point with sufficient toughness [73]. These crosslinking points are connected to other polymer chains to crosslink the hydrophilic polymer chains, forming a macroscopic three-dimensional hydrogel network and producing hydrophobic association physical hydrogels [74]. Gao et al. reported poly(butyl acrylate)(PBA) latex

particles toughening hydrogels with anionic sodium dodecyl sulfate (SDS) and amphoteric dodecyl dimethyl betaine [75]. As shown in Fig. 1.8, the attraction between the surfactants resulted in a relatively tight alignment to form a mixed micelle. The resulting hydrogels exhibited superior mechanical strength (~690 kPa).

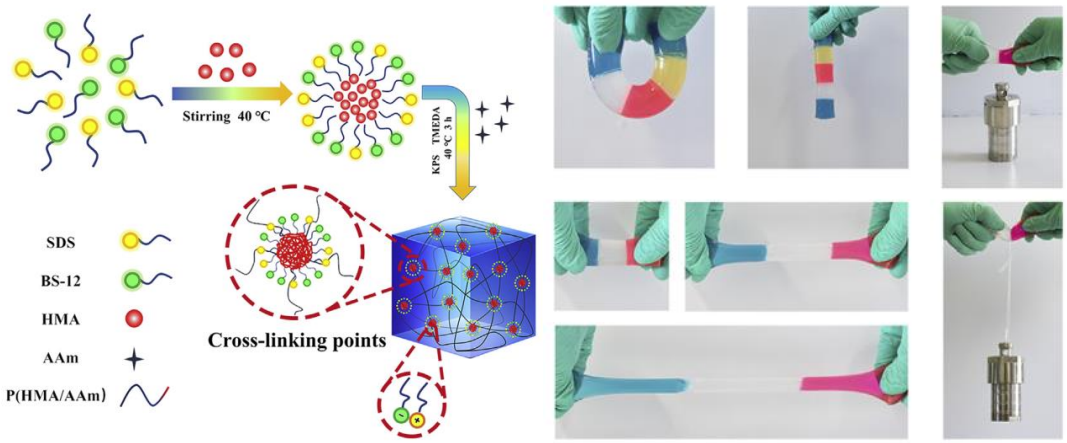

Fig. 1.8 Structure and superior characterizations of HA hydrogels with combined surfactants [76]

1.2.3 The enhancement of ionic bond/coordination bond

Hydrogels using dynamic ionic bond crosslinks have proven well-suited for the preparation of functional systems with properties including self-healing, shape memory, and stimuli-induced stiffness changes [77-79]. The ionic bond is stronger than the hydrogen bond and most of the non-covalent bonds, so it is widely used in self- healing hydrogels. Ionic bond self-healing hydrogel is also based on the movement of polymer chains as same as H-bond enhanced hydrogel, which can be reconstruction and completes the healing. Suo et al. [80] designed and prepared a double-network hydrogel with sodium alginate calcium ion cross-linking network and polyacrylamide chemical cross-linking network. During the tensile test, there is a synergistic effect between the ionic cross-linking network and the chemical cross-linking network, and the tensile stress reaches 156 kPa and the strain is 2300%. Shi et al. [3] used $-PO_4^-$ to modify hyaluronic acid and $MgSiO_3$ nanoparticles to prepare a two-component injection hydrogel. The Mg^{2+} ions form coordinate bond crosslinking with $-PO_4^-$ to

obtain a hydrogel dynamically crosslinked. The hydrogel is self-healing and is expected to be used for smart drug delivery (Fig. 1.9).

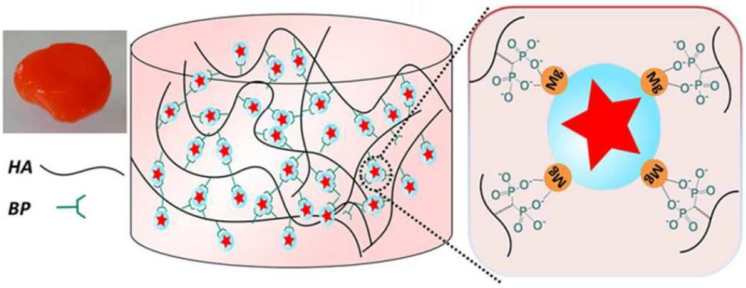

Fig. 1.9 Mg^{2+} and $-PO_4^-$ coordination hydrogel [3]

1.2.4 The enhancement of Dipole–Dipole interaction

High strength hydrogels were previously constructed based on dipole–dipole and hydrogen bonding reinforcement. In spite of the high tensile and compressive strengths achieved, the fracture energy of the hydrogels strengthened with sole noncovalent bondings was rather low due to the lack in energy dissipating mechanism. Bai et al. [81] fabricated dipole–dipole interaction hydrogels which can withstand tensile stress up to 3.5 MPa and excellent fatigue resistance.

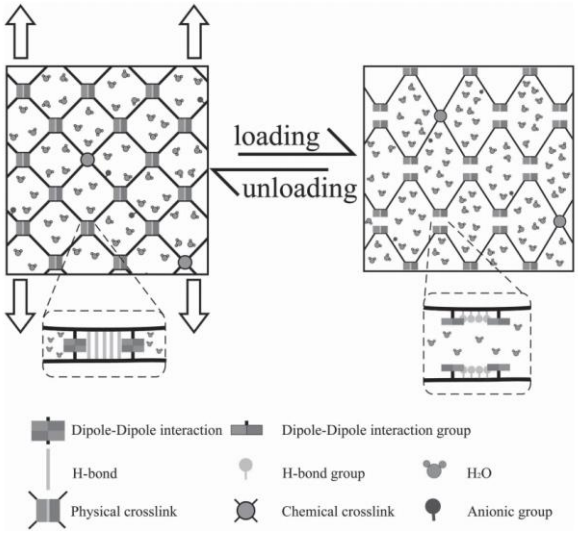

Fig. 1.10 Mechanism underlying the energy dissipation of Dipole–Dipole interaction hydrogel during the cycling test [82]

Liu et al. [82] constructed a high strength hydrogel with ultra-toughness by

introducing dual physical interactions of dipole–dipole pairings and hydrogen bonding into the networks at a much lower chemical crosslinking density. A dipole–dipole interacting contributed to the increased stiffness, and hydrophilic weaker hydrogen bondings among AAm would be easily fractured to dissipate energy (Fig.1.10).

1.3 Structure of hydrogels

More and more novel hydrogels have been reported. We going to introduce the four hydrogels with different structure, including nanocomposite gel (NC-gel) [83], topological gel (TP-gel) [84], macromolecular microsphere composite hydrogel (MMC-gel) [85], and double network gel (DN-gel) [86]. By systematic discussing the structure of these hydrogels, find out the relationship between their structure and mechanical properties, to develop a universal strategy for significantly enhancing the comprehensive mechanical properties of hydrogels.

1.3.1 Nanocomposite hydrogel

Nanocomposite hydrogel refers to a type of composite hydrogel in which the dispersed phase has a nanometer size (1-100 nm) in at least one dimension. The challenges of nanoparticles application could potentially be overcome by incorporation into hydrogels, which resulting in decreased risks to human health and the environment. In addition, the innovative combination of these two completely different types of materials was not only thought of as creating structural diversity but also generating a plurality of property enhancements. These performance enhancements were the main focus of hydrogel-nanoparticle composite materials research leading to improved mechanical strength and stimuli response [87]. For example, recently reported silica nanoparticle-hydrogel composite made of silica nanoparticles and modified polyethylene glycol demonstrated remarkable improvements in tissue adhesive property, mechanical stiffness and bioactivity compared to hydrogel without nanoparticles [5]. So far, researchers have reported three different supramolecular hydrogel-nanoparticle. i) micro or nano-gels stabilizing single/multiple nanoparticles,

ii) nanoparticles non-covalently immobilized in a hydrogel matrix, and iii) nanoparticles covalently immobilized in a hydrogel matrix (Fig. 1.11) [88].

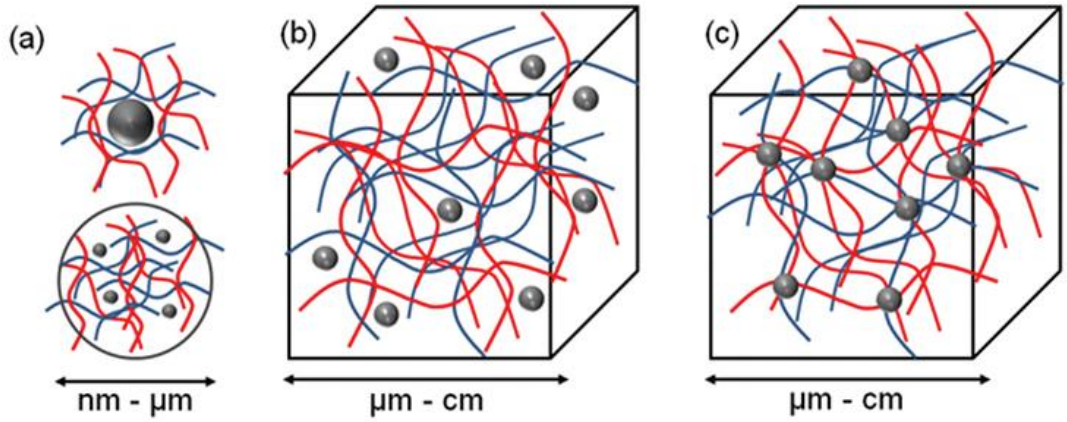

Fig. 1.11 Concept for combination of nanoparticles and hydrogel to form new functional materials [88]

1.3.2 Topology hydrogel

The TP-gel is also called the Slide-Ring Gel, which was synthesized by Okumura and Ito in 2001. Topological gels are obtained by crosslinking cyclodextrin on different chains of polyrotaxane based on PEG/α- cyclodextrin(α-CD) (Fig. 1.12) [50].

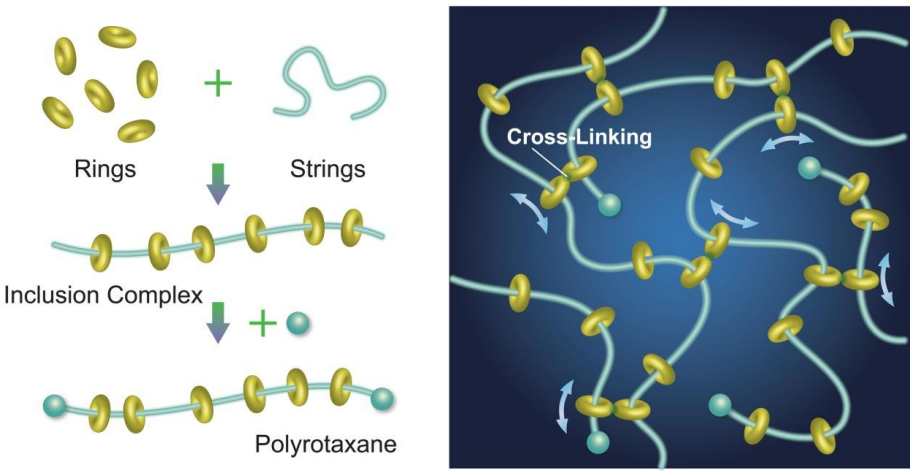

Fig. 1.12 Schematic diagram of PR and slide-ring hydrogel [50]

The difference in microstructure from traditional hydrogel is the random crosslinking points formed by the TP-gel, which slide along the segment while stretched by an external force, essentially acting like a “pulley”. It can evenly divide the

long chain into several short chains so that the force is evenly distributed to each segment [89]. The TP-gels usually have good tensibility and large swellability could be realized, the polymer chains with bulky end groups are neither covalently cross-linked like chemical gels nor attractively interacted like physical gels, but are topologically interlocked by figure-of-eight cross-links. Therefore, the polymer chains freely pass through the cross-links acting like pulleys, which are supposed to automatically equalize the nanoscopic heterogeneity in structure and stress [90].

1.3.3 Tetra-PEG hydrogel

Tetra-PEG hydrogels can be made from tetra-PEG macromers containing functional groups such as amines and esters [91]. These hydrogels are a different and unique class of tough materials. In this hydrogel, network defects are negligible and there are no trapped entanglements between the polymer chains (Fig. 1.13).

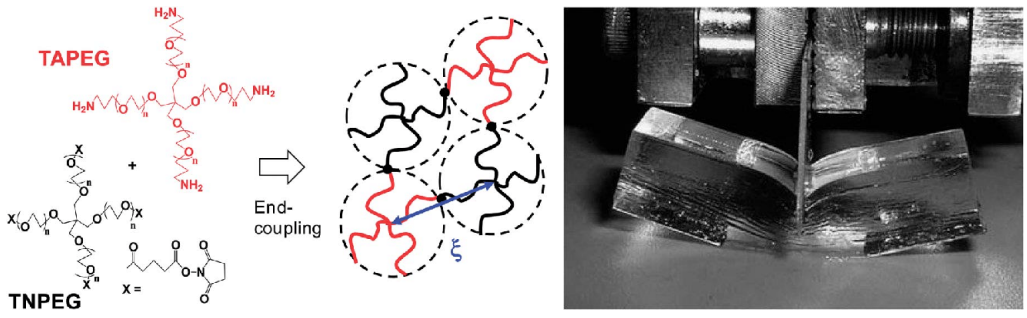

Fig. 1.13 Preparation and image of tetra-PEG gels [92]

Mechanical testing and scattering experiments suggest that the hydrogels consist of elastic polymer “blobs” (i.e., coils) that are packed within the hydrogels. For example, cross-end coupling of tetra-amine-terminated PEG and tetra-N-hydroxysuccinimide-glutaraldehyde-terminated PEG leads to hydrogel networks with high cross-linking efficiency and little hysteresis[93]. This behavior is very similar to that of an elastic rubber. Scattering studies show that these tetra-PEG hydrogels are mostly homogeneous with low concentration fluctuations comparable to those of the corresponding solutions [91]. Concentration fluctuations are changes in density within the same hydrogel. When the ratio of the reacting macromonomers is not

stoichiometric ratio, heterogeneity will occur due to an increase in structural defects. Kamata et al. [94] report the synthesis of injectable “nonswellable” hydrogels from hydrophilic and thermoresponsive polymers, in which two independently occurring effects (swelling and shrinking) oppose each other. The hydrogels can endure a compressive stress up to 60 MPa and can be stretched more than sevenfold without hysteresis.

1.3.4 Double-network hydrogel

DN-gels usually are both hard and strong, with comparable mechanical properties to that of rubbers and cartilages. The hydrogels consist of two interpenetrating polymer networks with contrasting mechanical properties. The design principle can be summarized as follows: first, rigid and brittle polyelectrolyte serves as the first network, while soft and ductile neutral polymer serves as the second network; second, the molar concentration of the second network is 20~30 times that of the first network; third, the first network is tightly (making it stiff and brittle) while the second network is loosely cross-linked (making it soft and stretchable) to achieve a strong asymmetric gel structure [86, 95-97]. The toughness is the ability of a material to absorb mechanical energy and deform without rupture. One of the definitions of material toughness is the fracture energy, which is the energy per unit area required to propagate a notch crack. DN-gels are tough because the internal fracture of the brittle network dissipates substantial amounts of energy under large deformation, while the elasticity of the second network is able to return to its original shape after deformation. The fracture energy of the double network can always be much larger than those of either of the corresponding single networks. Material gains toughness by sacrificing the rupture of the covalent bonds of the brittle first network [98]. Gong et al. [99] illustrate this brittle-ductile transition in double network gels adopting a two-spring model as shown in Fig. 1.14. With stretching, the ductile DN-gel (where the effective chain number density of the 2nd network is higher than that of the 1st network) experiences internal damage of the 1st network, while the brittle DN-gel (where chain density of the 1st

network is higher than that of the 2nd network) undergoes simultaneous fracture of the two networks, which leads to sample failure. Therefore, the material gains toughness by sacrificing the rupture of the covalent bonds of the brittle first network. The covalent bonds serve as "sacrificial bonds," which used to describe how bones fracture.

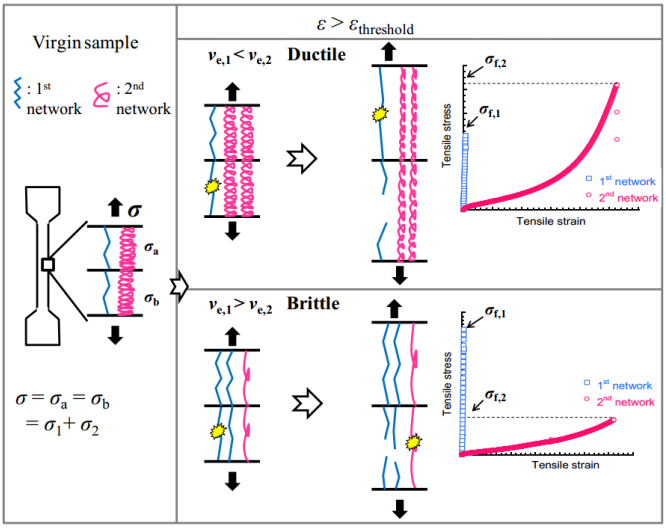

Fig. 1.14 Illustration of the tensile stretching of ductile and brittle DN-gels using two springs as model [99]

1.4 Benefits and limitations of hydrogels

The conventional hydrogels have their unique benefits including, biocompatible, can be injected in vivo as a liquid that then hydrogels at body, protect cells, good transport properties, timed released of medicines or nutrients, easy to modify, and can be biodegradable or bio-absorbable. However, the conventional hydrogels also have some limitations, for example, high cost, can be hard to handle, and difficult to sterilize. Hydrogels usually have high compressive strength and large elongation, but their tensile strength and modulus are not satisfied enough; furthermore, their high elastic properties show no hysteresis behavior, thus lacking a mechanism for mechanical energy dissipating. As a result, the mechanical properties are observably reduced when the hydrogels contain a defect.

1.5 Purpose of this research

Due to the poor mechanical properties of traditional single-crosslinked hydrogels, this greatly limits the application of hydrogels. Their resemblance to living tissue opens up many opportunities for applications in biomedical areas. Although hydrogels have brilliant future in the next decade, the mechanical properties of the hydrogel have some distance from their final application. Therefore, our goal is to design a hydrogel with the required mechanical properties to meet the requirements of various application fields. Recently, a lot of progress has been made in the construction of high-strength hydrogels, mainly as follows ideas: 1) Increase the interaction between the chains of polymer hydrogels and develop synergistic hydrogels, such as chemical crosslinking, hydrophobic interaction, hydrogen bond crosslinking, and ionic bond crosslinking, etc., using two or more of them to construct synergistic hydrogels; 2) In terms of spatial structure, build multiple networks between polymer networks to develop toughness hydrogels; 3) The combination of the above two forms. These construction ideas are currently one of the hot spots and development trends in the preparation of high-strength hydrogels.

In order to develop high-strength hydrogels that match the mechanical strength required by the application (modulus: $1\sim10^2$ MPa, water content 50%~90 wt%, tensile strength $1\sim10^2$ MPa, compressive strength $10\sim10^3$ MPa). Based on the above understanding, in this study, three kinds of high-strength hydrogels were prepared through different design.

References

[1] Ahmed EM. Hydrogel: Preparation, characterization, and applications: A review. Journal of Advanced Research. 2015;6(2):105-21.

[2] Gulrez S, Al-Assaf S, Phillips G. Hydrogels: Methods of Preparation, Characterisation and Applications. 2011.

[3] Bacelar A, Cengiz IF, Silva-Correia J, et al. "Smart" Hydrogels in Tissue Engineering and Regenerative Medicine Applications. 2017.

[4] Yuk H, Lu B, Zhao X. Hydrogel bioelectronics. Chemical Society Reviews, 2019;48(6):1642-67.

[5] Thoniyot P, Tan MJ, Karim AA, et al. Nanoparticle–Hydrogel Composites: Concept, Design, and Applications of These Promising, Multi-Functional Materials. Advanced Science. 2015;2(1-2):1400010.

[6] Han S-T, Peng H, Sun Q, et al. An Overview of the Development of Flexible Sensors. Advanced materials, 2017,29(33): 1700375.

[7] Chirani N, Gritsch L, Motta F L, et al. History and Applications of Hydrogels. Journal of biomedical sciences. 2015;4(2).

[8] Flory PJ. Introductory lecture. Faraday Discussions of the Chemical Society. 1974;57(0):7-18.

[9] Hoffman AS. Hydrogels for biomedical applications. Advanced Drug Delivery Reviews. 2012;64:18-23.

[10] Bahram M, Mohseni N, Moghtader M. An introduction to hydrogels and some recent applications. Emerging concepts in analysis and applications of hydrogels. 2016.

[11] Caló E, Khutoryanskiy VV. Biomedical applications of hydrogels: A review of patents and commercial products. European Polymer Journal. 2015;65:252-67.

[12] Fu J. Strong and tough hydrogels crosslinked by multi-functional polymer colloids. Journal of Polymer Science Part B: Polymer Physics. 2018;56(19):1336-50.

[13] Pan Y, Shi K, Peng C, et al. Evaluation of Hydrophobic Polyvinyl-Alcohol Formaldehyde Sponges As Absorbents for Oil Spill. ACS Applied Materials & Interfaces. 2014;6(11):8651-9.

[14] Wichterle O, LÍM D. Hydrophilic Gels for Biological Use. Nature. 1960;185(4706):117-8.

[15] Zhao D, Huang J, Zhong Y, et al. High-strength and high-toughness double-cross-linked cellulose hydrogels: a new strategy using sequential chemical and physical cross-linking. Advanced Functional Materials. 2016;26(34):6279-87.

[16] Zhao D, Huang J, Zhong Y, et al. High-Strength and High-Toughness Double-Cross-Linked Cellulose Hydrogels: A New Strategy Using Sequential Chemical and Physical Cross-Linking. Advanced Functional Materials. 2016;26(34):6279-87.

[17] Gun'ko VM, Savina IN, Mikhalovsky SV. Properties of water bound in hydrogels. Gels. 2017;3(4):37.

[18] Li X, Su X. Multifunctional smart hydrogels: potential in tissue engineering and cancer therapy. Journal of Materials Chemistry B. 2018;6(29):4714-30.

[19] Lin F, Wang Z, Shen Y, et al. Natural skin-inspired versatile cellulose biomimetic hydrogels. Journal of Materials Chemistry A. 2019;7(46):26442-55.

[20] Le X, Lu W, Zhang J, et al. Recent Progress in Biomimetic Anisotropic Hydrogel Actuators. Advanced Science. 2019;6(5):1801584.

[21] Shojaeiarani J, Bajwa D, Shirzadifar A. A review on cellulose nanocrystals as promising biocompounds for the synthesis of nanocomposite hydrogels. Carbohydrate Polymers. 2019;216:247-59.

[22] Zhao H, Liu M, Zhang Y, et al. Nanocomposite hydrogels for tissue engineering applications. Nanoscale. 2020;12(28):14976-95.

[23] Gyles D, Castro L, Junior J, et al. The Designs and Prominent Biomedical Advances of Natural and Synthetic Hydrogel Formulations. European Polymer Journal. 2017;88.

[24] Rodríguez-Rodríguez R, García-Carvajal ZY, Jiménez-Palomar I, et al. Development of gelatin/chitosan/PVA hydrogels: Thermal stability, water state, viscoelasticity, and cytotoxicity assays. Journal of Applied Polymer Science. 2019;136(10):47149.

[25] Qu X, Wirsén A, Albertsson AC. Novel pH-sensitive chitosan hydrogels: swelling behavior and states of water. Polymer. 2000;41(12):4589-98.

[26] Alehosseini A, Gomez del Pulgar E-M, Fabra MJ, et al. Agarose-based freeze-dried capsules prepared by the oil-induced biphasic hydrogel particle formation approach for the protection of sensitive probiotic bacteria. Food Hydrocolloids.

2019;87:487-96.

[27] Kim Y-W, Kim JE, Jung Y, et al. Non-swellable, cytocompatible pHEMA-alginate hydrogels with high stiffness and toughness. Materials Science and Engineering: C. 2019;95:86-94.

[28] Kondinskaia DA, Gurtovenko AA. Supramolecular complexes of DNA with cationic polymers: The effect of polymer concentration. Polymer. 2018;142:277-84.

[29] Luo K, Yang Y, Shao Z. Physically Crosslinked Biocompatible Silk-Fibroin-Based Hydrogels with High Mechanical Performance. Advanced Functional Materials. 2016;26(6):872-80.

[30] Wang D, Zhu L, Qiu J, et al. Poly(acrylic acid)/palygorskite microgel via radical polymerization in aqueous phase for reinforcing poly(vinyl alcohol) hydrogel. Applied Clay Science. 2020;185:105421.

[31] Jiang L, Yang T, Peng L, et al. Acrylamide modified poly(vinyl alcohol): crystalline and enhanced water solubility. RSC Advances. 2015;5(105):86598-605.

[32] Leone G, Consumi M, Lamponi S, et al. Thixotropic PVA hydrogel enclosing a hydrophilic PVP core as nucleus pulposus substitute. Materials Science and Engineering: C. 2019;98:696-704.

[33] Mansur HS, Oréfice RL, Mansur AAP. Characterization of poly(vinyl alcohol)/poly(ethylene glycol) hydrogels and PVA-derived hybrids by small-angle X-ray scattering and FTIR spectroscopy. Polymer. 2004;45(21):7193-202.

[34] Ma J, Lee J, Han SS, et al. Highly Stretchable and Notch-Insensitive Hydrogel Based on Polyacrylamide and Milk Protein. ACS Applied Materials & Interfaces. 2016;8(43):29220-6.

[35] Mondal S, Das S, Nandi AK. A review on recent advances in polymer and peptide hydrogels. Soft Matter. 2020;16(6):1404-54.

[36] Singhal R, Gupta K. A Review: Tailor-made Hydrogel Structures (Classifications and Synthesis Parameters). Polymer-Plastics Technology and Engineering. 2016;55(1):54-70.

[37] Zhao S, Zhou F, Li L, et al. Removal of anionic dyes from aqueous solutions by

adsorption of chitosan-based semi-IPN hydrogel composites. Composites Part B: Engineering. 2012;43(3):1570-8.

[38] Song G, Zhang L, He C, et al. Facile Fabrication of Tough Hydrogels Physically Cross-Linked by Strong Cooperative Hydrogen Bonding. Macromolecules. 2013;46(18):7423-35.

[39] Qin Y, Wang J, Qiu C, et al. A Dual Cross-Linked Strategy to Construct Moldable Hydrogels with High Stretchability, Good Self-Recovery, and Self-Healing Capability. Journal of Agricultural and Food Chemistry. 2019;67.

[40] Wang Z, Pan Q. An Omni-Healable Supercapacitor Integrated in Dynamically Cross-Linked Polymer Networks. Advanced Functional Materials. 2017;27(24):1700690.

[41] Peng X, Liu H, Yin Q, et al. A zwitterionic gel electrolyte for efficient solid-state supercapacitors. Nature communications. 2016;7(1):11782.

[42] Fang H, Wang J, Li L, et al. A novel high-strength poly(ionic liquid)/PVA hydrogel dressing for antibacterial applications. Chemical Engineering Journal. 2019;365:153-64.

[43] Jin S, Qiu J, Sun M, et al. Strain-Sensitive Performance of a Tough and Ink-Writable Polyacrylic Acid Ionic Gel Crosslinked by Carboxymethyl Cellulose. Macromolecular Rapid Communications. 2019;40(20):1900329.

[44] Harrison IP, Spada F. Hydrogels for Atopic Dermatitis and Wound Management: A Superior Drug Delivery Vehicle. Pharmaceutics. 2018;10(2):71.

[45] Cai G, Wang J, Qian K, et al. Extremely Stretchable Strain Sensors Based on Conductive Self-Healing Dynamic Cross-Links Hydrogels for Human-Motion Detection. Advanced Science. 2017;4(2):1600190.

[46] Yang G, Ding J, Yang B, et al. Highly stretchable electrochromic hydrogels for use in wearable electronic devices. Journal of Materials Chemistry C. 2019;7(31):9481-6.

[47] Kamaly N, Yameen B, Wu J, et al. Degradable Controlled-Release Polymers and Polymeric Nanoparticles: Mechanisms of Controlling Drug Release. Chemical Reviews. 2016;116(4):2602-63.

[48] Folkman J, Long DM. The use of silicone rubber as a carrier for prolonged drug therapy. Journal of Surgical Research. 1964;4(3):139-42.

[49] Abu Hashim II, El-dahan MS, Yusif RM, et al. Potential Use of Niosomal Hydrogel as an Ocular Delivery System for Atenolol. Biological and Pharmaceutical Bulletin. 2014;37(4):541-51.

[50] Takahashi S, Yamada N, Ito K, et al. Inclusion Complex of α-Cyclodextrin with Poly(ethylene glycol) Brush. Macromolecules. 2016;49.

[51] Fonseca L, Bergamo Trinca R, Felisberti M. Amphiphilic Polyurethane Hydrogels as Smart Carriers for Acidic Hydrophobic Drugs. International Journal of Pharmaceutics. 2018;546.

[52] Guo P, Liang J, Li Y, et al. High-strength and pH-responsive self-healing polyvinyl alcohol/poly 6-acrylamidohexanoic acid hydrogel based on dual physically cross-linked network. Colloids and Surfaces A: Physicochemical and Engineering Aspects. 2019;571:64-71.

[53] Huang H, Qi X, Chen Y, et al. Thermo-sensitive hydrogels for delivering biotherapeutic molecules: A review. Saudi Pharmaceutical Journal. 2019;27(7): 990-9.

[54] Kurkuri MD, Lee J-R, Han JH, et al. Electroactive behavior of poly(acrylic acid) grafted poly(vinyl alcohol) samples, their synthesis using a Ce(IV)glucose redox system and their characterization. Smart Materials and Structures. 2006;15(2):417-23.

[55] Zheng J, Xiao P, Le X, et al. Mimosa inspired bilayer hydrogel actuator functioning in multi-environments. Journal of Materials Chemistry C. 2018;6(6):1320-7.

[56] Di Turo F, Matricardi P, Di Meo C, et al. PVA hydrogel as polymer electrolyte for electrochemical impedance analysis on archaeological metals. Journal of Cultural Heritage. 2019;37:113-20.

[57] Someya T, Yokota T, Lee S, et al. Electronic Skins for Robotics and Wearables: proceedings of the 2020 IEEE 33rd International Conference on Micro Electro Mechanical Systems (MEMS). 18-22 Jan. 2020.

[58] Wang Z, Cong Y, Fu J. Stretchable and tough conductive hydrogels for flexible pressure and strain sensors. Journal of Materials Chemistry B, 2020,8(16): 3437-3459.

[59] Keplinger C, Sun J-Y, Foo CC, et al. Stretchable, transparent, ionic conductors. Science. 2013;341(6149):984-7.
[60] Yue YF, Haque MA, Kurokawa T, et al. Lamellar Hydrogels with High Toughness and Ternary Tunable Photonic Stop-Band. Advanced materials. 2013;25(22):3106-10.
[61] Smeds KA, Grinstaff MW. Photocrosslinkable polysaccharides for in situ hydrogel formation. Journal of Biomedical Materials Research. 2001;54(1):115-21.
[62] Fernandes-Cunha GM, Chen KM, Chen F, et al. In situ-forming collagen hydrogel crosslinked via multi-functional PEG as a matrix therapy for corneal defects. Scientific Reports. 2020;10(1):16671.
[63] Ding X, Wang Y. Weak bond-based injectable and stimuli responsive hydrogels for biomedical applications. Journal of Materials Chemistry B. 2017;5(5):887-906.
[64] Jiang Z, Bhaskaran A, Aitken HM, et al. Using Synergistic Multiple Dynamic Bonds to Construct Polymers with Engineered Properties. Macromolecular Rapid Communications. 2019;40(10):1900038.
[65] Zhou C, Li X, Gong Z, et al. Direct observation of single-molecule hydrogen-bond dynamics with single-bond resolution. Nature communications. 2018;9(1):807.
[66] Li A, Si Y, Wang X, et al. Poly(vinyl alcohol) Nanocrystal-Assisted Hydrogels with High Toughness and Elastic Modulus for Three-Dimensional Printing. ACS Applied Nano Materials. 2019;2(2):707-15.
[67] Liu Y, Zhang Q, Feng J. Fabricating dual-responsive shape memory PVA-based composites via reactive melt-mixing by skillfully utilizing excellent flowability and crosslinking heat of polyethylene. Polymer. 2018;146:267-74.
[68] Hu X, Vatankhah-Varnoosfaderani M, Zhou J, et al. Weak Hydrogen Bonding Enables Hard, Strong, Tough, and Elastic Hydrogels. Advanced materials. 2015;27(43):6899-905.
[69] Lin F, Wang Z, Chen J, et al. Bioinspired Hydrogen Bond Crosslink Strategy toward Toughening Ultrastrong and Multifunctional Nanocomposite Hydrogels. Journal of Materials Chemistry B. 2020;8.
[70] Andersen PO, Marstokk O, Nystr öm B, et al. Effects of Hydrophobic Modification

and Electrostatic Interactions on the Association Behavior in Aqueous Solutions of Poly(vinyl alcohol). A Pulsed Field Gradient NMR Study. Macromolecular Chemistry and Physics. 2001;202(8):1457-65.

[71] Ye L, Lv Q, Sun X, et al. Fully physically cross-linked double network hydrogels with strong mechanical properties, good recovery and self-healing properties. Soft Matter. 2020;16(7):1840-9.

[72] Xu J, Ren X, Gao G. Salt-inactive hydrophobic association hydrogels with fatigue resistant and self-healing properties. Polymer. 2018;150:194-203.

[73] Zhang Y, Hu C, Xiang X, et al. Self-healable, tough and highly stretchable hydrophobic association/ionic dual physically cross-linked hydrogels. RSC Advances. 2017;7(20):12063-73.

[74] Cui W, Zhang Z-J, Li H, et al. Robust dual physically cross-linked hydrogels with unique self-reinforcing behavior and improved dye adsorption capacity. RSC Advances. 2015;5(65):52966-77.

[75] Ren XY, Yu Z, Liu B, et al. Highly tough and puncture resistant hydrogels driven by macromolecular microspheres. RSC Advances. 2016;6(11):8956-63.

[76] Jiang H, Duan L, Ren X, et al. Hydrophobic association hydrogels with excellent mechanical and self-healing properties. European Polymer Journal. 2019;112:660-9.

[77] Ye L, Sun X, Lv Q, et al. Tough and Stretchable Dual Ionically Cross-Linked Hydrogel with High Conductivity and Fast Recovery Property for High-Performance Flexible Sensors. ACS Applied Materials & Interfaces. 2019.

[78] Zhou Y, Wan C, Yang Y, et al. Highly stretchable, elastic, and ionic conductive hydrogel for artificial soft electronics. Advanced Functional Materials. 2019;29(1):1806220.

[79] Zhu L, Qiu J, Sakai E. A high modulus hydrogel obtained from hydrogen bond reconstruction and its application in vibration damper. RSC Advances. 2017;7(69):43755-63.

[80] Sun J-Y, Zhao X, Illeperuma WRK, et al. Highly stretchable and tough hydrogels. Nature. 2012;489(7414):133-6.

[81] Zhang Y, Li Y, Liu W. Dipole–Dipole and H-Bonding Interactions Significantly Enhance the Multifaceted Mechanical Properties of Thermoresponsive Shape Memory Hydrogels. Advanced Functional Materials. 2015;25(3):471-80.

[82] Bai T, Zhang P, Han Y, et al. Construction of an ultrahigh strength hydrogel with excellent fatigue resistance based on strong dipole–dipole interaction. Soft Matter. 2011;7(6):2825-31.

[83] Akhlaghi EA, Badali Y, Altindal S, et al. Preparation of mixed copper/PVA nanocomposites as an interface layer for fabrication of Al/Cu-PVA/p-Si Schottky structures. Physica B: Condensed Matter. 2018;546:93-8.

[84] Yamamoto T, Inoue K, Tezuka Y. Hydrogel formation by the 'topological conversion' of cyclic PLA–PEO block copolymers. Polymer Journal. 2016;48(4):391-8.

[85] Zhou H, Wang M, Zhao W, et al. Supramolecularly Mediated Robust, Anti-Fatigue, and Strain-Sensitive Macromolecular Microsphere Composite Hydrogels. Macromolecular Materials and Engineering. 2020;305(5):2000080.

[86] Gong JP, Katsuyama Y, Kurokawa T, et al. Double-network hydrogels with extremely high mechanical strength. Advanced materials. 2003;15(14):1155-8.

[87] Skelton S, Bostwick M, O'Connor K, et al. Biomimetic adhesive containing nanocomposite hydrogel with enhanced materials properties. Soft Matter. 2013;9(14):3825-3833.

[88] Liu Y, Meng H, Konst S, et al. Injectable Dopamine-Modified Poly(ethylene glycol) Nanocomposite Hydrogel with Enhanced Adhesive Property and Bioactivity. ACS Applied Materials & Interfaces. 2014;6(19): 16982-92.

[89] Kato K, Ito K. Dynamic transition between rubber and sliding states attributed to slidable cross-links. Soft Matter. 2011;7:8737-40.

[90] Okumura Y. Topological Gel: a Third Kind of Gel Consisting of Linear Polymer Chains and Figure-of-Eight Cross-links. KOBUNSHI RONBUNSHU. 2005;62(8):380-9.

[91] Shibayama M, Li X, Sakai T. Precision polymer network science with tetra-PEG

gels—a decade history and future. Colloid and Polymer Science. 2019;297(1):1-12.

[92] Richtering W, Saunders B. Gel architectures and their complexity. Soft Matter. 2014;10.

[93] Sakai T, Matsunaga T, Yamamoto Y, et al. Design and Fabrication of a High-Strength Hydrogel with Ideally Homogeneous Network Structure from Tetrahedron-like Macromonomers. Macromolecules. 2008;41.

[94] Kamata H, Akagi Y, Kayasuga-Kariya Y, et al. “Nonswellable” Hydrogel Without Mechanical Hysteresis. Science. 2014;343(6173):873.

[95] Guo H, Hong W, Kurokawa T, et al. Internal Damage Evolution in Double-Network Hydrogels Studied by Microelectrode Technique. Macromolecules. 2019;52(18): 7114-22.

[96] Li L, Zhang K, Wang T, et al. Biofabrication of a biomimetic supramolecular-polymer double network hydrogel for cartilage regeneration. Materials & Design. 2020;189:108492.

[97] Zhang W, Liu X, Wang J, et al. Fatigue of double-network hydrogels. Engineering Fracture Mechanics. 2018;187:74-93.

[98] Zhang W, Hu J, Tang J, et al. Fracture Toughness and Fatigue Threshold of Tough Hydrogels. ACS Macro Letters. 2019,8(1):17-23.

[99] Ahmed S, Nakajima T, Kurokawa T, et al. Brittle–ductile transition of double network hydrogels: Mechanical balance of two networks as the key factor. Polymer. 2014,55(3):914-23.

Chapter 2 Materials, Experiments and Characterizations

2.1 Materials

2.1.1 Polyvinyl Alcohol (PVA)

PVA (Fig. 2.1), a hydrophilic, biodegradable and biocompatible synthetic polymer, has been widely used in different areas of the biomedical field. Nano-fillers expose their larger surface area for interaction with polymer that is the key concept in the enhancement of functional properties of polymeric nanomaterials. The biomedical uses of PVA include embolization particles, eye drops, contact lenses, meniscus, artificial cartilage, and adhesion barrier. PVA behaves as an embedding mat and matrix for metal/inorganic nanofiller for sensing, optoelectronic devices and many other applications. PVA nanocomposites may include nanofillers made from metals, nonmetals, metal oxides, metal sulfides, inorganic or combinations of these materials. Hoffman has successfully used PVA hydrogels to cultivate living cells, because such hydrogels have large pores and are capable of degradation. PVA can be used not only for bio-artificial materials but also for phantom materials commonly used in medical research. Forecasting soft tissue deformation by analyzing therapeutic interventions and performing minimally invasive surgery simulations may greatly improve the proposed treatment, as well as the accuracy of surgical procedures. Simulation experiments require the use of tissue-simulating objects that mimic the properties of human or animal tissues [1-3].

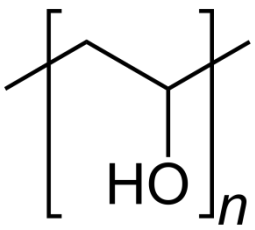

Fig. 2.1 Chemical structure of PVA

The mechanical properties of PVA hydrogels strongly depend on many factors including molecular weight of PVA, concentration of PVA in aqueous solution and synthesis method. The PVA hydrogels with satisfactory mechanical properties were hardly prepared from pure PVA precursors. Therefore, it is still a challenge to improve the performance of physically cross-linked PVA hydrogels. In this study, PVA (polymerization degree: 2000), were purchased from Nacalai Tesque.

2.1.2 Camphorquinone (CQ)

In recent years, photopolymerization has emerged as a valuable tool in biomedical applications because of its ability to rapidly convert a liquid monomer or macromer into 3D polymer networks under physiological conditions with temporal and spatial control. Camphorquinone (1,7,7-trimethylbicyclo[2.2.1]heptane-2,3-dione, CQ) belongs to the aliphatic a-diketones (Fig. 2.2) and is utilized as a photoinitiator for visible-light photo-crosslinking. It is most frequently applied among the commercial photo-initiators. CQ was provided by Tokyo Chemical industry Co., Ltd (Japan).

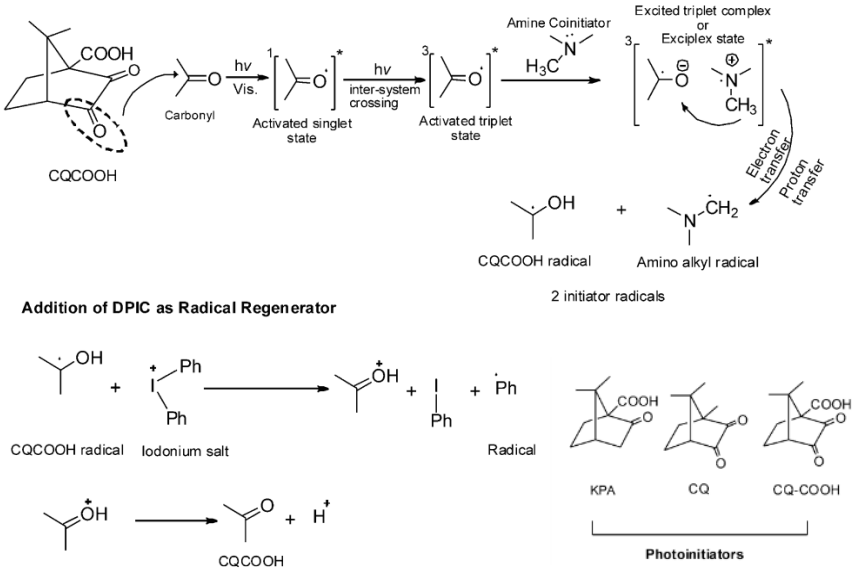

Fig. 2.2 Reaction mechanism of three-component photoinitiator system containing photoinitiator (CQCOOH), an electron donor (amine coinitiator), and an electron acceptor or accelerator (iodonium salt) [4]

2.1.3 Other chemical reagents

In this research, acrylic acid (AA), lithium chloride (LiCl) were purchased from Nacalai Tesque, Inc., (Japan). All chemical reagents were used as received. Distilled water was used in all experiments.

2.2 Synthesis method

2.2.1 Physically cross-linked hydrogels

The uniform hydrogel precursor solution was poured into a Teflon mold (2 mm × 100 mm × 100 mm) and the hydrogels were then fabricated by a FT method (Freezing at -20 ℃ for 24 h; thawing at 25 ℃ for 3 h).

2.2.2 Visible-light-trigger polymerized hydrogels

The hydrogel precursor solution was visible-light-trigger polymerized for 30 min using a visible light source (LS-M210, Sumita, Saitama, Japan).

2.3 Instruments and Characteristics

2.3.1 Tensile tests

The uniaxial elongation properties were tested at room temperature using a universal testing machine (Instron, 3385, extra 50 N load cell, Instron Co., Ltd., Canton, USA) in accordance with standard JIS K6251: 75 mm length, 4 mm width (w), 2 mm height (h), and 25 mm gauge length (l_0). For the cyclic tensile test, loading–unloading measurements were performed using the same universal testing machine at constant cross-head speed of 500 mm/min. Tensile stress (σ) was calculated as $\sigma = F/wh$; Tensile strain (ε) was calculated as $\varepsilon = (l - l_0)/l_0 \times 100\%$. Where F and l are the load and current length, respectively; The resilience (R) was calculated according to the Eq. 2-1:

$$R(\%) = \frac{\int_{Unloading} \delta d\varepsilon}{\int_{Loading} \delta d\varepsilon} \times 100\% \quad \text{2-1}$$

2.3.2 Compression tests

The compression properties were also measured by using the Instron 3385 at a cross-head speed of 1 mm/min. Before testing, hydrogels were cut in a disc shape (8 mm diameter and 2 mm height). The hysteresis energy loss (ΔU) was defined as the area of hysteresis loop encompassed by the loading-unloading curve, Eq. 2-2. The toughness was the total area under the stress-strain curve.

$$\Delta U = \int_{Loading} \delta d\varepsilon - \int_{Unloading} \delta d\varepsilon \quad \text{2-2}$$

2.3.3 Self-healing property test

The self-healing efficiency of hydrogel was measured by comparison of tensile tests between a healed sample and an original sample. In brief, the original sample with dumbbell shape was stretched at a velocity of 100 mm/min to obtain a critical stress (S_o). Then, the healed sample with the same shape and size was also stretched to obtain its critical stress (S_h). The healing efficiency (HE) was calculated according to the Eq. 2-3:

$$HE = S_h/S_o \times 100\% \quad \text{2-3}$$

2.3.4 Calculation of Fracture energy

Fracture energy $W(L)$ could be defined as the total mechanical work required per unit area of crack growth. Fig. 2.3 is the schematic diagram of calculating $W(L_c)$. One sample was non-notched, another sample was notched. The non-notched sample was used to measure the force-length curve. The area beneath the force-length curve gave the work done by the force to the non-notched sample, $W(L)$; The notched sample was used to measure the critical distance between the clamps, L_c when the notch turned into a running crack.

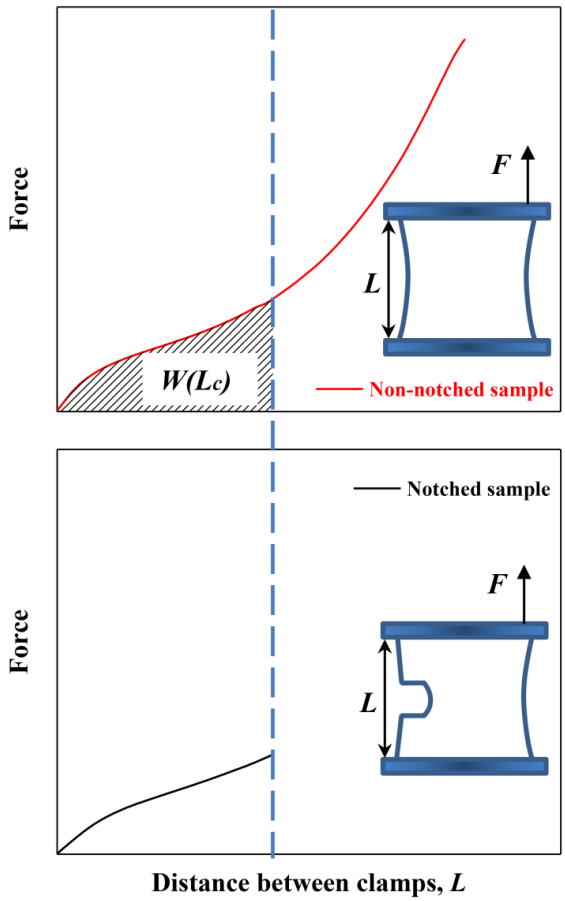

Fig. 2.3 Schematic diagram of calculating W(L_c)

2.3.5 Freeze-drying

The freeze-drying process was conducted by a freeze dryer (DC401, Yamato Scientific Co., Ltd., Japan). The wet hydrogels first were cut into a shape 10 mm×5 mm×2 mm, and then frozen in liquid nitrogen for 10 min. Finally, the frozen hydrogels were freeze-dried at 20 Pa for 12 h. The trap cooling temperature is -45 ℃.

2.3.6 Internal network of hydrogel

The microgel microstructure was observed using a scanning electron microscope (SEM) (Hitachi, Ltd S-4300, Japan). The freeze-dried samples were sputter coated with gold using an ion sputtering apparatus prior to the test.

2.3.7 Swelling experiments

Swelling experiments were performed by immersing the Gels and dried-Gels in conical flasks filled with distilled water. The flasks were placed in a temperature-controlled bath at 25 ℃ until constant. The swelling ratio (Q_m) was calculated by the following equation:

$$Q_m = W_s/W_a \quad 2\text{-}4$$

Where W_s is the weight of the swollen hydrogel and W_a is the weight of the as-prepared gels. Each swelling experiment was measured at least 3 times.

2.3.8 Moisture retention experiment

The hydrogels were exposed in the indoor environment (25 ℃ and RH =40%). The moisture retention ratio (SR_r) was calculated according to the Eq. 2-5:

$$SR_r=W_e/W_a \quad 2\text{-}5$$

where W_a is the as-prepared hydrogel, and W_e is the weight of the exposed hydrogels. Each moisture retention experiment was measured at least 3 times.

2.3.9 Thermal property

Thermal gravimetric analyzer (TGA) and Differential Thermal Analysis (DTA) of the samples were performed with TG instrument (DTG-60, Shimadzu Co., Ltd., Kyoto, Japan) at a scan rate of 10 ℃ min^{-1} from room temperature to 600 ℃ in N_2 atmosphere (flow rate of 50 mL/min). Samples (4-6 mg) were placed in aluminum crucibles by using an empty aluminum crucible as a reference. All of the samples were obtained from freeze-drying.

2.3.10 Fourier Transform Infrared Spectrometer (FT-IR)

A Thermo Fischer Scientific Nicolet iN 10MX infrared spectrometer was used for the analysis of FT-IR. The sample was measured in the range of 650 – 4000 cm^{-1} with a resolution of 4 cm^{-1}. Both KBr pellet and ATR technique were adopted in the test. A

total of 32 scans were accumulated.

2.3.11 X-ray diffraction (XRD)

The crystallinity of hydrogel was examined by X-ray diffraction system (XRD, X'pert Pro MPD, Malvern Panalytical, Netherlands) with Cu-Kα radiation at a scan step in θ of 0.01° and a range of 2θ from 5° to 70°.

2.3.12 Vibration experiment

For the experiments evaluating the damping performance, a commercially available test tube mixer was used as the vibration source; the vibration machine was equipped with a hydrogel vibration damper, a support plate, and a force sensor. The sampling frequency was set at 20 points per second.

References

[1] Hassan C M, Peppas N A. Structure and morphology of freeze/thawed PVA hydrogels. Macromolecules. 2000;33(7):2472-9.

[2] Jiang S, Liu S, Feng W. PVA hydrogel properties for biomedical application. Journal of the mechanical behavior of biomedical materials. 2011;4(7):1228-33.

[3] Peng Y, Yan B, Li Y, et al. Antifreeze and moisturizing high conductivity PEDOT/PVA hydrogels for wearable motion sensor. Journal of Materials Science. 2020;55(3):1280-91.

[4] Kamoun E A, Winkel A, Eisenburger M, et al. Carboxylated camphorquinone as visible-light photoinitiator for biomedical application: Synthesis, characterization, and application. Arabian Journal of Chemistry. 2016;9(5):745-54.

Chapter 3 Hydrophobic association effect enhanced PVA hydrogels

3.1 Introduction

Poly(vinyl alcohol) (PVA) has gained more and more interest over the last years due to its biodegradability and nontoxicity [1]. The physically cross-linked PVA hydrogels formed by freezing-thawing (FT) method has similar viscoelastic behavior with articular, making them attractive biomaterials for tissue engineering [2-4]. The high mechanical strength of PVA hydrogels is imparted by the large number of hydrogen bonds, which can be further strengthened by changing the conditions of FT method. The FT process could induce the formation of microcrystalline regions, resulting in physically cross-linked PVA hydrogels with enhanced mechanical properties [5]. The mechanical properties of PVA hydrogels strongly depend on many factors including molecular weight of PVA, concentration of PVA in aqueous solution and FT conditions. Table 3.1 listed several reported PVA hydrogels synthesized by FT method. It was seen that the PVA hydrogels with satisfactory mechanical properties were hardly prepared from pure PVA precursors. Therefore, it is still a challenge to improve the performance of physically cross-linked PVA hydrogels.

Table 3.1 Comparisons of physically cross-linked PVA hydrogels reported in literatures

FT condition	FT cycles	PVA polymerization degree	PVA solution concentration (wt%)	Modification/ addition agent	Crosslinked agent	Tensile strength (MPa)	Strain (%)	Literature
-20℃ for 24 h; 21℃ for 24 h	3	1750±50	15	none	none	0.4	-	[6]
-25℃ for 12 h; RT for 12 h	5	1750±50	20	none	none	0.935	-	[7]
-20℃ for 21 h; RT for 3 h	3	1750±50	10	none	phytic acid and POSS	0.4	360	[8]
−20°C for 14 h; 25℃ for 4 h	3	1750±50	10	MTM	none	1.3	300	[9]
-20℃ for 3 h; 30℃ for 6 h	2	1799	12.5	none	none	0.38	340	[10]
-20℃ for 16 h; RT for 8 h	3	Not available	15	agarose	none	0.9	200	[11]

RT means room temperature.

Many strategies have been attempted to improve the mechanical properties of physically cross-linked hydrogels. The hydrogel network can be constructed and enhanced by introducing hydrogen bonding [12], hydrophobic interactions [13], and interpolymer complexation [14]. For instance, physically cross-linked PVA hydrogels was strengthened by incorporating clay minerals [15]. Hydrogen bonding was formed between PVA and poly(acrylic acid) (PAA) to generate PVA/PAA hydrogels with improved properties [16]. Xing et al. [17] fabricated a double network polyacrylamide

(PAM)/PVA hydrogel with high tensile strength and good thermal conductivity. Another strategy to improve the PVA hydrogels is hydrophobic modification [18-20], i.e. the hydrophobically associated PVA hydrogels. These hydrogels presented diverse structural components that give them different texture, shape, and mechanical properties, which have widely been applied in soft human tissue engineering, drug delivery, and biosensors as functional materials [21, 22]. Chen et al. [23] introduced hydrophobic urethane and alkyl groups into PVA chains, resulting in an amphiphilic structure of PVA with high surface and interfacial activities, which could be used as a blood contacting material. Moreover, the mechanical properties and self-healing ability of the hydrogels could be improved by hydrophobic effect [13, 24-25]. Physically hydrophobic association interactions could toughen the hydrogels because the hydrophobic chains could be assembled into micelle-like aggregates by molecular entanglements. When the hydrogels were loaded and deformed, the curled hydrophobic chains could slide, extend and disentangle along with deformation of micelles, dissipating a large amount of energy [26].

Soybean oil (SO), consisted of triglycerides, is a relatively inexpensive biobased resource [27-31]. Thus, the derived epoxidized soybean oil (ESO) is environmental friendly and meets the requirements of green chemistry [32], which has been used to synthesize various polymers. It was reported that ESO can improve the thermal stability, adhesiveness, and flexibility properties of the modified polymeric blends [33]. For example, the long fatty acid chains can drive the use of ESO as plasticizers to toughen poly(lactic acid) (PLA) [34]; the stability of poly(vinyl chloride) (PVC) to heat and light can be improved by plasticizing with ESO [35]; the hydrophobic components of ESO can increase the interfacial adhesion between the grafted fibers and PLA matrix [36]. Furthermore, the hydrolyzed ESO-grafted hydroxyethyl cellulose polymeric emulsifier had excellent emulsifying properties and thus was used to synthesize functional hydrogel with N-vinylcaprolactam. [37]. However, to the best of our knowledge, there is no research on the modification of PVA hydrogels with ESO so far.

Herein, an ESO-modified PVA (PVA-ESO) hydrogel with excellent mechanical

properties (up to 1.4 MPa) was successfully prepared via FT for only 3 times. The ring-opening reactions between the epoxy rings of ESO and the hydroxyl groups of PVA have been proven. The strengthening mechanism and hydrophobically associated effect of ESO on the PVA-ESO hydrogels were systematically discussed.

3.2 Experimental

3.2.1 Materials

Poly(vinyl alcohol) (PVA, polymerization degree of 2000) was provided by Nacalai Tesque, Inc., Japan. Epoxidized soybean oil (ESO, average molar ratio of epoxy group/ESO of 4 mol) was purchased from Aladdin Inc., China. Sodium hydroxide was purchased from Nacalai Tesque, Inc., Japan.

3.2.2 Fabrication of hydrogels

Fig. 3.1 presents the preparation process of PVA-ESO hydrogel. 10 wt% PVA was added into distilled water and the mixture was stirred continuously at 90 ℃ for 6 h. Then, a certain amount of ESO (0, 1, 10, 15 and 20 wt%) was added to the mixture, and the resulting mixture were denoted as PVA, PVA-1% ESO, PVA-10% ESO, PVA-15% ESO and PVA-20% ESO, respectively. After adjusting the pH value to 12 by 10 wt% NaOH, the PVA-ESO solution was stirred continuously at 65 ℃ for 24 h to obtain homogeneous mixture. After being degassed, the PVA-ESO solution was cooled to room temperature. The uniform precursor solution was poured into a Teflon mold (2 mm × 100 mm × 100 mm) and the PVA-ESO hydrogels were then fabricated by a FT method (Freezing at -20 ℃ for 24 h; thawing at 25 ℃ for 3 h). The obtained hydrogels had a moisture content of ~85%.

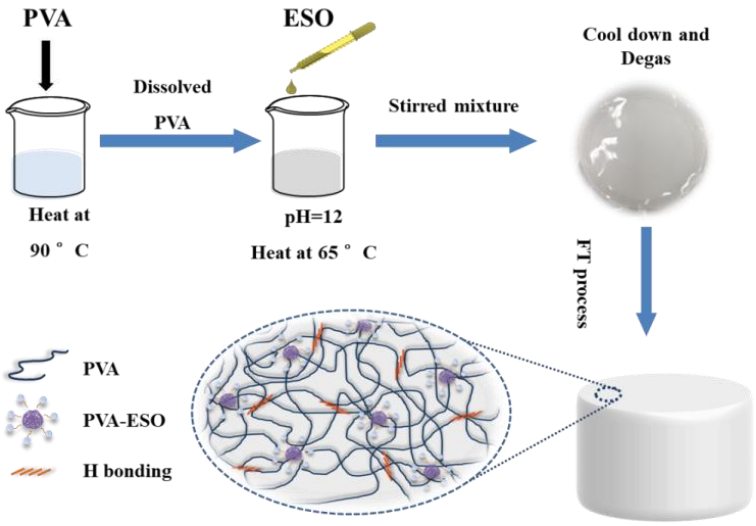

Fig. 3.1 Schematic of fabrication of PVA-ESO hydrogels

3.2.3 Characterization

A Fourier transform infrared spectroscopy (FT-IR, Nicolet iN10MX, Thermo Fischer Scientific) was used to investigate the chemical composition and chemical states of hydrogels at the range of 500-4000 cm^{-1} with a resolution of 4 cm^{-1} for 32 scans. The KBr pellet were adopted in the test.

Thermogravimetric analysis (TGA) and differential thermal analysis (DTA) were performed with TG instrument (DTG-60, Shimadzu, Japan) at a scan rate of 10 ℃/min from room temperature to 600 ℃ in N_2 atmosphere (flow rate of 50 mL/min). Samples (6-10 mg) were placed in aluminum crucibles by using an empty aluminum crucible as a reference. Before testing, the hydrogels were completely dried in vacuum oven at 40 ℃ for 48 h.

The crystallinity of hydrogel was examined by X-ray diffraction system (XRD, X'pert Pro MPD, Malvern Panalytical, Netherlands) with Cu-Kα radiation at a scan step in θ of 0.01° and a range of 2θ from 5° to 70°. Before testing, the hydrogels were completely dried via vacuum oven at 40 ℃ for 48 h. The crystallinity index (*CrI*) of samples were calculated using the relation [38]:

$$CrI = \frac{I_f - I_s}{I_f} \times 100 \qquad 3\text{-}1$$

Where I_f is the peak intensity of the fundamental band at 2θ = 18.5° - 22.0° and *I*s

is the peak intensity of the secondary band at 2θ = 22.0° - 25.0°. The *CrI* is a time-save empirical measure of relative crystallinity [39]:

$$\Delta(CrI)\% = \frac{(CrI)_{PVA\text{-}ESO} - (CrI)_{PVA}}{(CrI)_{PVA}} \times 100 \qquad 3\text{-}2$$

The tensile strength was measured using a universal testing machine (3385 series, Instron, USA) according to the standard of JIS K6251. Before testing, the wet hydrogels (moisture content ~85%) were cut into a dumbbell shape with a 75 mm length, 25 mm gauge length, 4 mm width and 2 mm thickness by a punching blade (JIS No.6, Asker, Japan). The tests were conducted at a cross-head speed of 500 mm/min (25 °C, RH=55%). Each sample was tested at least three times.

The mechanical properties of hydrogels were also determined by a dynamic mechanical analysis (DMA, RSA-G2, TA Instrument, USA). All wet hydrogels (8 mm in diameter and 2 mm in thickness, moisture content ~85%) were carried out through changing scanning dynamic frequency (0.1-100 Hz at 25 ℃) and temperature (30-45 ℃). The storage modulus and loss modulus were recorded during the tests.

The morphologies of hydrogels were characterized by scanning electron microscope (SEM, S-4300, Hitachi, Japan) with accelerating voltages of 5 kV. Before characterization, the hydrogel samples were prepared through freeze-drying method, and then all samples were sputter-coated with platinum by ion sputter (E-1030, Hitachi, Japan) to provide enhanced conductivity.

The contact angle of the PVA hydrogel (2 mm in thickness, moisture content ~85%) was analyzed by considering a liquid drop (deionized water and lubricating oil, 4 μL) resting on the hydrogel surface.

3.3 Results and discussion

3.3.1 Reaction mechanism of PVA-ESO hydrogels

The proposed reactions between ESO and PVA involve several reactions (Fig. 3.2). The main reaction I occurs between ESO and PVA through ring-opening reactions

between the epoxy rings on ESO and the hydroxyl groups of PVA, resulting in homogenized PVA-ESO solution. In the presence of a nucleophile, the ester groups of ESO could produce fatty acid and alcohol by basic hydrolysis; these hydrolyzed products containing –COOH and –OH groups would further react with the epoxy rings of ESO [40] (reaction II). The new generated –OH groups from reactions I and II are capable of further reacting with other epoxides to promote the self-polymerization of ESO [41].

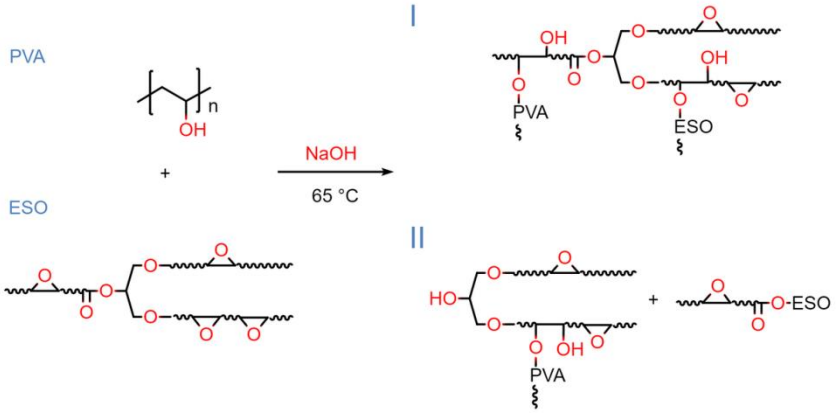

Fig. 3.2 Proposed reactions between PVA and ESO

To verify the reactions between PVA and ESO, the FT-IR spectra results of PVA, ESO, and PVA-ESO were shown in Fig. 3.3 For the spectrum of ESO, the bands at 1161 cm^{-1}, 1106 cm^{-1} and 832 cm^{-1} revealed C–O–C asymmetric stretching vibration, C–O–C symmetrical stretching vibration and epoxide ring vibrations, respectively [32, 42]. For the PVA-ESO, intensity of the C–O–C characteristic absorption band changed. Actually, the higher weight ratio of ESO to PVA, more ester groups took part in hydrogen bonds as hydrogen-bond acceptors, thus, the broad absorption band of O–H stretching vibration at 3360 cm^{-1} declined. These indicated that the epoxy groups successfully open the rings and reacted with the hydroxyl of PVA.

Moreover, it can be found from FT-IR spectra (Fig. 3.3) that PVA-ESO hydrogels showed asymmetric and symmetrical stretching vibration of COO^- at 1574 cm^{-1} and 1421 cm^{-1}, implying the formation of carboxylate. Therefore, there also were fatty acid salts due to the saponification reaction between ESO and aqueous alkali under heating condition.

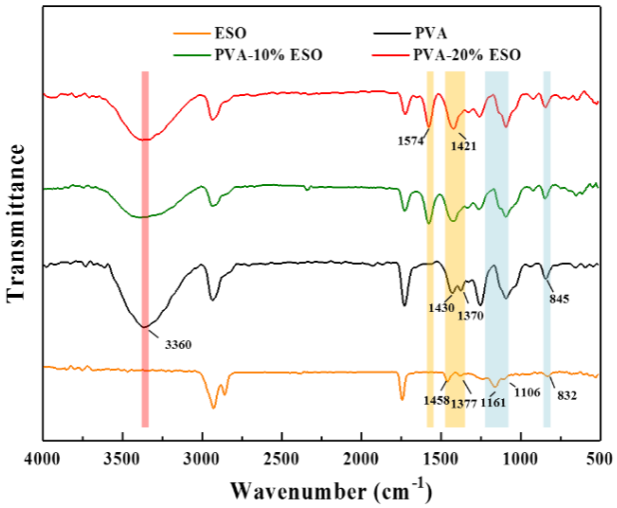

Fig. 3.3 FT-IR spectra of ESO, PVA and PVA-ESO

3.3.2 *Micro-structure of PVA-ESO hydrogels*

The internal structure of the freeze-dried hydrogels was shown in Fig. 3.4. Pure PVA exhibits a uniform structure without porous structure or defects (Fig. 3.4a and d). By contrast, the PVA-ESO hydrogels present porous structures. As the increase of ESO content, the evenly dispersed micro-pores (~3 μm in diameter, Fig. 3.4e) of PVA-10% ESO hydrogel change to the large concentrated pores (more than 10 μm in diameter, Fig. 3.4f) of PVA-20% ESO hydrogel.

Generally, during the polymerization of the hydrogel precursor, the produced polymer could not be dissolved in the solvent due to physical or chemical crosslinking. Thus, the hydrogel structure that consists of polymer matrix phase and solvent phase would form. For the freeze-drying process of hydrogel, the solvent phase would volatilize and then leading the porous structure. However, it was pointed out that the slow water evaporation during freeze-drying process that makes the PVA chains coming closer to each other, leading to a decrease in the pore size [43]. Therefore, the small pores of the pure PVA hydrogel can only be observed under more severe conditions of freeze-drying process.

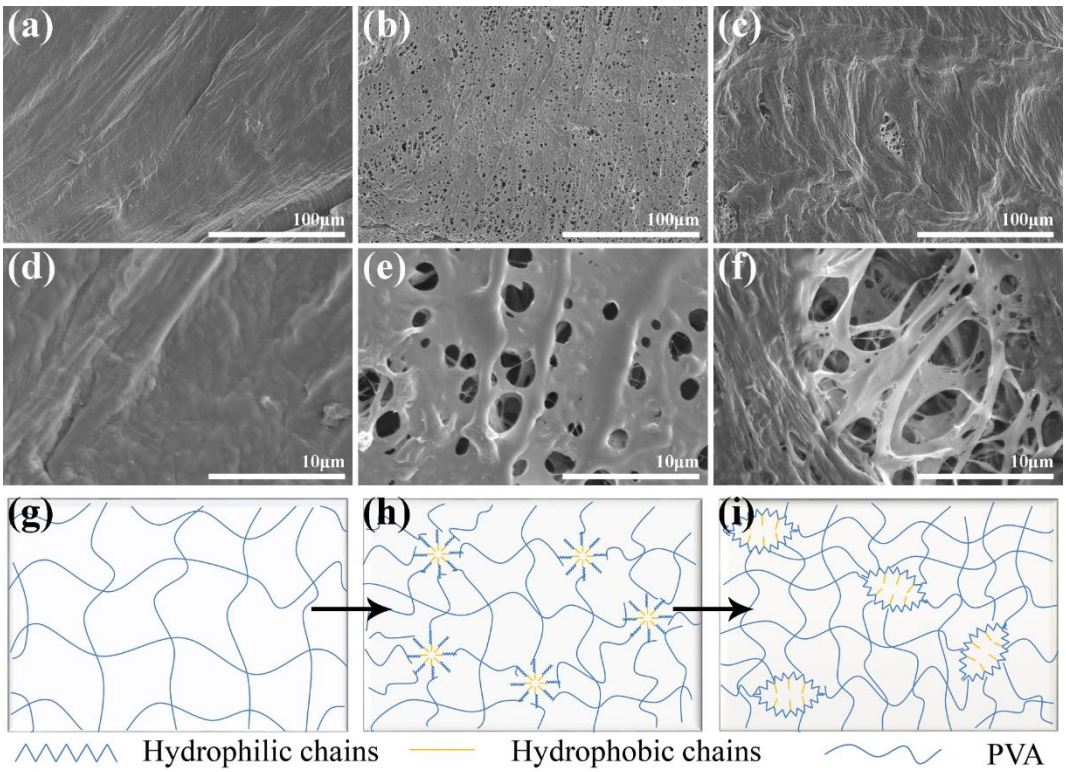

Fig. 3.4 SEM images of cutting surfaces and schematic structure of hydrogels (a, d and g) pure PVA; (b, e and h) PVA-10% ESO; (c, f and i) PVA-20% ESO

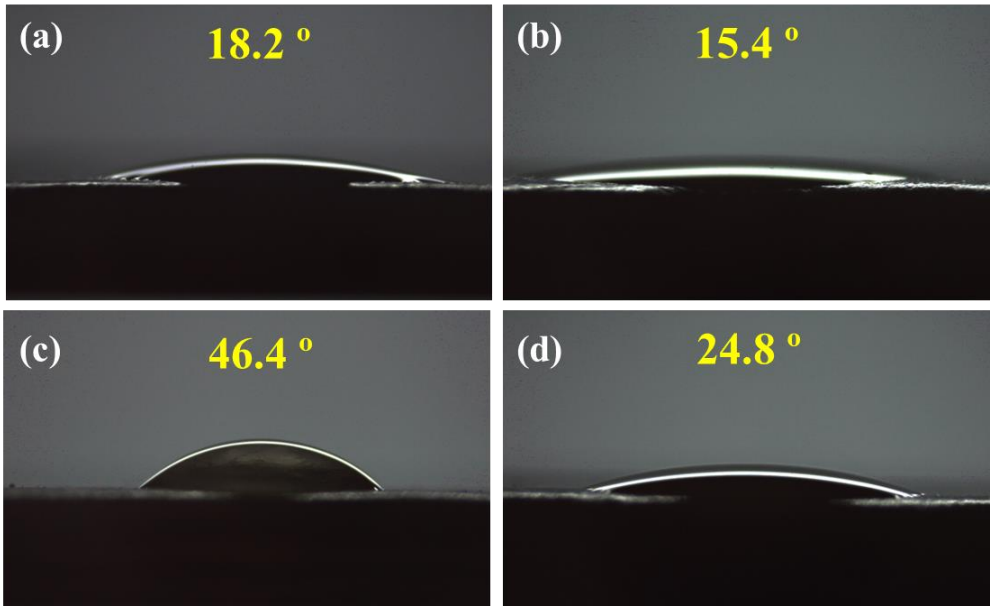

Fig. 3.5 Water contact angle of (a)PVA hydrogel and (b)PVA-10% ESO hydrogel; lubricating oil contact angle of (c) PVA and (d) PVA-10% ESO hydrogels

As to the PVA-ESO hydrogels, the porous structure can be observed after the

freeze-drying process at same conditions. With the addition of ESO, the cross-linking density of the polymers (PVA-ESO and unreacted PVA) increased due to the self-assembly and the hydrophobic segments and strong dipole-dipole interactions. Thus, the hydrophilic groups were extruded and the solvent (water + NaOH) was filled in the gaps [18], which results in the formation of the micelles (Fig. 3.4b-h) [44]. In the PVA-ESO hydrogel system, the more hydrophobic chains (ESO) grafted on hydrophilic chains (PVA), the bigger spherical micelles formed (Fig. 3.4f), and the more hydrophilic groups extruded. The micellar core corresponds to hydrophobic chains, the hydrophilic chain is in contact with the solution and wrapping the hydrophobic segment to form a porous structure (Fig. 3.4i) [45]. Generally, a porous hydrogel with a desired micro-structure can be obtained by controlling the amount of added ESO. What's more, the ESO modified PVA can also improves the amphipathic of hydrogels (Fig. 3.5).

3.3.3 *Mechanical properties of PVA-ESO hydrogels*

Fig. 3.6 presents the tensile test results of PVA and PVA-ESO hydrogels. The tensile strength of PVA-ESO hydrogels (72-319 kPa) was much higher than that of PVA hydrogel (47 kPa), after 1 time FT cycle (FT@1, Fig. 3.6b). With increasing contents of ESO, the hydrophobic segments of PVA-ESO entangle more tightly. Thus, when hydrogels are subjected to external forces, the hydrophobic segments act as cross-linking sites, allowing the stress to disperse and prevent the hydrogel from breaking. Therefore, it greatly improves the strength of hydrogel. On the other hand, it has been proved that the crystallinity of PVA hydrogel would increase as the number of cycle increases [22]. It was seen that the tensile strength of PVA and PVA-ESO hydrogels significantly increased with increasing the FT cycles (Fig. 3.6b). The highest strength of PVA-ESO hydrogels reached 1.4 MPa (Fig. 3.6b, PVA-20% ESO for FT@3), which was 2.4 times higher than that of pure PVA hydrogel prepared at same parameters. For the elongation at break of PVA-ESO hydrogels, its reduction is not significant and was finally stabilized at 325-350% (Fig. 3.6a).

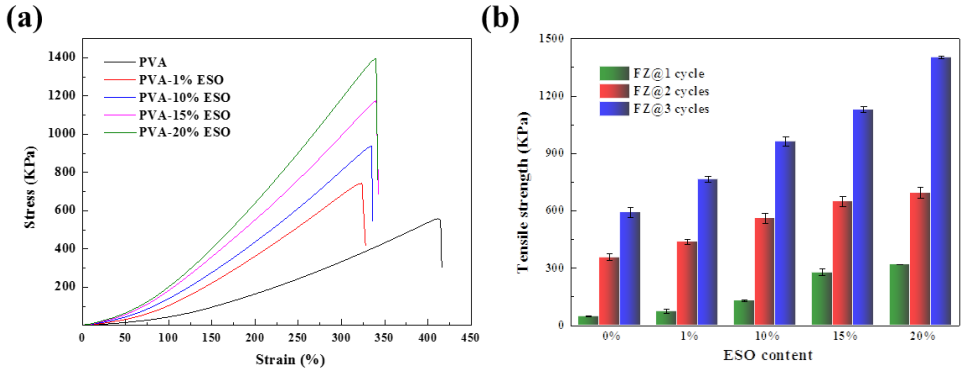

Fig. 3.6 Stress-strain curves of PVA and PVA-ESO hydrogels prepared under different times of freeze-thaw cycles: (a) three times (FZ-@3); (b) tensile strength results of PVA-ESO hydrogels by repetitive freeze-thaw cycles in comparison to control

For the pure PVA hydrogel with lower concentration (8 wt%, FT@1, Fig. 3.7), it still was viscous and had low fluidity, contrasting with a milky white and higher-strength PVA-20% ESO hydrogel (8 wt%, FT@1), which also indicating the significant enhancement of ESO to PVA.

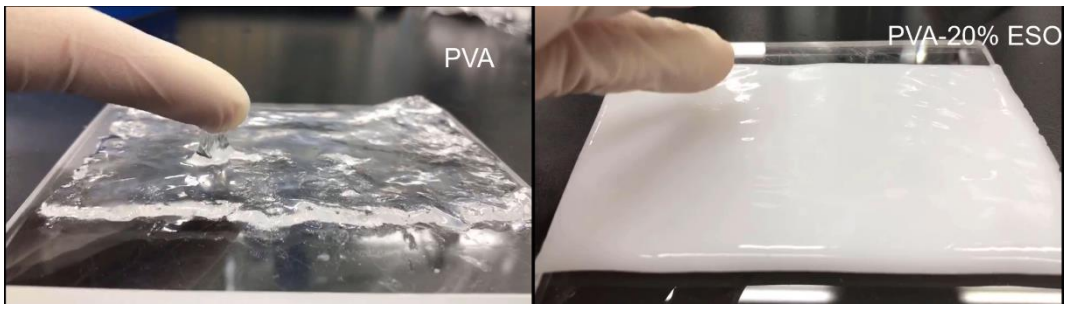

Fig. 3.7 The hydrogel appearance of PVA and PVA-20% ESO hydrogel through one freeze-thaw cycle process (8 wt% PVA sulotion), to further certify the hydrophobic association enhance the strength of hydrogels

In fact, after the addition of ESO into PVA, the efficient aggregation of hydrophobic chains can significantly enhance the mechanical properties of PVA-ESO hydrogels. The PVA-ESO is easier to form a hydrogel and the hydrogels are expected to exhibit enhanced viscosification ability as a result of intermolecular hydrophobic interaction between the hydrophobic groups in the structure, thus leading to the formation of polymolecular associations [20]. In addition, the moisture contents (Fig.

3.8) of the PVA-ESO hydrogels were significantly reduced compared with PVA for the increased molecular weight and the decrease in hydrophilic groups after reacting with ESO, indicated that the cross-linking density of the hydrogel gradually increased.

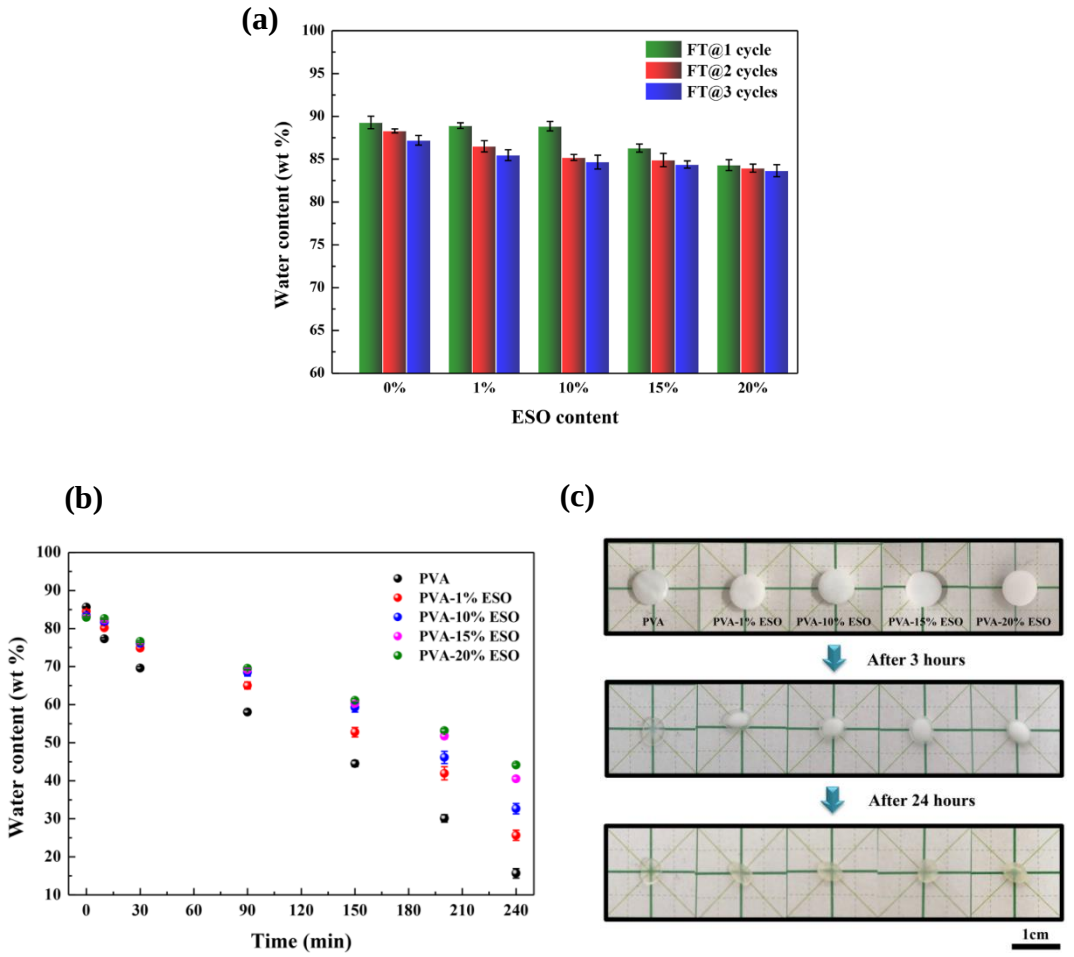

Fig. 3.8 (a) Moisture contents of PVA and PVA-ESO prepared by different times freeze-thaw cycles (b) Desorption behavior (water loss) of PVA and PVA-ESO hydrogels (c) Digital photo of desorption behavior

3.3.4 *Thermal property and crystal state of PVA-ESO hydrogels*

The thermal stability of PVA and PVA-ESO hydrogels were evaluated by thermogravimetric analysis (Fig. 3.9). A weight loss started at about 100 ℃ in TGA curves due to the evaporation of intermolecular H-bonded water. Pure PVA exhibited two thermal decomposition stages. The first stage occurred at 230-350 ℃ and the second stage appeared at 350-500 ℃. These two stages reflected the breakage of the

side and main backbone polymer chains, respectively [46]. The initial thermal decomposition temperature (T_o) of PVA was 230 ℃. The T_o of the PVA-ESO samples increased as the increase of ESO content. The temperature with 40% residual weights (T_{40}) of PVA was about 285 ℃, which was obviously lower than that of PVA-ESO. Moreover, the maximum decomposition temperatures (T_d) of PVA significantly increased after grafting with ESO (Fig. 3.9b). When the testing reached 600 ℃, the residual weights of hydrogels were basically stable. It can be found that the final residual weights decreased with increasing ESO content (from 13.80% of PVA-1% ESO to 9.27% of PVA-20% ESO, Fig. 3.9a). Notably, the final residual weights were lower than the estimated values (calculated by the combination of final residual weights of pure PVA and ESO), which also indicates the decomposition of PVA-ESO reaction product.

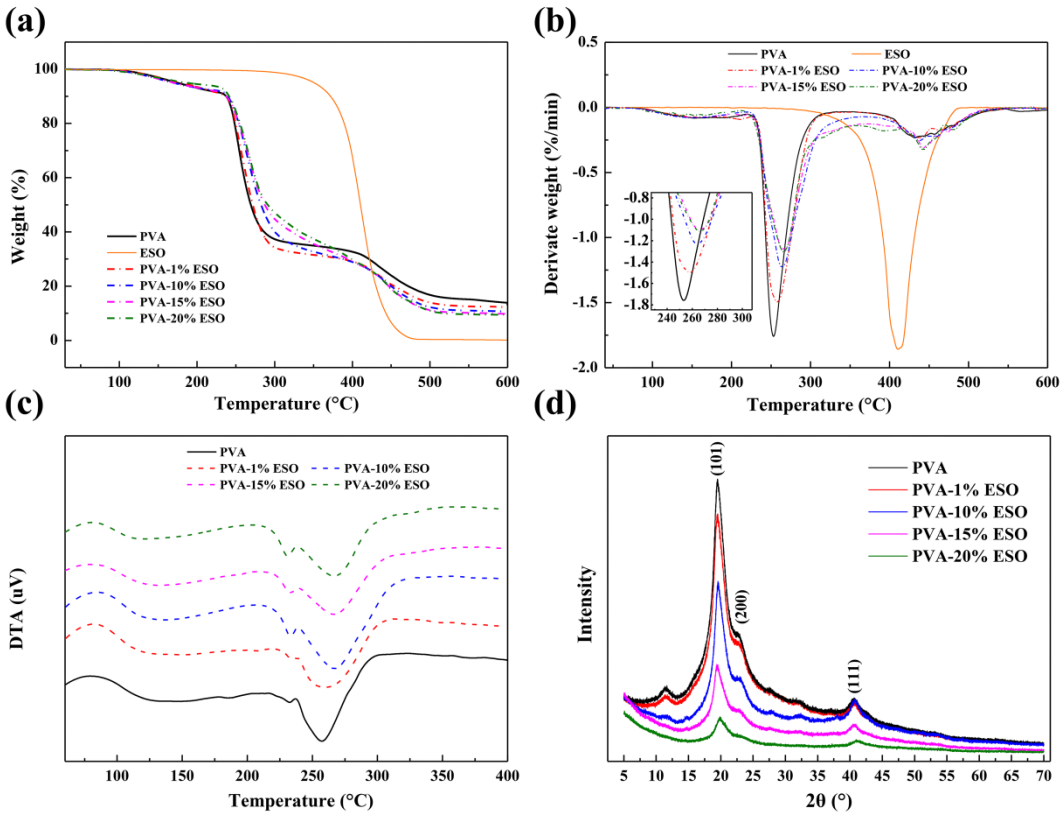

Fig. 3.9 Thermal degradation behavior of PVA and PVA-ESO hydrogels prepared by 3 times of freeze-thaw cycles: (a)TGA results; (b) DTG results; (c)DTA results; (d) XRD results

The DTA results (Fig. 3.9c) indicated that the crystallinity of PVA was changed by ESO. As shown in Table 3.2, the glass transition temperature (T_g) of the hydrogels slightly shifted from 104.77 ℃ to 100.66 ℃ with increasing the ESO contents. It was pointed out that the ESO as a plasticizer would reduce the T_g of polymers [47]. Actually, as the ESO content increases, the hydrogen bonding in the crystalline structure of PVA would be partially interrupted by the interaction between epoxies and PVA molecules. Moreover, the short branched chain introduced into the main chain of PVA (Fig. 3.2) could restrict the main chains to approached each other and cause an increase in degrees of freedom. Ultimately, the T_g of hydrogels was decreased with increasing the ESO contents. However, the melting peak shifted slightly to higher temperature with increasing content of ESO. The melting temperature (T_m) of PVA-1% ESO, PVA-10% ESO, PVA-15% ESO and PVA-20% ESO were 232.34, 232.63, 232.9 and 233 ℃, respectively. They can be attributed to the increased molecular weight and enhanced intermolecular forces. Further research about chains kinetics is needed to more clearly understand the effects.

Table 3.2 Summary of DTA and DTG thermograms of the PVA-ESO hydrogels

Samples	T_g	T_m	T_d
PVA	104.77	230.66	261.16
PVA-1% ESO	104.63	232.34	261.77
PVA-10% ESO	104.37	232.63	266.80
PVA-15% ESO	103.01	232.95	267.42
PVA-20% ESO	100.66	233.00	267.91
ESO	-	-	412.05

It was also pointed out that the crystallization region would limite the movement of the amorphous segment [2]. Since the hydrophilic groups are correspondingly reduced for the introduced ESO, the hydrogen bond decreased. On the one hand, the amorphous segments of PVA-ESO hydrogels could achieve the same degree of freedom as that of PVA hydrogel at lower temperature. On the other hand, with the

increase of flexible branches, the stereoregularity of the molecular chains are reduced, and it is difficult for the branched structure to co-crystallize with the main chain, which means the increasing the relative proportion of amorphous region [48].

Table 3.3 Crystallization of PVA and PVA-ESO hydrogels

Samples	Crystallinity index	△(CrI)%
PVA	54.77	-
PVA-1% ESO	52.50	4.13
PVA-10% ESO	52.37	4.37
PVA-15% ESO	46.93	14.31
PVA-20% ESO	39.44	27.98

To further reveal this point, the crystallinity index (*CrI*) of PVA and PVA-ESO samples were determined by XRD (Fig. 3.9d). The relative diffraction peaks at 20, 22.5 and 40.2 ° corresponded to the characteristic peaks ((101), (200) and (111), respectively) of PVA, which were consistent with literatures [2, 49, 50]. The XRD patterns of PVA-ESO exhibited the characteristics of pure PVA but with lower intensity of crystalline peaks. Thus, the crystalline zone of PVA was decreased upon mixing with different content of ESO. As calculated from Eq. 3-1 (Table 3.3), the *CrI* of PVA-ESO decreased with increasing ESO content to 39.44%.

3.3.5 *DMA analysis*

The liquid phase of hydrogel is constrained within a three-dimensional network thus existing visco-elastic properties [51]. It was found that all of the hydrogels have a similar pattern in the modulus versus temperature plot, i.e., the modulus is almost constant up to about 30-45 ℃, although their initial modulus were different [52]. Fig. 3.10a and b showed that curves of storage modulus (*E*'), loss modulus (*E*'') and tan δ as a function of temperature (30~45 ℃) for PVA and PVA-ESO hydrogel. The *E*' of PVA-ESO hydrogels were higher than that of pure PVA. The *E*' of the hydrogels declined slowly with the increase of temperature. When ESO content was over than

10%, there was little change in *E'*, *E"* and tan *δ*, and the changing trend of *E"* for the hydrogels were basically constant. These results indicated that PVA-10% ESO, PVA-15% ESO and PVA-20% ESO hydrogels have no significantly water evaporation, structural changes, and are thermally stable at least to 45 ℃ [53]. Moreover, with the increase of ESO, the dynamic thermal stability for the wet ESO-PVA hydrogel was enhanced, and the network structure could not be destroyed easily, the hardness and mechanical strength were improved.

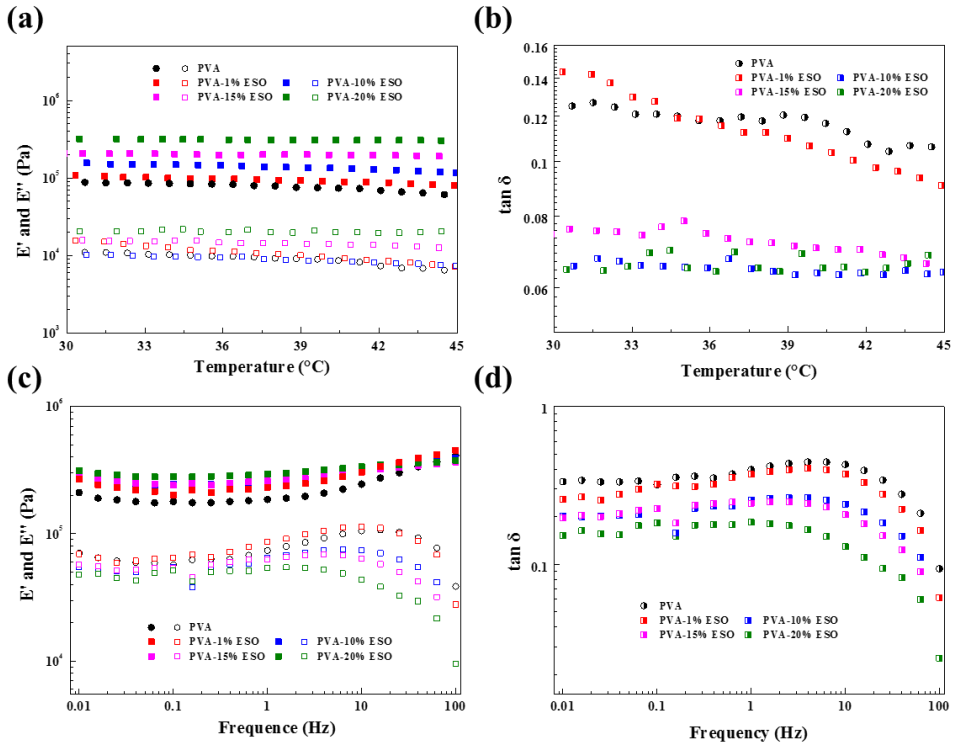

Fig. 3.10 DMA curves of PVA and PVA-ESO hydrogels: (a) and (b) Storage modulus *E'*, loss modulus *E"* and tan *δ* as a function of temperature; (c) and (d) Storage modulus and loss modulus as a function of frequency

Fig. 3.10c and d showed that curves of *E'*, *E''* and tan δ as a function of frequency (0.01~100 Hz) for PVA and PVA-ESO hydrogels. The *E'* of hydrogels increased slowly with the increased frequency, which was similar to the situation of natural cartilage. The *E"* declined slightly with the frequency, which indicated that most of the energy was stored in the hydrogel and consumed less. *E'* characterizes the elastic property of the material, and *E''* presents the viscous property of the material. For all

the samples, *E′* were much larger than *E″*, which indicates that the hydrogels have considerable strength that could suffer from pressure and resist to certain impact. The PVA-20% ESO hydrogel had the highest value of *E′* and the lowest tan δ over the entire wet hydrogels, which indicates that PVA-20% ESO hydrogel has a better elastic property.

3.4 Conclusions

High strength PVA-ESO hydrogels were successfully fabricated from hydrophilic PVA and hydrophobic ESO through the formation of hydrophobic association, hydrogen bonding, and chain entanglements. The thermal stability and mechanical properties of PVA hydrogels were significantly enhanced and good flexibility was observed, where the ESO acted as the physical entanglement point between the molecular chains and increased the elasticity of the hydrogels. With the increase of ESO content, the tensile strength of the hydrogels (FT@3) increased from 560 kPa to 1.4 MPa. In addition, a porous hydrogel having a certain microscopic morphology could be obtained by controlling the content of ESO. These results indicate that the vegetable oil-based hydrogels will find applications in personal care or health care areas due to its amphipathy, improved mechanical properties and controllability in wet conditions.

References

[1] Reguieg F, Ricci L, Bouyacoub N, et al. Thermal characterization by DSC and TGA analyses of PVA hydrogels with organic and sodium MMT. Polymer Bulletin. 2020;77(2):929-48.

[2] Holloway J L, Lowman A M, Palmese G R. The role of crystallization and phase separation in the formation of physically cross-linked PVA hydrogels. Soft Matter. 2013;9(3):826-33.

[3] Hasan A, Morshed M, Memic A, Hassan S, Webster T. J, Marei H. E.-S.

Nanoparticles in tissue engineering: applications, challenges and prospects. International journal of nanomedicine. 2018;13:5637-55.

[4] Wang Y, Xue Y, Wang J, Zhu Y, Zhu Y, Zhang X, Liao J, Li X, Wu X, Qin Y.-X, W. A composite hydrogel with high mechanical strength, fluorescence, and degradable behavior for bone tissue engineering. Polymers. 2019;11(7):1112.

[5] Hassan C. M, Peppas N. A. Structure and applications of poly (vinyl alcohol) hydrogels produced by conventional crosslinking or by freezing/thawing methods. Biopolymers ·PVA Hydrogels, Anionic Polymerisation Nanocomposites. 2000;37-65.

[6] Hago E.-E, Li X. Interpenetrating polymer network hydrogels based on gelatin and PVA by biocompatible approaches: synthesis and characterization. Advances in Materials Science and Engineering. 2013;2013:328763.

[7] Pan Y, Ding J, Chen Y, Shen Q. Study on mechanical and optical properties of poly(vinyl alcohol) hydrogel used as soft contact lens. Materials Technology. 2016;31(5): 266-73.

[8] Shao L, Li Y, Ma Z, Bai Y, Wang J, Zeng P, Gong P, Shi F, Ji Zh, Qiao Y, Xu R, Xu J, Zhang G, Wang C, Ma J. A Highly Sensitive Strain Sensor Based on Stretchable and Conductive Poly (vinyl alcohol)/Phytic Acid/NH2-POSS Hydrogel with a 3D Microporous Structure. ACS Applied Materials & Interfaces. 2020;12:26496-508.

[9] Luo X, Akram M Y, Yuan Y, Nie J, Zhu X. Silicon dioxide/poly (vinyl alcohol) composite hydrogels with high mechanical properties and low swellability. Journal of Applied Polymer Science. 2019;136(1): 46895.

[10] Sun Y, Xiang N, Jiang X, Hou L. Preparation of high tough poly (vinyl alcohol) hydrogel by soaking in NaCl aqueous solution. Materials Letters. 2017;194:34-7.

[11] Li H, Wu C, Wang S, Zhang W. Mechanically strong poly (vinyl alcohol) hydrogel with macropores and high porosity. Materials Letters. 2020;266:127504.

[12] Lin C, Liu Y, Xie X. GO/PVA nanocomposites with significantly enhanced mechanical properties through metal ion coordination. Chinese Chemical Letters. 2019;30:1100-4.

[13] Zhang Y, Song M, Diao Y, Li B, Shi L, Ran R. Preparation and properties of

polyacrylamide/polyvinyl alcohol physical double network hydrogel. RSC advances. 2016;6(113):112468-76.

[14] Rodríguez-Rodríguez R, García-Carvajal Z Y, Jiménez-Palomar I, Jiménez-Avalos J A, Espinosa-Andrews H. Development of gelatin/chitosan/PVA hydrogels: Thermal stability, water state, viscoelasticity, and cytotoxicity assays. Journal of Applied Polymer Science. 2019, 136(10):47149.

[15] Kokabi M, Sirousazar M, Hassan Z M. PVA–clay nanocomposite hydrogels for wound dressing. European polymer journal. 2007;43(3):773-81.

[16] Liu T, Jiao C, Peng X, Chen Y.-N, Chen Y, He C, Liu R, Wang H. Super-strong and tough poly (vinyl alcohol)/poly (acrylic acid) hydrogels reinforced by hydrogen bonding. Journal of Materials Chemistry B. 2018;6(48):8105-14.

[17] Xing L, Hu C, Zhang Y, Wang X, Shi L, Ran R. A mechanically robust double-network hydrogel with high thermal responses via doping hydroxylated boron nitride nanosheets. Journal of Materials Science, 2019, 54(4):3368-82.

[18] Yahya G O, Asrof Ali S K, Hamad E Z. Surface and interfacial activities of hydrophobically modified poly(vinyl alcohol) (PVA). Polymer. 1996;37(7):1183-8.

[19] Andersen P O, Marstokk O, Nyström B, Walderhaug H. Effects of Hydrophobic Modification and Electrostatic Interactions on the Association Behavior in Aqueous Solutions of Poly(vinyl alcohol). A Pulsed Field Gradient NMR Study. Macromolecular Chemistry and Physics, 2001, 202(8):1457-65.

[20] Jiang H, Duan L, Ren X, Gao G. Hydrophobic association hydrogels with excellent mechanical and self-healing properties. European Polymer Journal. 2019;112:660-9.

[21] Li X, Su X. Multifunctional smart hydrogels: potential in tissue engineering and cancer therapy. Journal of Materials Chemistry B. 2018;6(29):4714-30.

[22] Hoffman A S. Hydrogels for biomedical applications. Advanced drug delivery reviews. 2012;64:18-23.

[23] Chen X, Taguchi T. Hydrophobically modified poly(vinyl alcohol)s as antithrombogenic coating materials. Materials Science and Engineering: C.

2019;102:289-98.

[24] Tuncaboylu D C, Sari M, Oppermann W, Okay O. Tough and Self-Healing Hydrogels Formed via Hydrophobic Interactions. Macromolecules. 2011;44(12):4997-5005.

[25] Tuncaboylu D C, Sahin M, Argun A, Oppermann W, Okay O. Dynamics and Large Strain Behavior of Self-Healing Hydrogels with and without Surfactants. Macromolecules. 2012;45(4):1991-2000.

[26] Ren X, Huang C, Duan L, Liu B, Bu L, Guan S, Hou J, Zhang H, Gao G. Super-tough, ultra-stretchable and strongly compressive hydrogels with core–shell latex particles inducing efficient aggregation of hydrophobic chains. Soft Matter. 2017, 13(18):3352-8.

[27] Zhang C, Garrison T F, Madbouly S A, Kessler M R. Recent advances in vegetable oil-based polymers and their composites. Progress in Polymer Science. 2017;71:91-143.

[28] Stolp L J, Gronlund P J, Kodali D R. Soybean Oil Fatty Acid Ester Estolides as Potential Plasticizers. American Oil Chemists' Society. 2019, 96(6):727-38.

[29] Chelil O, Belhaneche-Bensemra N, GARCIA D L, Fernandez-Garcia M, Benaniba M T. Preparation of epoxidized sunflower oil metal soap derivatives and their use as heat stabilizers for polyvinyl chloride. Turkish Journal of Chemistry. 2019;43(2):582-93.

[30] Nakagawa K, Sowasod N, Tanthapanichakoon W, Charinpanitkul T. () Hydrogel based oil encapsulation for controlled release of curcumin by using a ternary system of chitosan, kappa-carrageenan, and carboxymethylcellulose sodium salt. LWT-Food Science and Technology. 2013;54(2):600-5.

[31] Alehosseini A, Gomez del Pulgar E.-M, Fabra M. J, Gómez-Mascaraque L G, Benítez-Páez A, Sarabi-Jamab M, Ghorani B, Lopez-Rubio A. Agarose-based freeze-dried capsules prepared by the oil-induced biphasic hydrogel particle formation approach for the protection of sensitive probiotic bacteria. Food Hydrocolloid. 2019;87:487-96.

[32] Wang Z, Zhang X, Wang R, Kang H, Qiao B, Ma J, Zhang L, Wang H. Synthesis and Characterization of Novel Soybean-Oil-Based Elastomers with Favorable Processability and Tunable Properties. Macromolecules. 2012;45:9010-9.

[33] Ammar S, Iling A.W.M, Ramesh K, Ramesh S. Development of fully organic coating system modified with epoxidized soybean oil with superior corrosion protection performance. Progress in Organic Coatings. 2020;140:105523.

[34] Liu W, Qiu J, Zhu L, Fei M, Qiu R, Sakai E, Ito K, Song G, Tang G. Tannic acid-induced crosslinking of epoxidized soybean oil for toughening poly (lactic acid) via dynamic vulcanization. Polymer. 2018;148:109-18.

[35] He W, Zhu G, Gao Y, Wu H, Fang Z, Guo K. Green plasticizers derived from epoxidized soybean oil for poly (vinyl chloride): Continuous synthesis and evaluation in PVC films. Chemical Engineering Journal. 2020;380:122532.

[36] Chen T, Wu Y, Qiu J, Fei M, Qiu R, Liu W. Interfacial compatibilization via in-situ polymerization of epoxidized soybean oil for bamboo fibers reinforced poly (lactic acid) biocomposites. Composites Part A: Applied Science and Manufacturing. 2020;138:106066.

[37] Yang X, Li Z, Liu H, Ma L, Huang X, Cai Z, Xu X, Shang S, Song Z. Cellulose-based polymeric emulsifier stabilized poly (N-vinylcaprolactam) hydrogel with temperature and pH responsiveness. International Journal of Biological Macromolecules. 2020;143:190-9.

[38] Segal L, Creely J J, Martin A E, Conrad C M. An Empirical Method for Estimating the Degree of Crystallinity of Native Cellulose Using the X-Ray Diffractometer. Textile research journal. 1959;29(10):786-94.

[39] Guirguis O W, Moselhey M T. Thermal and structural studies of poly (vinyl alcohol) and hydroxypropyl cellulose blends. National Science. 2012;4:57-67.

[40] Ahn B.-J. K, Kraft S, Sun X S. Chemical pathways of epoxidized and hydroxylated fatty acid methyl esters and triglycerides with phosphoric acid. Journal of Materials Chemistry. 2011;21(26):9498-505.

[41] Liu W, Qiu J, Zhu L, Fei M, Qiu R, Sakai E, Ito K, Song G, Tang G. Tannic

acid-induced crosslinking of epoxidized soybean oil for toughening poly(lactic acid) via dynamic vulcanization. Polymer. 2018;148:109-18.

[42] Huang J, Jiang P, Wen Y, Deng J, He J. Soy-castor oil based polyurethanes with octaphenylsilsesquioxanetetraol double-decker silsesquioxane in the main chains. RSC advances. 2016;6(73):69521-9.

[43] Gonzalez-Ortiz D, Pochat-Bohatier C, Gassara S, Cambedouzou J, Bechelany M, Miele P. Development of novel h-BNNS/PVA porous membranes via Pickering emulsion templating. Green Chemistry, 2018, 20(18): 4319-29.

[44] Rangel-Yagui CO, Pessoa Jr A, Tavares L C. Micellar solubilization of drugs. J Pharm Pharm Sci. 2005;8:147-63.

[45] Kwon G S, Kataoka K. Block copolymer micelles as long-circulating drug vehicles. Advanced drug delivery reviews. 1995;16(2-3):295-309.

[46] Zhu L, Liu Y, Jiang Z, Sakai E, Qiu J, Zhu P. Highly temperature resistant cellulose nanofiber/polyvinyl alcohol hydrogel using aldehyde cellulose nanofiber as cross-linker. Cellulose. 2019;26(9):5291-303.

[47] Krishnaswamy R K, Yang Q, Fernandez-Ballester L, Kornfield J A. Effect of the Distribution of Short-Chain Branches on Crystallization Kinetics and Mechanical Properties of High-Density Polyethylene. Macromolecules. 2008;41(5):1693-704.

[48] Tian Z, K. Chen, B. Liu, N. Luo, W. Du, F. Qian. Short-chain branching distribution oriented model development for Borstar bimodal polyethylene process and its correlation with product performance of slow crack growth. Chem Eng Sci 2015;130:41-55.

[49] Wang J, Ye L. Structure and properties of hydrophobic cationic poly(vinyl alcohol). Polymer international. 2012;61(4):571-80.

[50] Jiang L, Yang T, Peng L, Dan Y. Acrylamide modified poly(vinyl alcohol): crystalline and enhanced water solubility. RSC advances. 2015;5(105):86598-605.

[51] Parhi R. Cross-Linked Hydrogel for Pharmaceutical Applications: A Review. Advanced pharmaceutical bulletin. 2017;7(4):515-30.

[52] Slaughter B V, Khurshid S S, Fisher O Z, Khademhosseini A, Peppas N A.

Hydrogels in regenerative medicine. Advanced materials. 2009;21(32-33): 3307-29.

[53] Chen K, Liu J, Yang X, Zhang D. Preparation, optimization and property of PVA-HA/PAA composite hydrogel. Materials Science and Engineering: C. 2017;78:520-9. Materials Science and Engineering: C. 2017, 78: 520-529.

Chapter 4 Double network ionic hydrogel and its application in strain sensing

4.1 Introduction

Hydrogels are soft-wet materials with good flexibility and biocompatibility, which have attracted much attention in sensing, electronic skin, health detection [1-3]. For a hydrogel-based sensor [4-6], on the premise of satisfying the electrical conductivity, the selected hydrogel also needs certain mechanical strength, good stretchability, recovery and anti-fatigue property for stable signal transmission during it withstands repeated deformation at different speeds for a long duration [7, 8]. Up to now, various hydrogel strain sensors incorporated with conducting polymers, polyelectrolyte, inorganic salt and biomolecules have been developed [3]. Among them, inorganic salt-incorporated hydrogel provide the most simple and straightforward route to fabricate hydrogel-based sensor.

The ions introduced in the hydrogel can not only improve its electrical conductivity but also improve its stretchability because the cations can form coordination bonds with appropriate ligands, and the formed coordination bonds can dissociate and associate reversibly and rapidly [9]. However, the main mechanical properties of the hydrogel depend on its network structure [10]. For a hydrogel with heterogeneous network structure, the stress concentration on the shortest chain would cause the structural damage during stretching. This drawback can be improved by the design of a double network (DN) hydrogel.

Double-network hydrogel (DN-Gel) comprise of a tight rigid network and a loose soft network, which has superior mechanical property because the first brittle network serves as sacrificial bonds to efficiently disperse stress when the hydrogel is stretching [10]. Li, et al. [11] produced a supramolecular polymer DN-Gel with maximum young's modulus of 209 kPa and fracture toughness of 47 kJ/ m^3 for cartilage regeneration, which used methacrylated hyaluronic acid as rigid frame network and self-assembling peptides supramolecules as sacrificial second network.

However, many DN-Gels are usually synthesized by multiple steps, particularly complicated synthesis process and high costs [10, 12]. Moreover, although these DN

hydrogels demonstrate improved properties over their corresponding single-network hydrogels, the mechanical properties do not improve as significantly as expected. In fact, if covalent bonds serve as the unique cross-links of a DN-gel, the covalent bond cannot be recovered once the brittle network is broken, the excellent energy hysteresis cannot be preserved for a long-term and the recovery capability is limited [13]. Therefore, the double cross-linked hydrogel (DC-Gel) [14] with dynamic physical cross-linked (ionic bonding [15] or hydrogen bonding [16]) and chemically cross-linked networks are expected to exhibit excellent stretchability and self-healing ability [17].

Visible light graft polymerization has the characteristics of simple steps, low energy consumption, and easy control of reaction time [18]. Compared with the ultraviolet light initiation system, the visible light reaction conditions are more mild and safe, so it can have a broader application prospect in the field of biology. In this work, we facilely synthesized a DC-Gel with polyvinyl alcohol (PVA) and poly (acrylic acid) (PAA) double-networks via visible-light-trigger polymerization. After immersing in LiCl solution, the PVA-PAA@LiCl hydrogels with dynamic physical ionic bonding exhibit good electrical conductivity, instantaneous recovery, anti-fatigue, and resilience. The distinguished comprehensive mechanical properties of our DC-Gels ensure a stable and sensitive signal transmission when it is served as a capacitance-based sensor.

4.2 Experimental

4.2.1 Materials

Polyvinyl alcohol (PVA, polymerization degree: 2,000), acrylic acid (AA) and lithium chloride (LiCl) were purchased from Nacalai Tesque, Inc., (Japan). Camphorquinone (CQ) was provided by Tokyo Chemical industry Co., Ltd (Japan).

4.2.2 Synthesis of hydrogels

Acrylic acid (AA) and photo-initiator CQ (0.5 wt% based on AA) were sequentially added into a 10 wt% PVA liquid. The mass ratios of PVA: AA were kept at 1: 1, 1: 5

and 1: 9. The solution was stirred 1 h for homogenization and degassed under vacuum for 10 min. The obtained solution was slowly poured into the mold (100 mm × 100 mm × 2 mm or 100 mm × 100 mm × 1 mm), and covered with a transparent plate (5 mm thickness). A visible light source (LS-M210, Sumita) was used to induce the precursor solution polymerization at the luminous emittance of 215 Klux for 30 min. Finally, the polymerized PVA-PAA hydrogel was immersed into a saturated LiCl solution for 8 h to prepare PVA/PAA@LiCl ionic hydrogel. The double crosslinked composite hydrogels were named as DC-X, where X denoted the weight ratio of AA to PVA, i.e., DC-1, DC-5 and DC-9. The synthesis process of the hydrogels was shown in Fig. 4.1.

Fig. 4.1 Appearance of the synthesis process of hydrogels

4.2.3 Characterizations

A Fourier transform infrared spectroscopy (FTIR, Nicolet iN10MX, Thermo Fischer Scientific) was used to investigate the chemical composition of the hydrogels. Thermal stabilities and glass transition temperatures of the freeze dried samples were analyzed by a TG instrument (DTG-60, Shimadzu) at the scan rate of 10 ℃/min from room temperature to 600 ℃ and a differential scanning calorimeter (DSC, SII X-DSC 7000, Hitachi) at the heating rate of 20 ℃/min from -30 ℃ to 120 ℃ in N_2 atmosphere. Mechanical properties were tested by using a universal testing machine (Instron 3385, Instron). More experimental details were described in Supporting Information, respectively.

For the application in capacitance sensors, the ionic hydrogel was cut into the shape with 15 mm in width, 1 mm in thickness, and 45 mm in length. Two layers of the ionic hydrogel sandwiched a VHB tape (4905, 3M) to fabricate a strain sensor. The real-time electrical signals of the strain sensors based on the capacitance variations

were obtained by a capacitance meter (830C, BK Precision).

4.3 Results and discussion

4.3.1 Reaction mechanism

Fig. 4.2 proposed the polymerization mechanism of the PVA-PAA hydrogel triggered by visible light, i.e., free-radical grafting polymerization with CQ initiator. The CQ firstly decomposed to triplet 3CQ* via visible light, which subsequently abstracted hydrogen from -OH groups of PVA backbone to form alkoxy radicals [18-20]. The AA monomer would be polymerized on the PVA backbone under the initiation of the alkoxy radicals, resulting in a polymer network with grafted structure. After the yellow precursor solution was exposed to visible light, a colorless transparent hydrogel was successfully formed (Fig. 4.1).

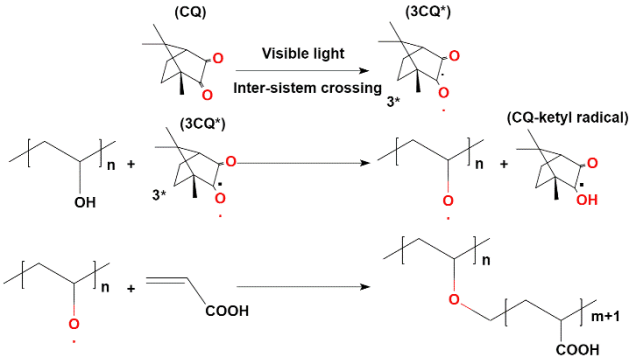

Fig. 4.2 The polymerization mechanism of PVA-PAA triggered by visible light

The schematic illustration of the ionic DC-Gel and its FT-IR results were presented in Fig. 4.3a and b, respectively. For the FTIR spectra, the absorption bands at 3450 cm^{-1} are suggested to the O−H vibration [21]. The two strong peaks of DC-Gels displayed at 1452 cm^{-1} and 1250 cm^{-1} are attributed to the asymmetric and symmetric stretching vibration of the carboxylate (COO^-) and stretching vibration of C−O, respectively [22]. Moreover, with increasing the AA content, the relative intensities and wavenumbers of O−H at around 3450 cm^{-1} and 1650 cm^{-1} are lower than that of PVA, at the same time, the width of O−H stretch vibration increased, indicating the increasing of H-bounds and the reduction of −OH content. In summary, PAA was successfully grafting polymerized onto PVA [23].

Actually, the complexation between carboxyl groups and hydroxyl groups would be promoted by Li^+, and the molecular chains of the hydrogels would shrink when the DC-Gels are exposed to a saturation lithium solution [24]. It is believed that the anion sites in the composites segment increase electrostatic attraction and the degree of ionic crosslinking of the hydrogel, and therefore would increase the toughness of hydrogels [25, 26]. Moreover, the cationic charge shielding effect protects COO^- and effectively prevents the electrostatic repulsion between anions. The protonation of COO^- and hydrogen bonding make the hydrogel volume shrink rapidly in a short time to achieve the enhancement in toughness [27]. It was seen that the volume of the hydrogel was shrunk significantly after the salt impregnation (Fig. 4.1).

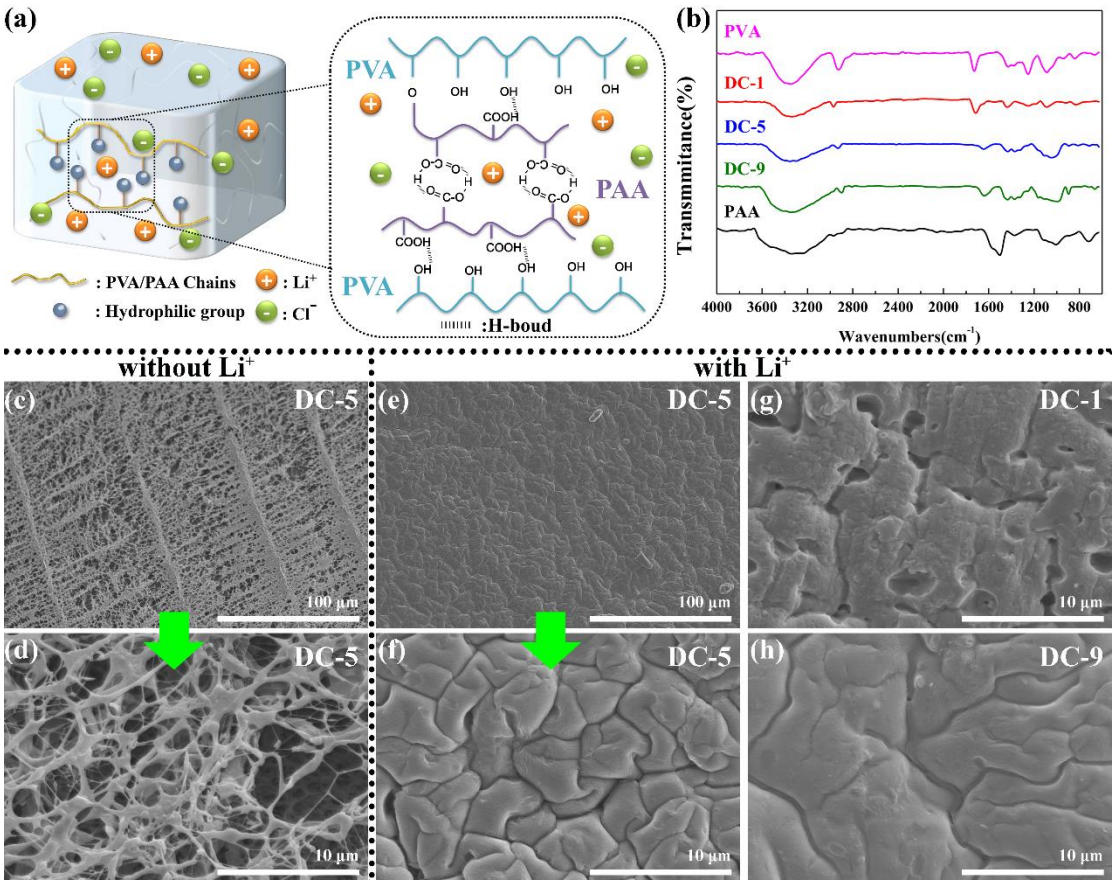

Fig. 4.3 (a) Schematic illustration of the DC-Gel; (b) FTIR spectra of PVA, PAA, DC-1, DC-5 and DC-9; (c and d) SEM images of DC-5; (e and f) SEM images of ionic DC-5; (g) SEM image of ionic DC-1; (h) SEM image of ionic DC-9. The salt impregnation duration was 8 h

The SEM images revealed the cross-sectional morphologies of DC-Gels (Fig. 4.3c-h). It was seen that the internal structures of the DC-Gels changed significantly

as the content of AA and immersing of LiCl solution. The hydrogels without LiCl presented a sponge-like internal morphology (Fig. 4.3cd), which is similar to the reported lyophilized hydrogels [13, 28, 29]. After impregnation in LiCl, the DC-Gels showed a dense, homogeneous and wrinkled microstructure (Fig. 4.3e-h) due to the strong interaction between Li^+ ions and the PVA/PAA chain. As the increase of AA contents, the phase separation between PVA and PAA domains decreased, which reflects a more dense structure and large wrinkled units (DC-9, Fig. 4.3h).

4.3.2 Thermal stabilities of DC-Gels

Fig. 4.4 showed the thermal stability of the DC-Gels. The weight loss of the hydrogels below 100 ℃ (Fig. 4.4a) was observed due to the evaporation of intermolecular H-bonded water. The first stage of degradation occurs between 200 and 340 ℃, which is mainly reflected by the dehydration of polymer chains and accompanied by the formation of polyene structure. In the second decomposition stage, polyene chains are degraded to produce carbon and hydrocarbons to form the acetaldehyde and acetic acid (340 to 500 ℃), where the sharp weight loss is attributed to the thermal decomposition of the carbon skeleton of the PVA and PAA molecules. For the temperature >500 ℃, the weights gradually remained stable. Moreover, it was seen that the first decomposition stages of the DC-Gels were similar to those of PVA, and the decomposition-completion lies of the DC-Gels were similar to those of PAA. For the DTA curves (Fig. 4.4b), it was seen that both the first begining decomposition temperature (T_o) and the maximum decomposition rate temperature (T_m) of DC-Gels were higher those than of PVA. Simultaneously, the weight loss rate of DC-Gels decreased with increasing ratio of AA. This demonstrates that the DC-Gels have good thermal stability.

The chains' thermal motion of the DC-Gels was shown in the DSC curves (Fig. 4.4cd). The crystallization endothermic peaks of the DC-Gels slightly shifted from 49.79 to 56.69 ℃ with increasing AA content (Fig. 4.4c). Moreover, two glass transition temperatures (T_gs) were observed on the DSC curve of PAA at 36.09 and 64.56 ℃, respectively. The first peak should be attributed to the formation of ion aggregation on PAA chains, while the second peak could be explained by the formation of free micelles in the bulk [26]. However, there was only one T_g on the curves of the DC-Gels, which indicates the homogeneous interconnected phase of the

DC-Gels. In addition, it was reported that the chains' thermal motion would be affected by introducing ions into polymer [30]. The entropy of the DC-Gels significantly increased from 12.79 to 23.94 J/g with the AA content. During the impregnation in LiCl solution, a large amount of ions would diffuse into the composite molecular chains, cause a superior interfacial adhesion between PAA and PVA, and decrease the intermolecular repulsive force. Therefore, the mobility of the molecular chains was reduced and the T_gs of the DC-Gels were increased [31, 32].

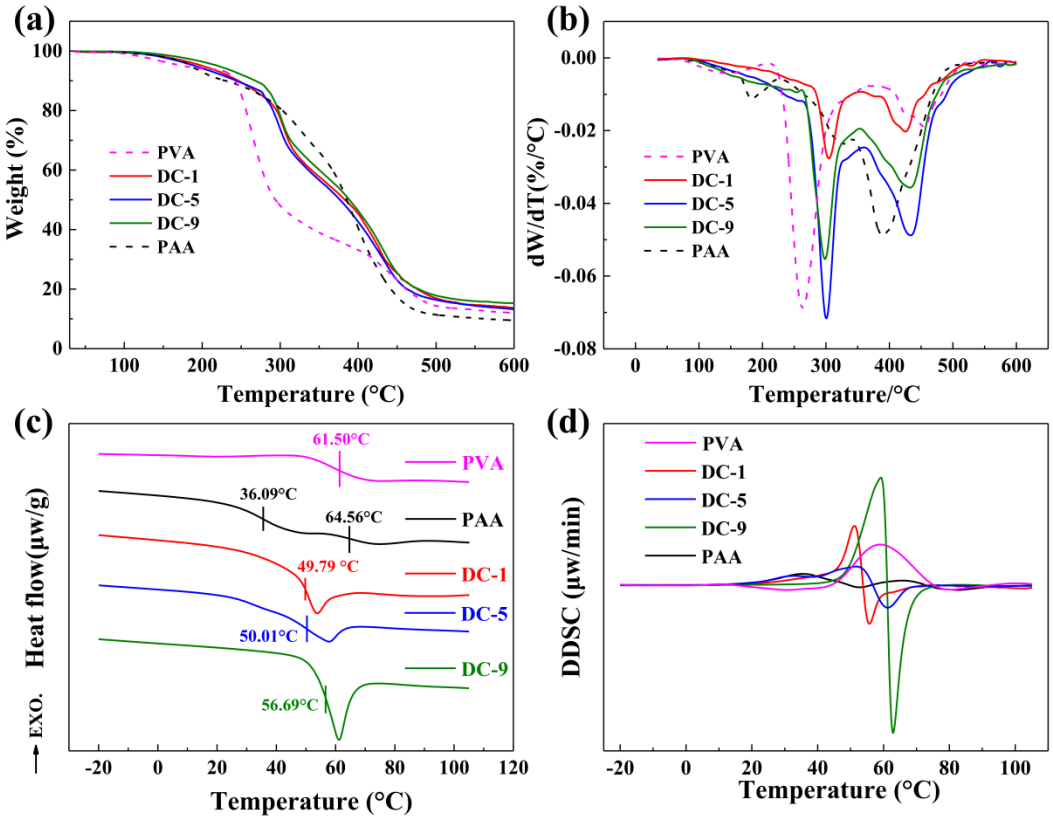

Fig. 4.4 Thermodynamics of the DC-Gels (a) TGA curves; (b) DTG curves; (c) DSC curves; (d) DDSC curves

4.3.3 Mechanical properties of DC-Gels

The ionic DC-Gels became tough and strong with LiCl salt impregnation. To further quantitatively evaluate the change in mechanical properties of the DC-5 with the immersing time, the tensile testing was performed (Fig. 4.5). With the increasing of immersing time, the tensile strength and elongation at break of DC-5 increased and reached the maximum values at the immersing time of 8 h, which reached 4.58 ± 0.67 MPa and 721 ± 23%, respectively. After the immersing duration prolonged from 8 to

12 h, few enhancement in tensile strength but significant decrease in elongation at break of DC-5 were observed.

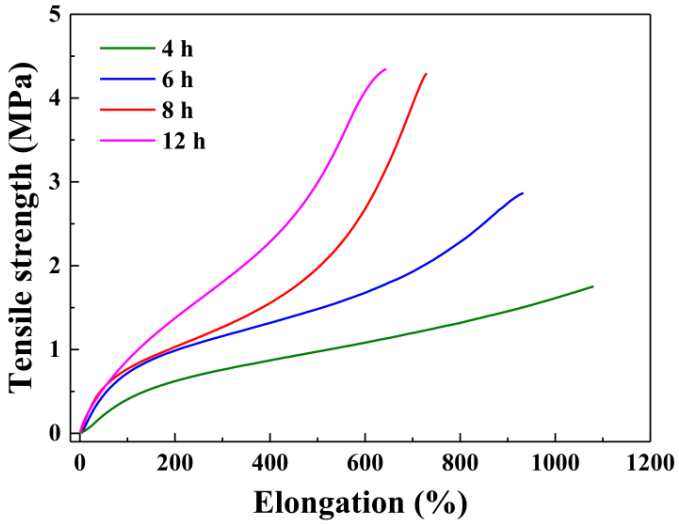

Fig. 4.5 Stress−strain curves of DC-5 with different immersing time

Fig. 4.6 showed that the mechanical strength of the DC-Gels increased with the AA dosage. DC-9 hydrogel achieved the highest tensile strength and toughness of ~7 MPa and ~ 20 MJ/m^3 (Fig. 4.6a). These tough DC-Gels are capable of withstanding large compressive stress. The maximum compressive strength at a 70% strain of DC-Gels reached 90 MPa (DC-9, Fig. 4.6b). The increasing addition of AA improved the strength of hydrogen bonding between the copolymer chains, leading to a denser structure and a smoother appearance of cross-section (Fig. 4.3f-h).

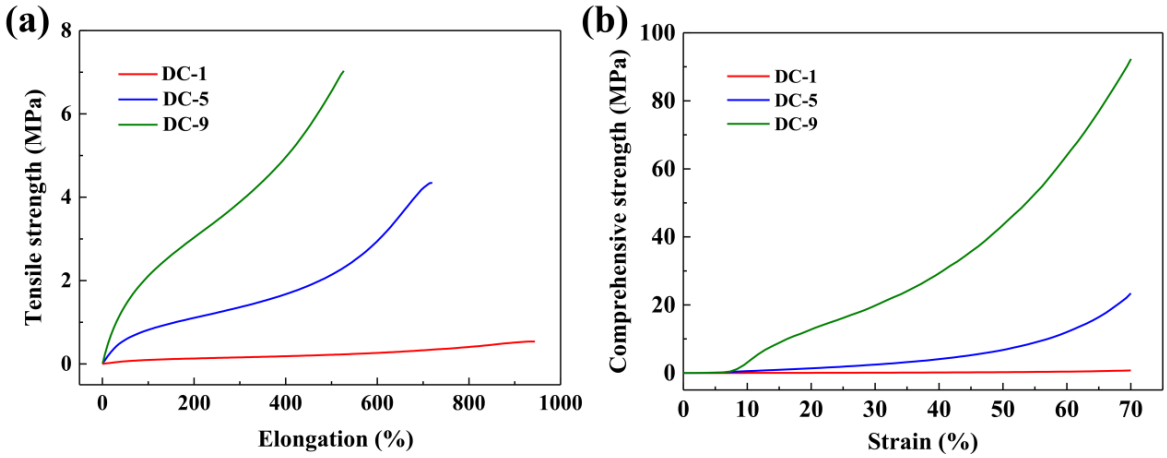

Fig. 4.6 Stress–strain curves of ionic DC-Gels with different AA contents (a) Tensile strength; (b) compressive strength

It was seen that salt solutions with different cations can significantly vary the modulus, fracture stress, and toughness of the DC-Gel; which immersed in LiCl

solution exhibited the best mechanical properties than that in other salt solutions (Fig. 4.7). On the one hand, the different dissolution capabilities of metal ions in solvent (water or water-like environment) [33] can be used to explain it. Overall, the high molarity Li^+ can better dissolve in both water and PAA than other metal ions. As a result, the dissolution of PAA in water would be reduced (salt out effect), leading to a dense and wrinkled structure (Fig. 4.3). On the other hand, it is generally believed that the smaller ion with a monovalent charge (Li^+) would better promote the diffusion of salt in the narrow gaps of polymer due to the less structural and electrostatic hindrances. It was also pointed out that the full potential of the complexation between COO- and OH- might be promoted when the hydrogel precursor was exposed to a concentrated lithium solution [34].

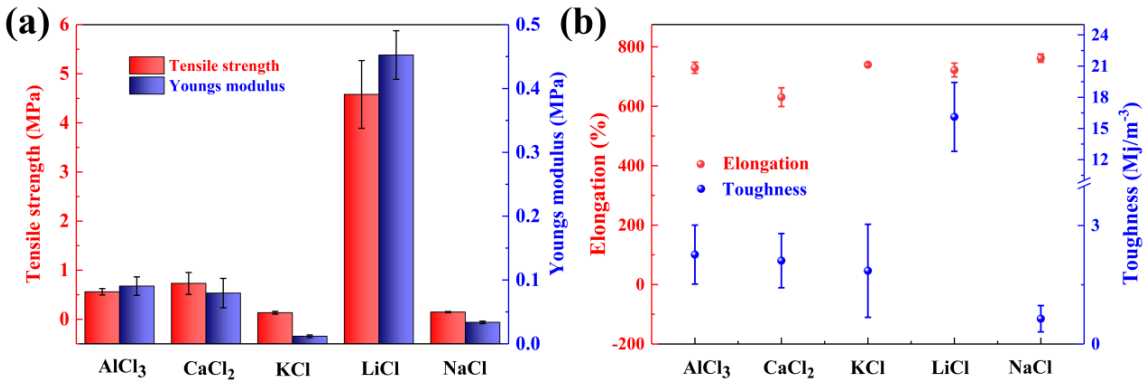

Fig. 4.7 The mechanical properties of DC-5 after immersing in saturated solution with different cations for 8 h. (a) Young's modulus and tensile strength; (b) Toughness and elongation at break

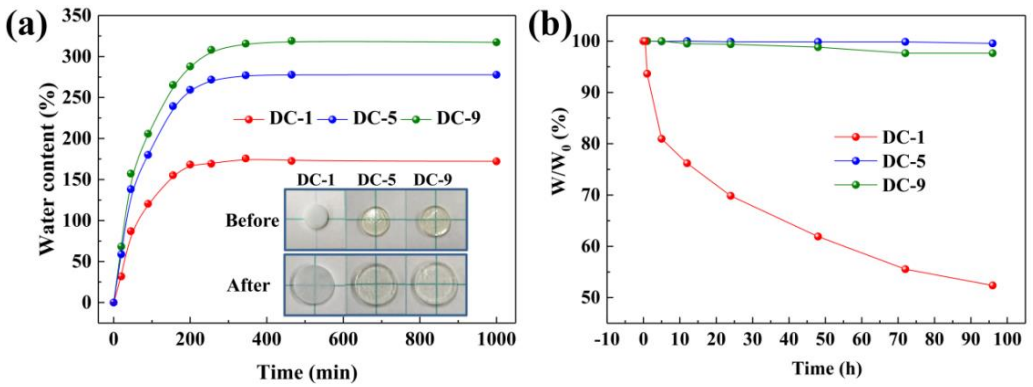

Fig. 4.8 (a) Water absorption ability of ionic DC-Gels and (b) moisture retention ability of ionic DC-Gels

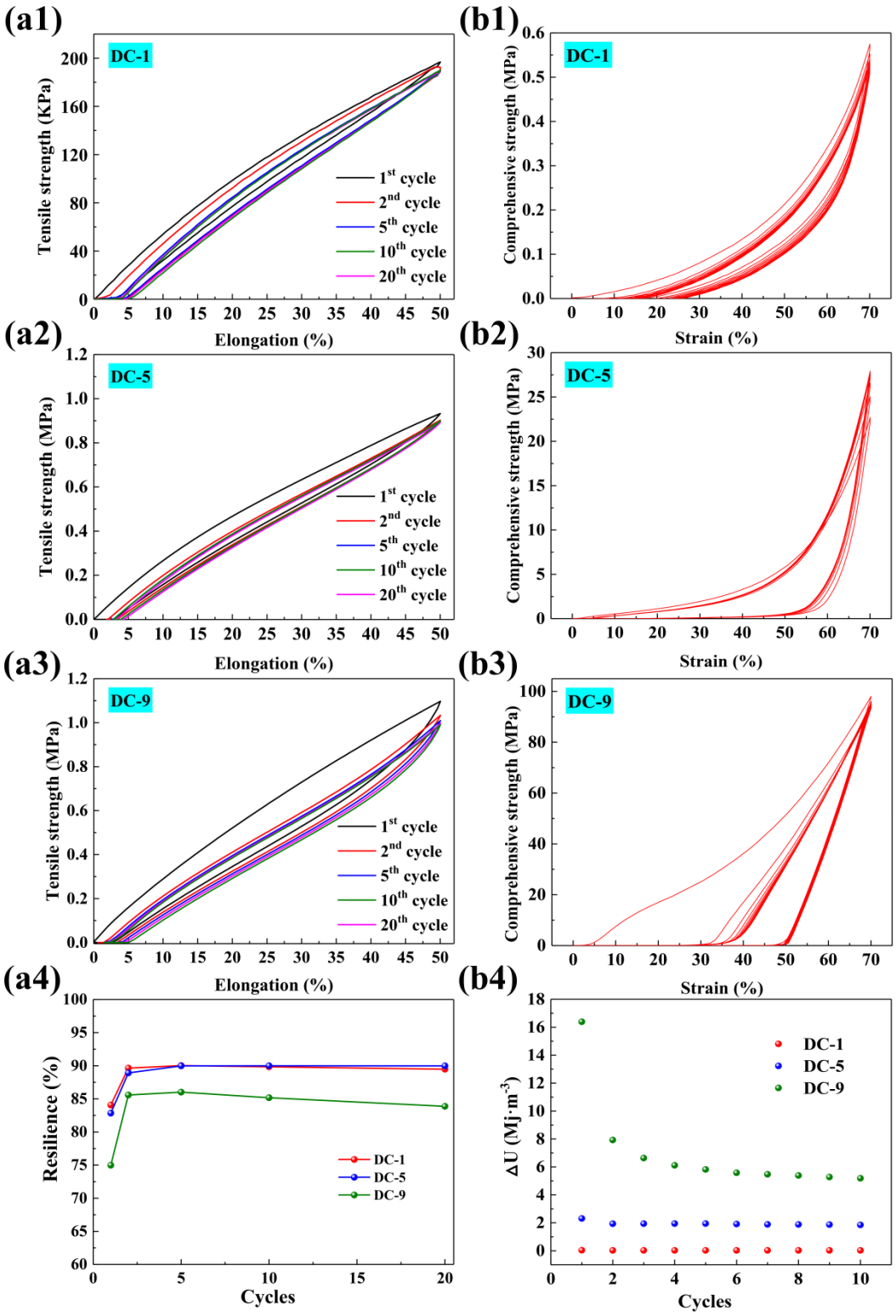

Fig. 4.9 (a1-a3) Cyclic tensile stress-strain curves of the DC-gels; (a4) Resilience of the DC-Gels at a strain of 50 % for 20 cycles; (b1-b3) Successive cyclic compression tests of the DC-gels at a 70 % strain for 10 cycles. (b4) The calculated disperse energy of the DC-Gels

The cyclic tensile stress-strain curves of DC-Gels at 50% strains showed the typically hysteresis loop in the first cyclic test (Fig. 4.9a1-a3). This phenomenon is known as the Mullins effect, which has been reported in the double-network hydrogels [35]. The disentanglement or sliding of polymer chains as well as the rupture of network would appear during the stretching process of the hydrogel, which results in the hysteresis loop [36]. Moreover, once a distinct hysteresis loop is observed in the first cycle, a large drop in stress would generally appear in the second cycle (Fig. 4.9a3). The hysteresis phenomenon becomes much smaller if the next cycle is conducted immediately after the previous cycle. It was seen that the stress-strain curves after the first cycle were almost overlapping (Fig. 4.9a1-a3), which indicates that the DC-Gel reached a stable state.

The high dosage of AA (DC-9) significantly contributed to a high network density, resulting in a high stiffness. The low mechanical cyclic stability of DC-9 (Fig. 4.9a3) is attributed to the drop of effective junction points after the initial cycle [37]. By comparison, DC-5 exhibited the best elastic properties after the initial cycle (Fig. 9a4). It also had good water retention ability (Fig. 4.8). These properties ensure the stable mechanical properties of DC-5 during suffering in the successive cyclic tensile system. It is reported that the combination of high stretchability and low modulus would make hydrogels well adaptable to the epidermis [25]. Fig. 4.7a showed that DC-5 had a similar tensile modulus (450 kPa) to the human skin (140-600 kPa of modulus for the epidermis [38]).

Fig. 4.9b1-b3 showed the compression stress−strain curves of the DC-Gels. No substantial plastic deformation and strength reduction were observed on DC-1 and DC-5 when compared to DC-9. The dissipation energies (ΔU, Eq. 2-2) of DC-1 and DC-5 slightly decreased for the first cycle to the second cycle (Fig. 4.9b4) and then remained unchanged.

However, the ΔU of DC-9 decreased sharply after the first cycle, which is microscopically caused by the accumulation of irreversible damage and fragmentation of the brittle first network. The compressive strength at the strain of 70% drastically increased from 0.58 ± 0.03 to 97.83 ± 2.62 MPa with the increased dosage of AA (Fig. 4.9b1-b3). The maximum stress of DC-5 slightly increased from 22.69 to 27.92 MPa after the 5th cycle, and then remained steady. It can be explained by the self-healing

of the broken ionic cross-links and H-bonds at either the original sites or other accessible sites after the compression in a rather short time [37]. Moreover, after the first four loading–unloading cycles, the rest cycles of the recovered DC-5 started to remain stable and still exhibited a similar loop to the initial one. The compressive strength remained high and almost unchanged. These indicated that the DC-5 had excellent high compression stability. Hydrogels usually failed to recover to the original and have high residual strain after stress-strain cyclic tests [39-41]. By comparison, the DC-5 has an excellent self-recovery capacity and mechanical flexibility.

4.3.4 Rapid recovery ability and tensile cyclic stability of DC-5

Stable mechanical properties such as resilience, tensile strength, and residual strain are crucial for the application of the hydrogel [12, 42, 43]. To examine the recovery ability and tensile cyclic stability of DC-5, the cyclic loading–unloading tests with varying stretching conditions were conducted (Fig. 4.10). The curves of DC-5 almost remained constant even if the number of stretching continues to increase and the rest time had little effect on the curves (Fig. 4.10a), indicating the rapid recovery ability of DC-5.

The resilience, residual strain, and maximum stress of DC-5 after each stretching were still stabilized at 95%, less than 7%, and 1.8 MPa, respectively. The slight strength degradation and plastic deformation of the hydrogels at the high strain of 150% were negligible. The area between the loading–unloading curves represents the dissipated energy caused by the dissociated hydrogen bonding [44, 45]. For the various strains, the energy dissipation gradually increased as the maximum strain increases from 100% to 500% (Fig. 4.10b). The hysteresis loop of DC-5 steadily increased, which indicates the hydrogels with excellent recovery ability and tensile cyclic stability at various strains.

The resilience of the DC-5 was calculated from the loading–unloading curves according to Eq. 2-1 (Fig. 4.10c). The significant softening of DC-5 after the first loading–unloading was attributed to the Mullins effect [36], and the resilience reached a high and stable value after the second loading–unloading. The softening increases progressively with the maximum strain of DC-5 (25 to 500%). The resilience of DC-5

remained over 80% at various strains, indicating the excellent performance in resilience and self-recovery of DC-5. As to the insignificant residual strains of DC-5 under various strains, which were mainly resulted from both the rupture of the hydrogel network, and the slight slip at the fixture and soft hydrogel. Fig. 4.10d proved the excellent mechanical performance of DC-5. A strip of DC-5 with a diameter of 3 mm lifted up and shifted the steel blocks with a weight of 1.5 kg without obvious failure and damage.

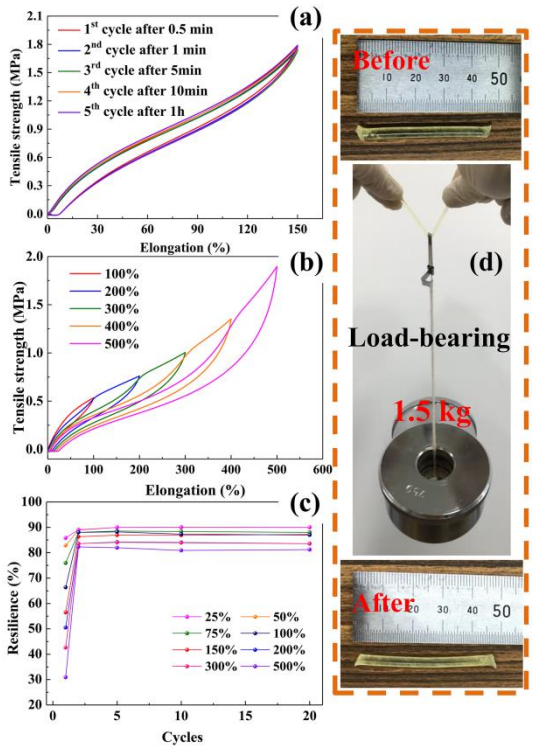

Fig. 4.10 (a) Intermittent cyclic loading–unloading curves of DC-5 with different rest time under a constant strain (150%); (b) Continuously cyclic loading–unloading curve under various strains; (c) Resilience of DC-5 after cyclic loading–unloading with different cycles under different strains; (d) A DC-5 strip with a diameter of 3 mm lifting up two steel blocks (1.5 kg)

4.3.5 Strain sensitivity of DC-Gel as a wearable sensor

Inorganic salt-incorporated hydrogels are widely used to assemble the strain sensor [3]. In general, there are mainly two types of hydrogel-based strain sensors according to the used signals, i.e., resistive [4-6, 46] and capacitive [25, 28, 47] sensors. The resistive sensor has been studied extensively due to its simple structure and sensitivity

to stimulus. However, the Joule heat generated on the resistive sensor during the long work duration might affect its sensing stability. As to the capacitive sensors, it can monitor both stretching and pressing actions. Moreover, it can be used to design some special electronic skins, due to the different working principle of capacitive sensor than that of resistive sensor.

For the stable mechanical properties and excellent recovery ability give the DC-5 potential application hydrogel-based sensors. In this work, the capacitance changes of the strain sensor assembled by DC-5 were tested (Fig. 4.11). The strain sensor was stretched to different deformation with the finger bending to angles of 0 °, 30 °, 60 °, and 90 ° respectively, and the capacitance signal correspondingly and sensitively changed with different amplitudes (Fig. 4.11a). After the finger was straightened again, the capacitance immediately returned back to the original value (C_0).

The $\Delta C/C_0$ of strain sensor assembled by DC-5 showed a good linear correlation to stretch in a range (Fig. 4.11b). When a uniaxial force successively was applied to stretch the sensor reaching a strain of 200% with various speeds (0.5-12 mm/s), the $\Delta C/C_0$ remained at nearly 190% (Fig. 4.11c). This indicates that the capacitance variation of strain sensor dramatically depends on the stretch of sensor [25].

The excellent recovery ability of DC-5 was shown on the strain sensor (Fig. 4.11d). The $\Delta C/C_0$ increased from 50 to 300% when the sensor was continuously cyclic stretched with the strain. It indicates that DC-5 owns a relatively large sensing range and is superior to previously reported hydrogel-based strain sensor before the strain sensor near rupture [48, 49]. Moreover, we stimulated the sensor through two instantaneous stretching movements (strain of ~ 100%) at different speeds (type A and B, Fig. 4.11e), the sensor showed a timely instant response to the stimulus (~ 0.06 and 0.2 s, respectively), and its capacitance quickly returned to the initial state after the stimulus was removed. Notably, it is generally believed that a stable gauge factor is very important to the sensor. For the hydrogel-based resistance sensor, the gauge factor is defined as $(\Delta R/R_0)/\varepsilon$, where $\Delta R/R_0$ is relative resistance change, R_0 is the resistance at 0% strain, and ε is the applied strain [14, 48, 50].

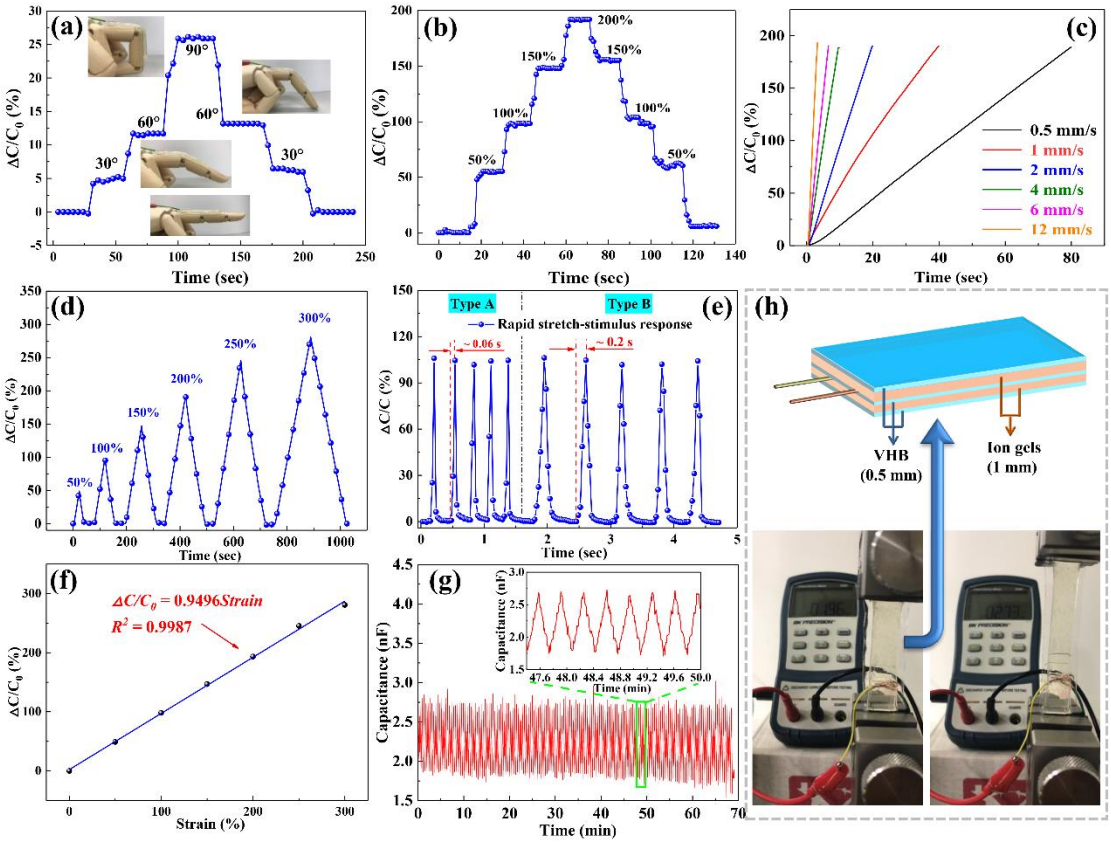

Fig. 4.11 Sensory and electrical performance of DC-5 (a) Capacitance change ratio variations ($\Delta C/C_0$) at different angels; (b) $\Delta C/C_0$ at different tensile strains; (c) $\Delta C/C_0$ at varies tensile strain speeds; (d) $\Delta C/C_0$ of the sensor when a uniaxial force successively loaded–unloaded onto it from strain of 50 to 300% with a fixed speed of 4 mm/s; (e) $\Delta C/C_0$ at instantaneous tensile deformation with 100% strain; (f) Variation of $\Delta C/C_0$ as a function of strain and the linear fitting curves; (g) Capacitance change of sensor when cyclic stretching with 50% strain for 300 cycles at a speed of 4 mm/s; (h) Assembly method of the sensor, and photos of the sensor at the uniaxial force stretched from an undeformed state to a deformed state

Similarly, we can also define the gauge factor of hydrogel-based capacitance sensor as $(\Delta C/C_0)/\varepsilon$. Sun, et al. [25] have investigated the capacitance change of hydrogel-based sensor after considering the deformations of length, width and thickness of the sensor, which was scaled as $C = C_0\lambda$, where λ is the stretched factor. This formula can be transformed into $\Delta C/C_0 = \varepsilon$. As shown in Fig. 4.11f, the experimentally measured capacitance increased linearly with the stretch, and matched well with the theoretical prediction, the gauge factor was calculated as ~ 0.95 in a

range of 0 to 300%. In addition, electrical stability is another vital property of strain sensor for long-time service. Therefore, we pulled the strain sensor at stain of 50% for 300 cycles and recorded its capacitance (Fig. 4.11g). In general, the sensor exhibited a favorable reproducibility in capacitance, which was attributed to the lower residual deformation (less than 5%) and excellent self-recovery ability of strain sensor during tests.

4.3.6 Self-healing property of DC-5

The self-healing property of the DC-5 was further evaluated (Fig. 4.12). Firstly, one piece cylindrical DC-5 was cut into two parts (Fig. 4.12b). Then, keep the fresh surfaces of the two parts in contact at room temperature for 24 h and the healed DC-5 was obtained. The healed DC-5 can be horizontally sustained with a hanging load of 100 g on the joint without any damage (Fig. 4.12d and e).

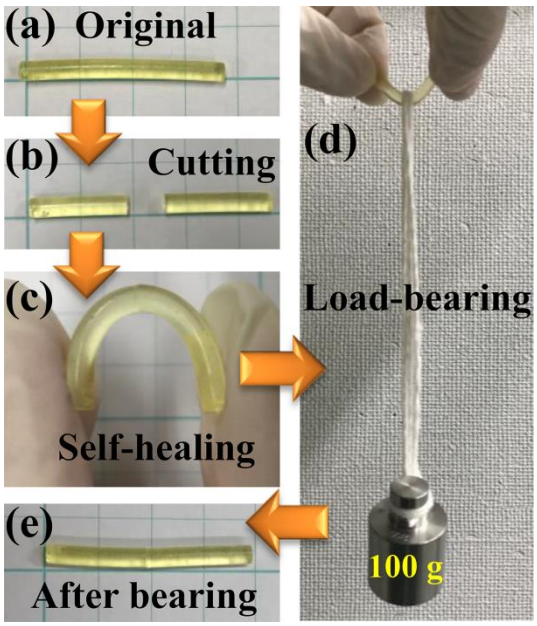

Fig. 4.12 Self-healing property of DC-5 (a) Original DC-5; (b) Cutting DC-5; (c) Self-healed DC-5 after 24 h; (d) Self-healed DC-5 with a diameter of 3 mm lifting up a mass of 100 g; (e) Self-healed DC-5 after bearing the mass of 100 g

Moreover, the self-healing property of the healed DC-5 was further evaluated by using the tensile test and the comparison of tensile stress at break between the DC-5 and healed DC-5 was made (Fig. 4.13). The healed DC-5 possessed extensibility and can be stretched to a strain of 200% (~ 1 MPa) without breaking, indicating the good

self-healing effect of the DC-5.The healing efficiency of the DC-5 reached ~ 30% after self-healed for 24 h. It indicates that the polymer chains of DC-5 had a low mobility [51] and the self-healing property of DC-5 mainly depends on the new reconstruction of H-bounds and the new reconstruction of the metal ionic coordination bonds in the whole hydrogel networks [24, 46].

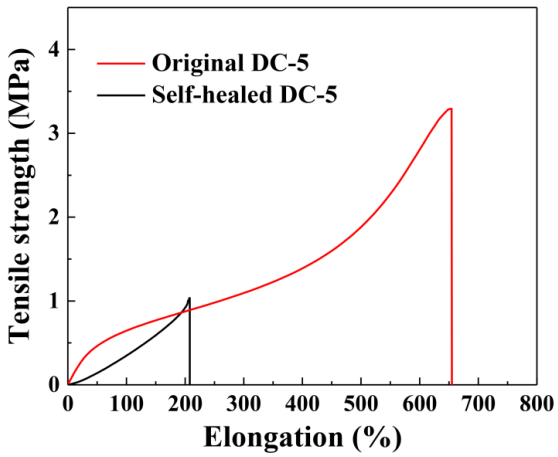

Fig. 4.13 Stress−strain curves of the original DC-5 and the healed DC-5 after self-healed for 24h

4.4 Conclusions

A tough, conductive and self-healable DC-Gel was developed by a facile polymerization triggered by visible light and salt impregnation. The DC-Gel exhibits a rubber-like flexible hydrogel network and a homogeneous interconnected phase. The superior interfacial adhesion and low intermolecular repulsive force of the DC-Gel caused by the ionic diffusion of LiCl into PVA/PAA molecular chains can ensure a smooth stress-transfer and recoverable energy dissipation to give the hydrogels with excellent mechanical strength (6.59 ± 1.21 MPa) and toughness (19.27 ± 3.3 MJ/m^3). Moreover, the DC-5 exhibited remarkable recovery properties (resilience > 80% and 95% for successively and intermittently cyclic tensile tests, respectively, and residual strain < 3%). The high strain sensitivity of DC-5 was proved by assembling a capacitance-based strain sensor, and the sensor could precisely, quickly and continuously distinguish the deformation (0-300%). In general, this work provides a positive exploration in the fabrication of conductive hydrogels and application in

wearable electronic sensors.

References

[1] Xia S, Zhang Q, Song S, et al. Bioinspired Dynamic Cross-Linking Hydrogel Sensors with Skin-like Strain and Pressure Sensing Behaviors. Chemistry of Materials. 2019;31(22):9522-31.

[2] Yang JC, Mun J, Kwon SY, et al. Electronic Skin: Recent Progress and Future Prospects for Skin-Attachable Devices for Health Monitoring, Robotics, and Prosthetics. Advanced materials. 2019;31(48):1904765.

[3] Zhang D, Ren B, Zhang Y, et al. From design to applications of stimuli-responsive hydrogel strain sensors. Journal of Materials Chemistry B. 2020;8(16):3171-91.

[4] Wang Z, Zhou H, Chen W, et al. Dually Synergetic Network Hydrogels with Integrated Mechanical Stretchability, Thermal Responsiveness, and Electrical Conductivity for Strain Sensors and Temperature Alertors. ACS Applied Materials & Interfaces. 2018;10(16):14045-14054.

[5] Wang Z, Zhou H, Lai J, et al. Extremely stretchable and electrically conductive hydrogels with dually synergistic networks for wearable strain sensors. Journal of Materials Chemistry C. 2018;6(34):9200-7.

[6] Zhou H, Jin Z, Yuan Y, et al. Self-repairing flexible strain sensors based on nanocomposite hydrogels for whole-body monitoring. Colloids and Surfaces A: Physicochemical and Engineering Aspects. 2020;592:124587.

[7] Zhou Y, Wan C, Yang Y, et al. Highly stretchable, elastic, and ionic conductive hydrogel for artificial soft electronics. Advanced Functional Materials. 2019;29(1):1806220.

[8] Feig VR, Tran H, Lee M, et al. Mechanically tunable conductive interpenetrating network hydrogels that mimic the elastic moduli of biological tissue. Nature communications. 2018;9(1):1-9.

[9] Lin P, Ma S, Wang X, et al. Molecularly Engineered Dual-Crosslinked Hydrogel with Ultrahigh Mechanical Strength, Toughness, and Good Self-Recovery. Advanced materials. 2015;27(12):2054-59.

[10] Chen Q, Chen H, Zhu L, et al. Fundamentals of double network hydrogels. Journal of Materials Chemistry B. 2015;3(18):3654-76.

[11] Li L, Zhang K, Wang T, et al. Biofabrication of a biomimetic supramolecular-polymer double network hydrogel for cartilage regeneration. Materials & Design. 2020;189:108492.

[12] Wang Y, Xue Y, Wang J, et al. A composite hydrogel with high mechanical strength, fluorescence, and degradable behavior for bone tissue engineering. Polymers. 2019;11(7):1112.

[13] Xing L, Hu C, Zhang Y, et al. A mechanically robust double-network hydrogel with high thermal responses via doping hydroxylated boron nitride nanosheets. Journal of Materials Science. 2019;54(4):3368-82.

[14] Xia S, Song S, Gao G. Robust and flexible strain sensors based on dual physically cross-linked double network hydrogels for monitoring human-motion. Chemical Engineering Journal. 2018;354:817-24.

[15] Liang Y, Ye L, Sun X, et al. Tough and Stretchable Dual Ionically Cross-linked Hydrogel with High Conductivity and Fast-Recovery Property for High-Performance Flexible Sensors. ACS Applied Materials & Interfaces. 2020;12(1):1577-87.

[16] Liu T, Jiao C, Peng X, et al. Super-strong and tough poly (vinyl alcohol)/poly (acrylic acid) hydrogels reinforced by hydrogen bonding. Journal of Materials Chemistry B. 2018;6(48):8105-14.

[17] Dai X, Zhang Y, Gao L, et al. A mechanically strong, highly stable, thermoplastic, and self‐healable supramolecular polymer hydrogel. Advanced materials, 2015;27(23): 3566-71.

[18] Kamoun EA, Winkel A, Eisenburger M, et al. Carboxylated camphorquinone as visible-light photoinitiator for biomedical application: Synthesis, characterization, and application. Arabian Journal of Chemistry. 2016;9(5):745-54.

[19] Brandt W, Schneider LF, Frollini E, et al. Effect of different photo-initiators and light curing units on degree of conversion of composites. Brazilian oral research. 2010;24:263-70.

[20] Tsai L, Charney E. Triplet states of. alpha.-dicarbonyls. Camphorquinone. The Journal of physical chemistry. 1969,73(7):2462-3.

[21] Mansur HS, Sadahira CM, Souza AN, et al. FTIR spectroscopy characterization of poly (vinyl alcohol) hydrogel with different hydrolysis degree and chemically crosslinked with glutaraldehyde. Materials Science and Engineering: C, 2008;28(4):539-48.

[22] Max J-J, Chapados C. Infrared Spectroscopy of Aqueous Carboxylic Acids: Comparison between Different Acids and Their Salts. The Journal of Physical Chemistry A. 2004;108(16):3324-37.

[23] Kurkuri MD, Lee J-R, Han JH, et al. Electroactive behavior of poly(acrylic acid) grafted poly(vinyl alcohol) samples, their synthesis using a Ce(IV)glucose redox system and their characterization. Smart Materials and Structures. 2006;15(2):417-423.

[24] Zhang Y, Hu C, Xiang X, et al. Self-healable, tough and highly stretchable hydrophobic association/ionic dual physically cross-linked hydrogels. RSC Advances. 2017;7(20):12063-73.

[25] Sun JY, Keplinger C, Whitesides GM, et al. Ionic skin. Advanced materials. 2014;26(45):7608-14.

[26] Pragatheeswaran AM, Chen SB. The influence of poly (acrylic acid) on micellization and gelation characteristics of aqueous Pluronic F127 copolymer system. Colloid and Polymer Science. 2016;294(1):107-17.

[27] He J, Zhang L. Polyvinyl alcohol grafted poly (acrylic acid) as water-soluble binder with enhanced adhesion capability and electrochemical performances for Si anode. Journal of Alloys and Compounds. 2018;763:228-40.

[28] Lin F, Wang Z, Shen Y, et al. Natural skin-inspired versatile cellulose biomimetic hydrogels. Journal of Materials Chemistry A. 2019;7(46):26442-55.

[29]Jin S, Qiu J, Sun M, et al. Strain-Sensitive Performance of a Tough and Ink-Writable Polyacrylic Acid Ionic Gel Crosslinked by Carboxymethyl Cellulose. Macromolecular Rapid Communications. 2019;40(20):1900329.

[30]Gao Y, Choudhury NR, Dutta N, et al. Effect of the ionic aggregation on the crystallization behavior of polyethylene part of ionomer. Journal of Thermal Analysis and Calorimetry. 2003;73:361-380.

[31]Seida Y, Nakano Y. Effect of salt on the property of adsorption in thermosensitive polymer hydrogel. JOURNAL OF CHEMICAL ENGINEERING OF JAPAN. 1996;29(5):767-72.

[32]Kundu SK, Yoshida M, Shibayama M. Effect of Salt Content on the Rheological Properties of Hydrogel Based on Oligomeric Electrolyte. The Journal of Physical Chemistry B. 2010;114(4):1541-7.

[33]Zhang Z, Yang Y, Tang X, et al. Effects of Ionic Strength on Chemical Forces and Functional Properties of Heat-induced Myofibrillar Protein Gel. Food Science and Technology Research, 2015;21(4):597-605.

[34]Zhao X, Wang M, Chen Y, et al. Puncture-Resistant Hydrogel: Placing Molecular Complexes Along Phase Boundaries. ACS Applied Materials & Interfaces. 2019;11(21):19421-8.

[35]Guo H, Hong W, Kurokawa T, et al. Internal Damage Evolution in Double-Network Hydrogels Studied by Microelectrode Technique. Macromolecules. 2019;52(18):7114-22.

[36]Merckel Y, Brieu M, Diani J, et al. A Mullins softening criterion for general loading conditions. Journal of the Mechanics and Physics of Solids. 2012;60(7):1257-64.

[37]Xu L, Wang C, Cui Y, et al. Conjoined-network rendered stiff and tough hydrogels from biogenic molecules. Science advances. 2019;5(2):eaau3442.

[38]Liu S, Zheng R, Chen S, et al. A compliant, self-adhesive and self-healing wearable hydrogel as epidermal strain sensor. Journal of Materials Chemistry C. 2018;6(15):4183-90.

[39]Qin Z, Sun X, Yu Q, et al. Carbon Nanotubes/Hydrophobically Associated Hydrogels as ultrastretchable, highly sensitive, stable strain, and pressure sensors. ACS Applied Materials & Interfaces. 2020;12(4):4944-53.

[40]Tong R, Chen G, Tian J, et al. Highly Stretchable, Strain-Sensitive, and Ionic-Conductive Cellulose-Based Hydrogels for Wearable Sensors. Polymers. 2019;11(12):2067.

[41]You J, Xie S, Cao J, et al. Quaternized Chitosan/Poly(acrylic acid) Polyelectrolyte Complex Hydrogels with Tough, Self-Recovery, and Tunable Mechanical Properties. Macromolecules. 2016;49(3):1049-59.

[42]Lei Z, Wang Q, Sun S, et al. A bioinspired mineral hydrogel as a self‐healable, mechanically adaptable ionic skin for highly sensitive pressure sensing. Advanced materials. 2017;29(22):1700321.

[43]Wang D, Zhu L, Qiu J, et al. Poly(acrylic acid)/palygorskite microgel via radical polymerization in aqueous phase for reinforcing poly(vinyl alcohol) hydrogel. Applied Clay Science. 2020;185:105421.

[44]Zhao D, Huang J, Zhong Y, et al. High‐strength and high‐toughness double‐cross‐linked cellulose hydrogels: a new strategy using sequential chemical and physical cross‐linking. Advanced Functional Materials. 2016;26(34):6279-87.

[45]Gong JP, Katsuyama Y, Kurokawa T, et al. Double‐network hydrogels with extremely high mechanical strength. Advanced materials. 2003;15(14):1155-8.

[46]Deng Z, Guo Y, Zhao X, et al. Multifunctional stimuli-responsive hydrogels with self-healing, high conductivity, and rapid recovery through host–guest interactions. Chemistry of Materials. 2018;30(5):1729-42.

[47]Lei Z, Wang Q, Sun S, et al. A Bioinspired Mineral Hydrogel as a Self-Healable, Mechanically Adaptable Ionic Skin for Highly Sensitive Pressure Sensing. Advanced materials. 2017;29(22):1700321.

[48]Wang Z, Chen J, Cong Y, et al. Ultrastretchable strain sensors and arrays with high sensitivity and linearity based on super tough conductive hydrogels. Chemistry of Materials. 2018;30(21):8062-9.

[49] Guo R, Jiao T, Xing R, et al. Hierarchical AuNPs-loaded Fe3O4/polymers nanocomposites constructed by electrospinning with enhanced and magnetically recyclable catalytic capacities. Nanomaterials. 2017;7(10):317.
[50] Cai G, Wang J, Qian K, et al. Extremely Stretchable Strain Sensors Based on Conductive Self-Healing Dynamic Cross-Links Hydrogels for Human-Motion Detection. Advanced Science. 2017;4(2):1600190.
[51] Wu J, Li P, Dong C, et al. Rationally designed synthetic protein hydrogels with predictable mechanical properties. Nature communications. 2018;9(1):620.

Chapter 5 Multi-sacrificial bonds enhanced double network hydrogel with high toughness, resilience, damping and notch-insensitivity

5.1 Introduction

Hydrogels are wet and soft materials that have drawn great attention in recent years due to their promising applications, and have been widely used as scaffolds for tissue engineering [1], vehicles for drug delivery [2], wearable electronics, and in hydrogel-based soft machines [3]. Mechanically strong and tough hydrogels are the first choice for artificial tissues, but most hydrogels are not adequate due to the demanding requirements of such applications [4]. For example, hydrogel-made knee cartilage is expected to sustain peak stresses of 4 to 9 MPa for 1 million cycles per year [5]. Moreover, the hydrogel-made skin needs to meet the a high stiffness level of ~100 MPa, a high fracture energy of ~3,600 J/m^2, and high water content of 40~70 wt% [6,7]. When hydrogels are used in robotic arms, repeated stretching and immediate restoration must be possible [8]. Moreover, engineering hydrogels rarely possess both high stiffness and toughness because hydrogels usually become brittle when excess crosslinkers are added to make them stiff [9]. These brittle hydrogels are notch-sensitive, i.e., their high stretch ability and strength decrease markedly when the samples contain notches or any other features that cause inhomogeneous deformation [10]. This factor greatly limits their applications. Specifically, general hydrogel performs poorly under prolonged static and cyclic loads. Overall, the existing hydrogels tested so far have difficultly providing these comprehensive mechanical properties at the same time.

Several strategies with different mechanisms of energy dissipation have been developed to synthesize tough hydrogels, including double network (DN) hydrogels, nano- and micro-composite hydrogels, and tri-block copolymers and hydrophobic associated hydrogels [11-15]. The fracture energy of hydrogels has been enhanced by

orders of magnitude from 10 to 10,000 J/m^2 [10]. Among them, the high toughness of DN hydrogel attributes the interpenetration between the first brittle and second soft networks. When a DN hydrogel is stretched, the sacrificed the first brittle network ruptures and dissipates energy, while the second soft network retains elasticity. However, when the sample is subjected to excessive forces, conventional DN hydrogel suffers from internal network fractures and irreversible deformation due to the fracture of chemical sacrificial bonds, which leads to poor recovery and anti-fatigue properties [16, 17]. Therefore, sacrificing reversible noncovalent bonds instead of covalent bonds has been advocated. Zheng et al. [18] reported a novel tetra-PEG/reduced graphene oxide nanocomposite hydrogel with a fracture energy of ~200 J/m^2, tensile strength of ~700 kPa, and Young's modulus of ~120 kPa. Gao et al. [19] prepared a high strength hydrogel with core-shell hybrid nanoparticles made of cross-linked polyacrylamide as the first network and Ca^{2+} cross-linked alginate as the second network, featuring a fracture stress of ~1 MPa, a Young's modulus of 54 kPa, and a toughness of ~10 MJ/m^3. However, these improvements are still limited.

In this work, we synthesized a composite polyvinyl alcohol (PVA)/poly (acrylic acid) (PAA)/silicone hydrogel (tensile strength of ~21 MPa, fracture elongation of ~700%, Young's modulus of ~3.5 MPa, and toughness of ~49 MJ/m^3) via visible-light-trigger polymerization and the introduction of dynamic physical ionic bonds. Moreover, this hydrogel exhibited high resilience, damping and notch-insensitivity. In this study, hydrolyzed silane (silanol) was grafted onto PAA/PVA chains to create a dynamic chemical crosslinking network. In this way, numerous hydrogen bonds were formed among the hydrophilic groups, and the hydrogen bonds enhanced by ions formed reversible physical crosslinking. In this way, a tough hydrogel was obtained. When the hydrogel was stretched, the reversible fracture-reorganization of the hydrogen bonds dissipated the energy, which significantly improved the resilience of the hydrogel. This work provides new clues for designing hydrogels with excellent comprehensive mechanical properties.

5.2 Experimental

5.2.1 Sample preparation

10 wt.% of triethoxyvinylsilane (TEVS, Sigma-Aldrich, Japan) was added to deionized water at room temperature and vigorously stirred for 12 h until a transparent dispersion solution of vinyl silanetriol (VSTO) solution was obtained.

Acrylic acid (AA, Nacalai Tesque, Japan), 0.5 wt.% photo-initiator camphorquinone (CQ, Tokyo Chemical Industry, Japan) based on AA, and VSTO (0, 0.1, 0.5, 1, 5 wt% based on AA) were sequentially added into a 10 wt.% polyviny alcohol (PVA, degree of polymerization of 2000, Nacalai Tesque, Japan) solution. The mass ratio of PVA: AA was kept at 1: 9. The mixture solution was stirred for 1 h to achieve homogenization and then degassed under a vacuum for 10 min. Afterward, the obtained precursor solution was slowly poured into a transparent mold (100 mm × 100 mm × 2 mm). Then the precursor solution was visible-light-trigger polymerized for 30 min using a visible light source (LS-M210, Sumita, Japan). Finally, the polymerized double network hydrogels were immersed in a saturated LiCl (Nacalai Tesque, Japan) solution for 8 h to prepare the composite double network ion hydrogel (CDN-gel). The CDN-gels were named GEL-X, where X denotes the weight ratio of the TEVS to AA, e.g., GEL-0, GEL-0.1, GEL-0.5, GEL-1, and GEL-5.

5.2.2 Characterization

The morphologies of the CDN-gels were characterized by a scanning electron microscope (SEM, S-4300, Hitachi, Japan). Before characterization, the hydrogel samples were prepared via the freeze-drying method, and then all samples were sputter-coated with platinum to provide enhanced conductivity.

The mechanical properties of the CDN-gels were tested using a universal testing machine (Instron 3385, Instron, USA). For the tensile mode, the CDN-gel was cut into a size according to the standard of JIS K6251, and the CDN-gel with a diameter of 8 mm and a height of 2 mm was used in compression mode. A dynamic mechanical analysis (DMA, RSA-G2, TA Instrument, USA) was used to measure the storage modulus and loss modulus of the CDN-gels at a frequency from 1 to 100 Hz under constant strain amplitude (1%). Before measurement, the CDN-gels (8 mm in diameter

and 2 mm in thickness) were subjected to an axial force (0.981 N). All of the mechanical characterizations of hydrogels were conducted at an indoor environment (25 ℃, RH=55%).

The damping ability of the CDN-gel was evaluated by a homemade evaluation device, whose details have been described in our previous work [20]. The CDN-gel was placed under a vibration source (Present mixer 2013, Taitec, Japan) as a shock-absorbing material, and the signal change caused by the shock of the vibration source was recorded by a force sensor placed under the hydrogel to evaluate the damping ability of the CDN-gel.

The notch-sensitivity of the CDN-gels was analyzed by calculating the change in the fracture energy using a method introduced by Rivlin and Thomas [5,21]. The CDN-gels (width a_0 = 50 mm and thickness b_0 = 2 mm) with 4-mm-long notches (processed by a razor blade) were used to evaluate the notch-sensitivity when the gels were stretched, and the non-notched sample was pulled to measure the force–length curve. During stretching, the distance between the two clamps was L_0 = 10 mm, and the cross-head speed was 30 mm/min. When the two clamps were pulled to distance L, the area beneath the force–length curve revealed the results of the applied force $W(L)$. The notched sample was then pulled, and the critical distance (L_c) was recorded when the notch turned into a running crack (Fig. 2.3). The fracture energy was calculated using Eq. 5-1:

$$\Gamma = W(L_C)/(a_0\, b_0), \qquad 5\text{-}1$$

5.3 Results and discussions

5.3.1 Synthesis of the CDN-gel

Visible light is a safe, low cost, and easily acquired trigger that has attracted attention in synthesis of polymers via radical-initiated polymerization in recent years [22, 23]. Fig 4.1 presents the preparation process and interactions of the CDN-gel. The alkoxy groups are first hydrolyzed into silanol groups in the presence of water, and the silanol groups then condensate to form a siloxane bond [24, 25]. The free-radical grafting polymerization mechanism of the PVA/PAA hydrogel triggered by visible light with a CQ initiator was proposed in our previous work [20]. Specifically, CQ uses light to dissociate the initiator molecules into free radicals, which react with double bonds in

the monomers or pre-polymers, thus allowing crosslinking to occur. In this work, monomer AA not only grafted with VSTO, leading to the formation of nanobrush gelators, but was also polymerized on the PVA backbone, resulting in a polymer network with a grafted structure. Simultaneously, the silanol can be adsorbed to the PVA on its OH-rich chains through hydrogen bonding, further leading to siloxane bridges [25]. Finally, the visible light-induced hydrogels were exposed to a saturation lithium solution to increase the crosslinking sites between the polymer chains by metal doping. The CDN-gels created by this method were expected to have a network structure constructed through a combination of ion-mediated reversible physical cross-linking, intra- and inter-polymer chain hydrogen bonding, physical entanglement of the polymer chains, and covalent cross-linking.

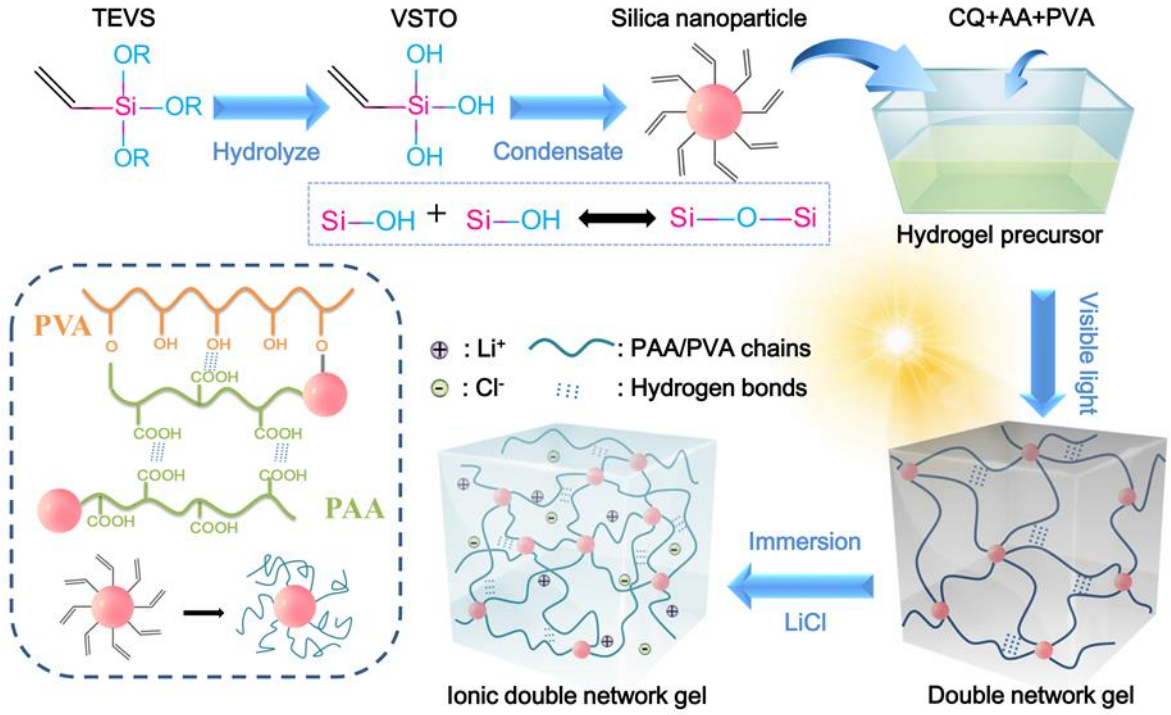

Fig. 5.1 Schematic diagram of the preparation process and network structure of the composite double network ionic hydrogel (CDN-gel)

5.3.2 Morphology of the CDN-Gel

Fig. 5.2 shows SEM images of the inner structure of the freeze-dried CDN-gels with different VSTO ratios. The inner structures of the CDN-gels presented a sponge-like morphology, similar to most lyophilized gels [26, 27]. As with the introduction of VSTO, the structures of the CDN-gels changed significantly as a result of strong

interactions. For GEL-0 (Fig. 5.2a), a porous main network structure and a relatively finer mesh structure were observed. When the VSTO was introduced into the CDN-gel, the finer mesh structure disappeared and an interconnected, uniform, and complete network structure was formed (GEL-0.5, Fig. 5.2b). However, an increased pore size difference was clearly observed on GEL-5 (Fig. 5.2c).

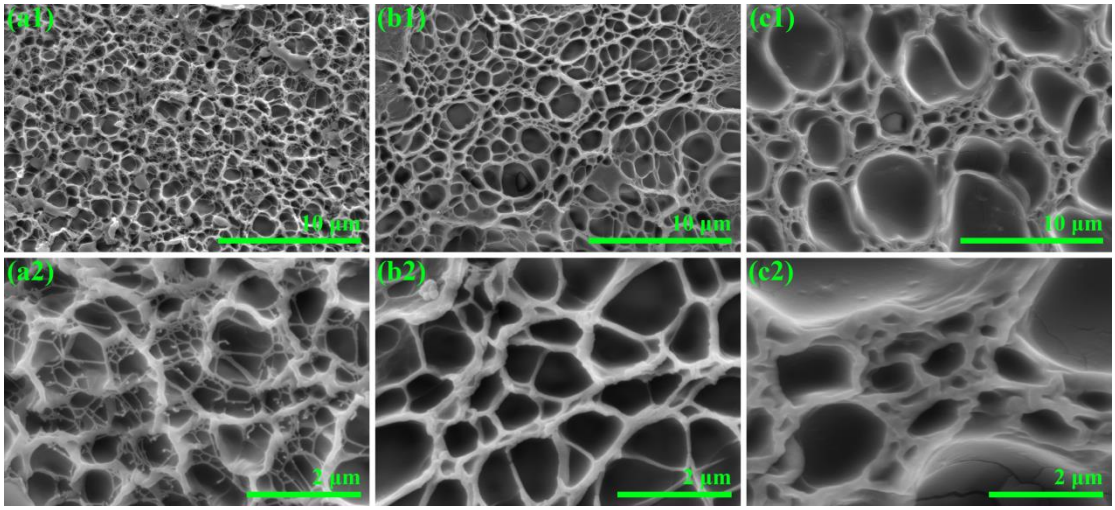

Fig. 5.2 Broken sections of CDN-gels (a1 and a2) GEL-0; (b1 and b2) GEL-0.5; (c1 and c2) GEL-5

The introduction of VSTO can have two effects on the crosslinking network of the CDN-gels. On the one hand, VSTO as a multifunction cross-linking agent can increase the crosslinking density of the CDN-gels and contribute to the formation of a uniform porous network structure [28]. On the other hand, excessive VSTO is distributed in a disordered manner throughout the whole network and causes the chain links to become different in length. Moreover, the regularity of molecular chains is also destroyed by an increase in cross-linking points [29].

It is believed that the swelling capacity of hydrogel reflects the homogeneity of its network [30]. The water contents of all CDN-gels showed a tendency to increase first and then stabilize over time (Fig. 5.3). Notably, the equilibrium of the moisture content of the CDN-gels showed a trend of increasing first and then decreasing with an increase of VSTO. Indeed, an appropriate amount of VSTO can facilitate the formation of a more complete and uniform network structure and increase the flexibility of the molecular chains [31,32]. A large amount of VSTO would lead to more new polymerization chains, making the length of the segment between the cross-linking

points shorter and more dense. The elastic contraction force that hinders the swelling of the CDN-gel thus increases sharply, the network space of the CDN-gel becomes smaller (Fig. 5.2c), and the free water decreases (Fig. 5.3). In general, the elastic interconnected network structure being enhanced by the correct amount of VSTO indicates that more effective energy dissipation could be achieved, resulting in an improvement of the mechanical properties and elasticity of the hydrogels.

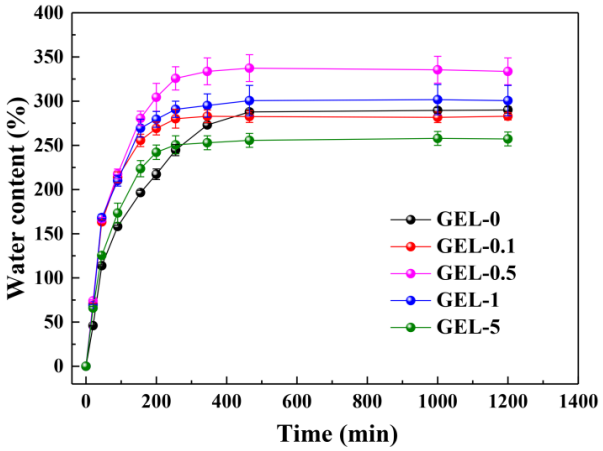

Fig. 5.3 Water absorption ability of CDN-gels

5.3.3 High Strength and Toughness of CDN-Gels

The mechanical properties of CDN-gels were investigated using tensile tests (Fig. 5.4). It can be seen that GEL-0 presented relatively poorer mechanical performance (a tensile strength of ~6 MPa, elongation at break of ~600%, toughness of ~20 MJ/m^3, and Young's modulus of ~2.8 MPa) than the other CDN-gels, despite offering better performance than most reported hydrogels in the literature (Fig. 5.5). Materials include the PVA-PAA- Silanol ion gel in this work, P(AAm-co-HFBMA) composite gel [33], PAMPS/PAAM double network hydrogel [34], alginate/polyacrylamide hydrogels [35], polyampholytes gel [36], PVA-PAAm gel [37], tetra-PEG/rGO nanocomposite (NC) hydrogel [18], PVA/HA-Fe^{3+} gel [38], PVA/PAA gels [39], as well as native cartilage [40] and skin [41].

Significant enhancements in mechanical performance were observed for GEL-0.1, -0.5, -1, and -5. Notably, the tensile strength, elongation at break, toughness, and Young's modulus of the optimal CDN-gel (GEL-0.5) reached ~21 MPa, ~700%, ~49

MJ/m^3, and 3.5 MPa, respectively. Moreover, the as-synthesized GEL-0.5 was further observed to withstand different deformations, such as twisting and large stretching after twisting (Fig. 5.4c). Fig. 5.4d illustrates that GEL-0.5 was strong enough to lift a hydrothermal reactor autoclave weighing 4.2 kg. In general, the synergy between the multiple cross-linking points gives GEL-0.5 excellent mechanical performance.

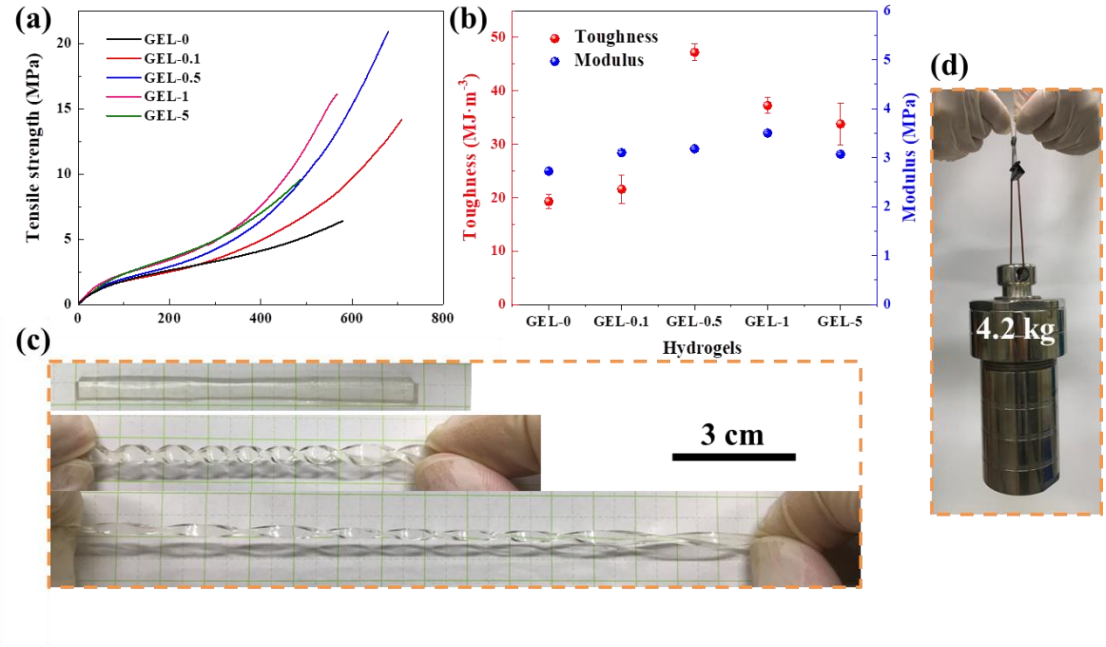

Fig. 5.4 (a) Tensile curves of CDN-gels; (b) toughness and Young's modulus of CDN-gels; (c) twisting and stretching after being twisted for GEL-0.5; and (d) carrying a heavy steel block weighing 4.2 kg using GEL-0.5 (width = 4 mm, thickness = 2 mm)

The mechanical performance of GEL-0 was explained in our previous work [20] (i.e., a double cross-linked hydrogel with dynamic physical cross-linking (ionic bonding and hydrogen bonding) and chemically cross-linked PVA/PAA networks). Herein, the introduction of VSTO (multiple function covalent cross-linking agents) into GEL-0 resulted in further significant improvements in mechanical strength, extensibility, toughness, and resilience (Fig. 5.4a or Fig. 5.6).

During the stretching process, the hydrogen bonds in the CDN-gels network dissipate energy through reversible break-reformation and homogenize the network. VSTO can maintain the elasticity of the network and act as a transfer center to

homogenize the stress distribution in the network [42]. The applied stress is then absorbed and redistributed by the VSTO, thus the crack propagation is delayed by the numerous grafted PAA/PVA chains.

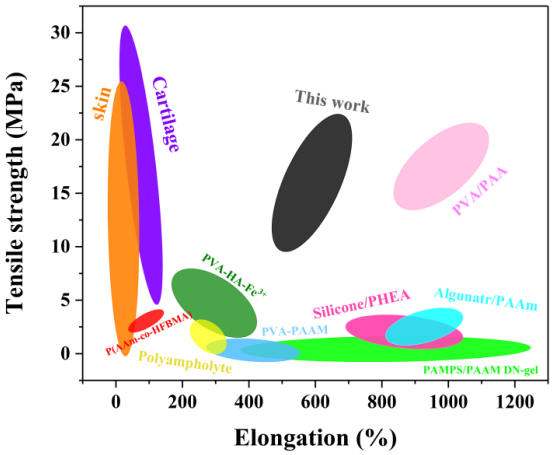

Fig. 5.5 Comparison of CND-gels and various soft materials obtained from literatures in tensile strength and elongation

However, too much VSTO (GEL-5) will increase the number of initiation points for polymer growth for a fixed AA monomer concentration. Consequently, the average polymer length will be reduced, thereby reducing the flexibility of the PAA/PVA chains. Similar phenomena have been reported by Zhong, et al. [43]. In that work, vinyl-hybrid silica nanoparticles (VSNP) were used as covalent cross-linking agents with ferric ions as ionic crosslinkers, ultimately obtaining tough and stretchable nanocomposite ionic cross-linked VSNP/PAA physical hydrogels. Nevertheless, the mechanical performance of our GEL-0.5 is still much higher than that of the VSNP/PAA hydrogel (tensile strength 860 kPa, elongation at break ~2300%).

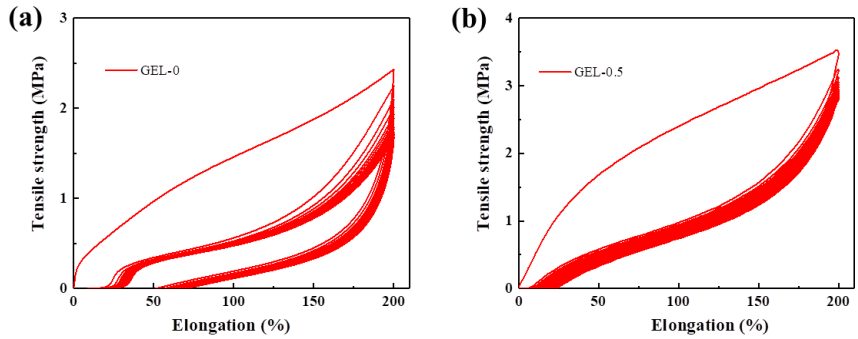

Fig 5.6 Cyclic tensile tests of (a) GEL-0 and (b) GEL-0.5 at strain of 200%

5.3.4 Excellent Recoverability of GEL-0.5

Tensile cyclic loading–unloading tests were conducted to evaluate the hysteresis behaviors of GEL-0.5 (Fig. 5.7) during the stretching fracture process of the gel samples [44, 45]. For the successive cyclic loading–unloading tests of the new GEL-0.5 at various strains ranging from 100 to 600% (Fig. 5.7a), the dissipated energy of GEL-0.5 increased with the deformation strain (Fig. 5.7b).

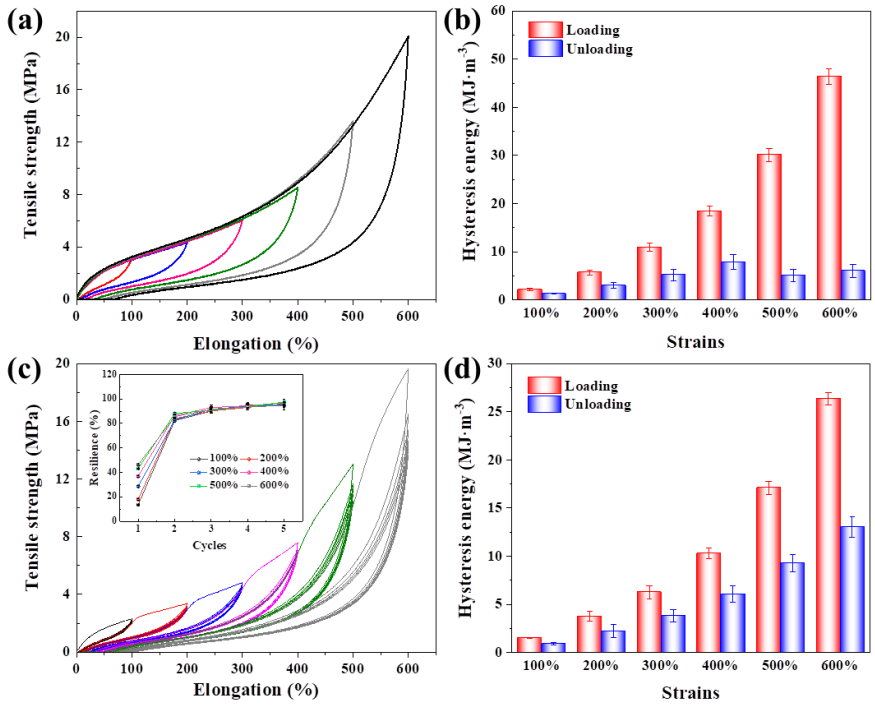

Fig. 5.7 (a) Loading–unloading curves of GEL-0.5 stretched for one cycle under different strains (new GEL-0.5 for every cycle); (b) the calculated hysteresis energy during the cyclic tensile tests in (a); (c) loading–unloading responses of the same GEL-0.5 submitted to gradient increasing strain (increase the strain after 6 cycles under every fixed strain); and (d) the calculated hysteresis energy of (c) during the first cycle of the softening process

For the gradient cyclic tensile test (Fig. 5.7c), the subsequent cyclic loading–unloading curves (2–6 cycles) remained almost overlapping and presented similar dissipated energies (resilience > 80%, inset figure in Fig. 5.7c) after the first stretching–releasing cycle. The observed material softening phenomenon, whereby a lower resulting stress appears after the first load and the hydrogel response curves coincide

during the following cycles at the same applied strain, could be explained by the Mullins effect [16, 46]. The softening increases progressively with the maximum strain (Fig. 5.7c), and the dissipated energies of the first cycle of softened GEL-0.5 at different strains were smaller than those of the unsoften GEL-0.5 (Fig. 5.7b, d). Moreover, it can be observed from the first loading curves under each strain of the repeatedly stretched GEL-0.5 (Fig. 5.7c) that they nearly continued to increase along the trajectories of the previous tensile test, thus indicating the excellent resilience of GEL-0.5.

5.3.5 Cyclic Compressive Tests

The compression cycle results of GEL-0.5 are presented in Fig. 5.8, which shows basic stable stress–strain curves. GEL-0.5 presented a compressive strength of ~60 MPa at a strain of 90% and the ability to rapidly return to its original position. As the strain increased, the network structure of GEL-0.5 changed slightly. The curves of the second cycle were observably inconsistent with those of the first cycle when the compression strain was over 50%, indicating that an overly large deformation could cause irreversible damage to the network structure.

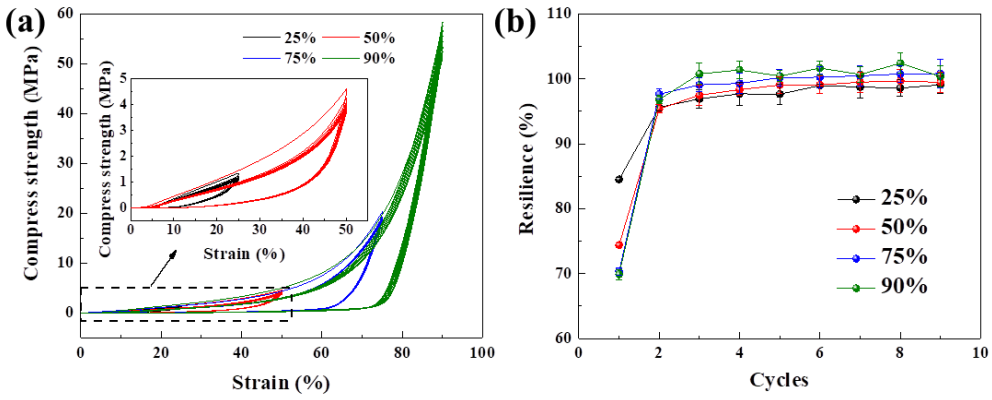

Fig. 5.8 (a) Loading–unloading curves of GEL-0.5 during successive compression cycles at different strains; (b) the calculated resilience of GEL-0.5 during the cyclic tensile tests

Nevertheless, the resilience of GEL-0.5 was still above 70% (from the first cycle) at a compressive strain of 90% and reached a stable and high value from the second cycle (>95%), as shown in Fig. 5.8b. Moreover, the stable hysteresis energy dissipation of GEL-0.5 could be attributed to both the dissociation of ionic and hydrogen bonds and

the friction between polymer chains [47, 48]. After the applied stress was removed, the sacrificial bonds were able to reform rapidly, and thereby restore the integrity of GEL-0.5. Above all, GEL-0.5 exhibited excellent compressive properties during successive process cycles.

5.3.6 High Recovery Properties

Most of the reported hydrogels possess obviously time-dependent recovery properties that significantly increase with an increase in rest time [49]. To further investigate the recovery properties of GEL-0.5, several tensile operations were conducted, as shown in Fig. 5.9.

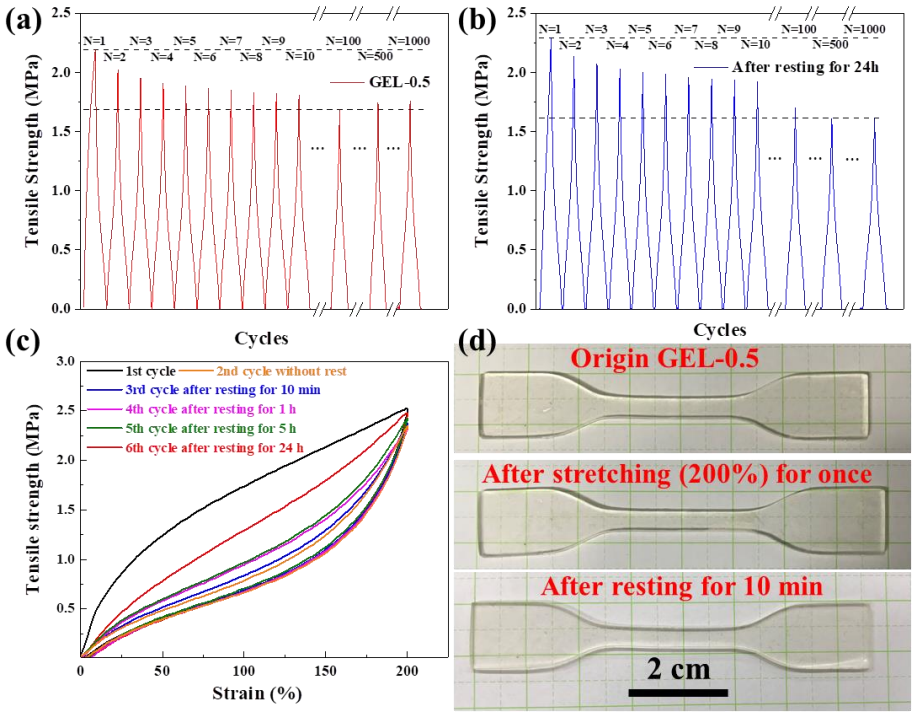

Fig. 5.9 (a) Cyclic tensile curves of GEL-0.5 obtained after 1000 tests at a strain of 200%; (b) the same operation as (a) was performed after GEL-0.5 rested for 24 h; (c) cyclic stress–strain curves of GEL-0.5 at a 200% strain with different rest times; and (d) digital photos of GEL-0.5 with fast resilience

After being stretched 1000 times at a strain of 200%, the maximum stress of each cycle decreased from 2.2 to 1.7 MPa (Fig. 5.9a). After GEL-0.5 rested for 24 h at room temperature, the reloading curves were almost the same as those for the first 1000 cycles (Fig. 5.9b). The observed slight increase in maximum stress could be due to

self-healing of the broken ionic and hydrogen bonds [50]. Fig. 5.9c illustrates the recovery speed of GEL-0.5. It can be observed that GEL-0.5 was much weaker when the second load was applied immediately and recovered somewhat if the second load was applied one day later. GEL-0.5 showed negligible hysteresis, and the sample fully recovered its original length after resting for 10 min (Fig. 5.9d). The pronounced hysteresis and relatively small permanent deformation (<25%) of GEL-0.5 were further demonstrated by loading–unloading tests (20 times) at a strain of 200% (Fig. 5.6). In a word, the GEL-0.5 has an excellent fatigue resistance and rapidly recovery ability by introducing multiple sacrificial bonds.

5.3.7 Dynamic Mechanical Analysis

The liquid phase of hydrogel is constrained within its three-dimensional network, thus producing visco-elastic properties [51, 52]. To investigate the influence of VSTO on the viscoelasticity of CDN-gels, a DMA was conducted from 1 to 100 Hz. Meanwhile, the storage modulus E' (a measure of elasticity and stiffness), the loss modulus E'' (a measure of viscous), and *Tan* δ (E''/E') were measured.

As shown in Fig. 5.10, E' is always higher than E'' in the frequency range of 1–100 Hz, which indicates that the CDN-gels have considerable strength to withstand pressure and resist certain impacts. Moreover, both the E' and E'' of all CDN-gels increased as the frequency increased, indicating that the energy dissipation caused by intermolecular friction was proportional to the frequency. For the E' of CDN-gels at 1 Hz (E'_1), the E'_1 dropped drastically after the VSTO was added and then gradually increased from 400 to 700 kPa with the VSTO content. It was reported that the E' in the low frequency relates to the effective network chain density (N), which can be depicted as follows [47]:

$$E' = \lambda NRT, \tag{5-2}$$

where λ is the hydrogel-based constant and R and T are the gas constant and absolute temperature, respectively. For the CDN-gels with VSTO, the increased E' can be explained by the increase in the effective network chain density with VSTO content, while the drastic decrease of E' after the VSTO was introduced could be attributed to a change in λ, which reflects a large change in the flexibility of molecular chains. An excessive amount of VSTO (GEL-5) would limit the movement of polymer chains, resulting in a decrease in viscosity (reflects by E'', Fig. 5.10b). *Tan* δ, also known as

damping, is determined by the ratio of the storage modulus and loss modulus [53]. After introducing VSTO into CDN-gels, GEL-0.5 presented the highest *tan δ* from 1 to 100 Hz (Fig. 5.10c). The high *tan δ* of GEL-0.5 reflects moderate viscoelasticity, which indicates its potential application in the field of vibration absorption.

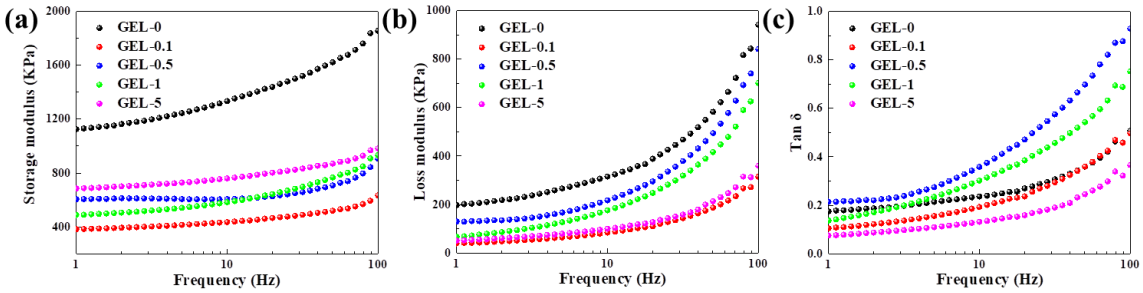

Fig. 5.10 Viscoelasticity of CDN-gels (a) Storage modulus; (b) loss modulus; (c) tan δ

5.3.8 Damping Ability

Fig. 5.11 shows the vibration signals after using different shock absorption materials as a buffer. When no damping material was placed, the vibrator beat violently on the metal plate, and the amplitude of the detected force was ~5 N. Under shock absorption, the force signals quickly converged to a stable range after experiencing a large shock at the moment when the power was turned on. The force amplitude of the spring, a traditional excellent shock absorption material, reduced to ~0.05 N. In this work, the CDN-gels exhibited certain damping abilities. For GEL-0, the force amplitude was still high (~1N) and not very stable. After the addition of VSTO, GEL-0.5 reflected much better damping ability (~0.4N) than GEL-0.

Indeed, the damping ability of the CDN-gel mainly depends on its elasticity. A stiff hydrogel cannot absorb enough of the shock, while a soft hydrogel does not have a sufficient response speed to resolve vibrations within a certain frequency [54, 55]. The excellent elasticity and recovery properties of GEL-0.5 provide it with good damping ability. As a shock absorbing material, hydrogel has the advantages of higher quality and space reduction over metal springs, although the damping ability of hydrogel is still not as good as that of metal springs.

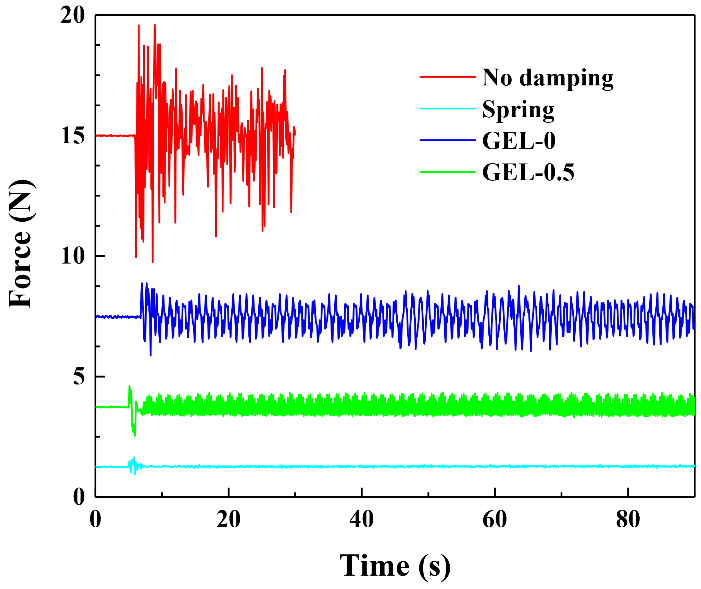

Fig. 5.11 Comparison of the damping effect of different vibration dampers

5.3.9 Notch-Insensitive Properties

Elastic hydrogel is known to be brittle and notch-sensitive. That is, the stretchability and strength of this material decrease markedly when the samples contain notches or any other features that cause inhomogeneous deformation [56]. In this work, different dynamic physical crosslinks (hydrogen and ionic bonds) of hydrogel were shown to effectively dissipate energy through the fracture-reformation process during stretching. Moreover, VSTO, a multifunctional crosslinking point, can make the network uniformly stressed to reduce the stress concentration [43]. Therefore, CDN-gels are expected to have good notch-insensitive properties.

When stretching the CDN-gels with notches (Fig. 5.9), the notches on the edges of the CDN-gels are the domain where stress concentration can easily occur. GEL-0.5 was shown to have better tensile cycle stability and higher uniaxial stress (120 N) stability than GEL-0 (40 N) (Fig. 5.12a, b), indicating better resistance to cracks or notch expansion in GEL-0.5. Under a strain of 100%, the notch in GEL-0.5 did not expand significantly during the stretching process (Fig. 5.12d). Fig. 5.12c presents the changes in the highest fracture energy and critical stretch with the VSTO contents. Compared with the non-notched CDN-gels, the notched CDN-gels can withstand less deformation, but can still be stretched to 2–3 times their original length, presenting excellent stretchability and notch-insensitive properties. The highest fracture energy can be

obtained by integrating the stress–strain curves of non-notched CDN-gels at the corresponding elongation. The notched GEL-0.5 presented the highest fracture energy (Fig. 5.12c), which is several orders of magnitude similar to natural rubber (~10^4 J/m^2) [57]. For the notched GEL-5, the PAA/PVA chains were densely crosslinked with a high concentration of VSTO. Only a small zone around the root of the notch was stressed enough to break the PAA/PVA chains (hard and brittle), so the fracture energy was low.

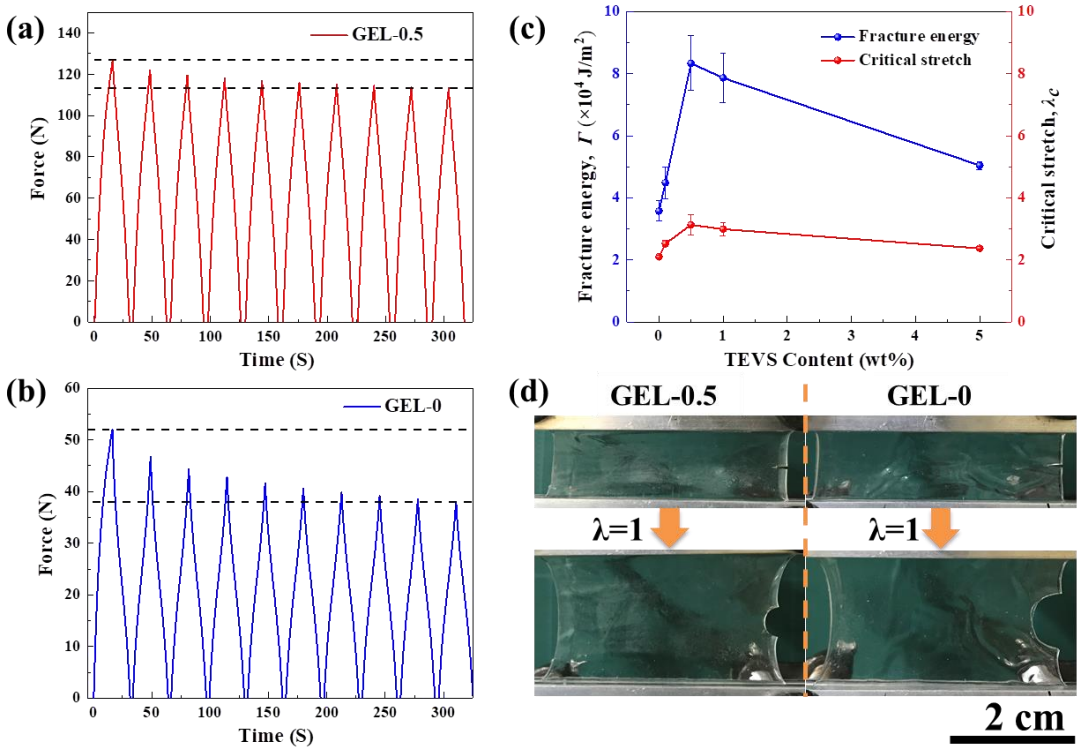

Fig. 5.12 (a) Cyclic tensile curves for 10 cycles of GEL-0.5 with single-notch (4 mm) at a strain of 100%; (b) cyclic tensile curves for 10 cycles of GEL-0 with a single-notch (4 mm) at a strain of 100%; (c) the ratios of the fracture critical stretch (λ) and the fracture energy (Γ) of the CDN-gels; (d) photos of notch deformation of GEL-0 and GEL-0.5 during stretching

Overall, VSTO can strengthen the network of CDN-gels, increase the gels' density, and contribute to forming cross-linking points, allowing the gels to bear more stress and dissipate more energy. As a result, VSTO can prevent crack propagation more effectively.

5.4 Conclusions

In this work, we presented a simple method to synthesize a composite double network ionic hydrogel by visible light triggering polymerization and salt impregnation. The VSTO, as a multi-crosslinking point, not only introduces an energy dissipation unit, but also homogenizes the network of CDN-gels. The right amount of VSTO can significantly improve the mechanical properties and swelling ratio of CDN-gel. The tensile strength, fracture elongation, modulus, and toughness of the optimized CDN-gel (GEL-0.5) can reach up to ~21 MPa, ~700%, ~3.5 MPa, and ~49 MJ/m^3, respectively. GEL-0.5 exhibited stable mechanical properties in repeated tensile and compression tests thanks to its excellent resilience. The damping test results show that the resilient GEL-0.5 has a good shock absorption property. Moreover, GEL-0.5 exhibits a certain ability to resist crack propagation. Overall, this kind of hydrogel with excellent comprehensive mechanical properties is expected to be used as artificial tissues, such as cartilage and achilles tendon.

References

[1] Kim H.D, Lee Y, Kim Y, Hwang Y, Hwang N.S. Biomimetically reinforced polyvinyl alcohol-based hybrid scaffolds for cartilage tissue engineering. Polymers. 2017;9(12):655.

[2] Song F, Li X, Wang Q, Liao L, Zhang C. Nanocomposite hydrogels and their applications in drug delivery and tissue engineering. Journal of biomedical nanotechnology. 2015;11(1):40-52.

[3] Zhang D, Ren B, Zhang Y, Xu L, Huang Q, He Y, Li X, Wu J, Yang J, Chen Q. From design to applications of stimuli-responsive hydrogel strain sensors. Journal of Materials Chemistry B. 2020;8(16):3171-91.

[4] Hoffman A.S. Hydrogels for biomedical applications. Advanced Drug Delivery Reviews. 2012;64:18-23.

[5] Lin S, Liu X, Liu J, Yuk H, Loh H.-C, Parada G.A, Settens C, Song J, Masic A, McKinley G.H. Anti-fatigue-fracture hydrogels. Science Advances. 2019;5(1):eaau8528.

[6] Graham H.K, McConnell J.C, Limbert G, Sherratt M.J. How stiff is skin? Experimental Dermatology. 2019;28:4-9.

[7] Zhao H, Xu K, Zhu P, Wang C, Chi Q. Smart hydrogels with high tunability of stiffness as a biomimetic cell carrier. Cell Biology International. 2019;43(2):84-97.

[8] Yang J.C, Mun J, Kwon S.Y, Park S, Bao Z, Park S. Electronic skin: Recent progress and future prospects for skin-attachable devices for health monitoring, robotics, and prosthetics. Advanced Materials. 2019;31(48):1904765.

[9] Kim Y.-W, Kim J.E, Jung Y, Sun J.-Y. Non-swellable, cytocompatible phema-alginate hydrogels with high stiffness and toughness. Materials Science and Engineering: C. 2019;95:86-94.

[10] Sun J.-Y, Zhao X, Illeperuma W.R.K, Chaudhuri O, Oh K.H, Mooney D.J, Vlassak J.J, Suo Z. Highly stretchable and tough hydrogels. Nature. 2012;489(7414):133-6.

[11] Fu J. Strong and tough hydrogels crosslinked by multi-functional polymer colloids. Journal of Polymer Science Part B: Polymer Physics. 2018, 56, 1336-1350.

[12] Bai R.; Yang Q, Tang J, Morelle X.P, Vlassak J, Suo Z. Fatigue fracture of tough hydrogels. Extreme Mechanics Letters. 2017;15:91-6.

[13] Jiang H, Duan L, Ren X, Gao G. Hydrophobic association hydrogels with excellent mechanical and self-healing properties. European Polymer Journal. 2019;112:660-9.

[14] Xu F, Li Y, Deng Y, Xiong J. Porous nano-hydroxyapatite/poly (vinyl alcohol) composite hydrogel as artificial cornea fringe: Characterization and evaluation in vitro. Journal of Biomaterials Science, Polymer Edition. 2008;19(4):431-9.

[15] Chen Q, Chen H, Zhu L, Zheng J. Fundamentals of double network hydrogels. Journal of Materials Chemistry B. 2015;3(18):3654-76.

[16] Webber R, Creton C. Large strain hysteresis and mullins effect of tough

double-network hydrogels. Macromolecules. 2007;40(8):2919-27.

[17] Fukao K, Tanaka K, Kiyama R, Nonoyama T, Gong J.P. Hydrogels toughened by biominerals providing energy-dissipative sacrificial bonds. Journal of Materials Chemistry B. 2020;8:5184-8.

[18] Wang L, Lei K, Li Z, Wang X, Xiao H, Zheng Z. Tetra-peg-based nano-enhanced hydrogel with excellent mechanical properties and multi-functions. Macromolecular Materials and Engineering. 2018;303(11):1800325.

[19] Xia S, Song S, Gao G. Robust and flexible strain sensors based on dual physically cross-linked double network hydrogels for monitoring human-motion. Chemical Engineering Journal. 2018;354:817-824.

[20] Sun M, Qiu J, Jin S, Liu W, Sakai E. Visible light induced synthesis of high toughness, self-healing ionic hydrogel and its application in strain sensing. Colloids and Surfaces A: Physicochemical and Engineering. 2020;607:125438.

[21] Long R, Hui C.-Y. Fracture toughness of hydrogels: Measurement and interpretation. Soft Matter. 2016;12(39):8069-86.

[22] Kamoun E.A, Winkel A, Eisenburger M, Menzel H. Carboxylated camphorquinone as visible-light photoinitiator for biomedical application: Synthesis, characterization, and application. Arabian Journal of Chemistry. 2016;9(5):745-54.

[23] Jin S, Qiu J, Sun M, Huang H, Sakai E. Strain-sensitive performance of a tough and ink-writable polyacrylic acid ionic gel crosslinked by carboxymethyl cellulose. Macromolecular Rapid Communications. 2019;40(20):1900329.

[24] Dou Y, Wang Z.-P, He W, Jia T, Liu Z, Sun P, Wen K, Gao E, Zhou X, Hu X. Artificial spider silk from ion-doped and twisted core-sheath hydrogel fibres. Nature Communications. 2019;10(1):5293.

[25] Wu L, Zhuang Z, Li S, Ma X, Diao W, Bu X, Fang Y. Ultrastretchable, super tough, and rapidly recoverable nanocomposite double-network hydrogels by dual physically hydrogen bond and vinyl-functionalized silica nanoparticles macro-crosslinking. Macromolecular Materials and Engineering. 2019;304(5):1800737.

[26] Wang X, Wang H, Brown H. Jellyfish gel and its hybrid hydrogels with high mechanical strength. Soft Matter. 2010;7(1):211-9.

[27] Wu Y, Xia M, Fan Q, Zhu M. Designable synthesis of nanocomposite hydrogels with excellent mechanical properties based on chemical cross-linked interactions. Chemical Communications. 2010;46(41):7790-2.

[28] Herz F.A.D, Nobis M, Wendel D, Pahl P, Altmann P.J, Tillmann J, Weidner R, Inoue S, Rieger B. Application of multifunctional silylenes and siliranes as universal crosslinkers for metal-free curing of silicones. Green Chemistry. 2020;22:4489-97.

[29] Lee J.-Y, Park N, Lim S, Ahn B, Kim W, Moon H, Paik H.-j, Kim W. Influence of the silanes on the crosslink density and crosslink structure of silica-filled solution styrene butadiene rubber compounds. Composite Interfaces. 2017;24(7):711-27.

[30] Kaberova Z, Karpushkin E, Nevoralová M, Vetrík M, Šlouf M, Dušková-Smrčková M. Microscopic structure of swollen hydrogels by scanning electron and light microscopies: Artifacts and reality. Polymers. 2020;12(3):578.

[31] Zhang X, Lin G, Kumar S.R, Mark J.E. Hydrogels prepared from polysiloxane chains by end linking them with trifunctional silanes containing hydrophilic groups. Polymer. 2009;50(23):5414-5421.

[32] Melo R.P.d, Aguiar V.d.O, Marques M.d.F.V. Silane crosslinked polyethylene from different commercial PE's: Influence of comonomer, catalyst type and evaluation of HLPB as crosslinking coagent. Materials Research. 2015;18(2):313-9.

[33] Zhang B, Wang C, Wang Y, Li T, Zhai K, Zhang F, Bai Y, Tan Y, Ma Y, Xu K. A facile method to synthesize strong salt-enhanced hydrogels based on reversible physical interaction. Soft Matter. 2020;16(3):738-46.

[34] Zhang W, Liu, X, Wang J, Tang J, Hu J, Lu T, Suo Z. Fatigue of double-network hydrogels. Engineering Fracture Mechanics. 2018;187:74-93.

[35] Zhang W, Hu J, Tang J, Wang Z, Wang J, Lu T, Suo Z. Fracture toughness and fatigue threshold of tough hydrogels. ACS Macro Letters. 2019;8(1):17-23.

[36] Sun T.L, Luo F, Kurokawa T, Karobi S.N, Nakajima T, Gong J.P. Molecular structure of self-healing polyampholyte hydrogels analyzed from tensile behaviors.

Soft Matter. 2015;11(48):9355-66.

[37] Li J, Suo Z, Vlassak J.J. Stiff, strong, and tough hydrogels with good chemical stability. Journal of Materials Chemistry B. 2014;2(39):6708-13.

[38] Li A, Si Y, Wang X, Jia X, Guo X, Xu Y. Poly(vinyl alcohol) nanocrystal-assisted hydrogels with high toughness and elastic modulus for three-dimensional printing. ACS Applied Nano Materials. 2019;2(2):707-15.

[39] Liu T, Jiao C, Peng X, Chen Y.-N, Chen Y, He C, Liu R, Wang H. Super-strong and tough poly(vinyl alcohol)/poly(acrylic acid) hydrogels reinforced by hydrogen bonding. Journal of Materials Chemistry B. 2018;6(48):8105-14.

[40] Schmidt M.B, Mow V.C, Chun L.E, Eyre D.R. Effects of proteoglycan extraction on the tensile behavior of articular cartilage. Journal of Orthopaedic Research. 1990;8(3):353-63.

[41] Tran T.T, Hamid Z.A, Cheong K.Y. A review of mechanical properties of scaffold in tissue engineering: Aloe vera composites. Journal of Physics: Conference Series. 2018;1082(1):012080.

[42] Sun J, Pu X, Liu M, Yu A, Du C, Zhai J, Hu, W, Wang Z.L. Self-healable, stretchable, transparent triboelectric nanogenerators as soft power sources. ACS Nano. 2018;12(6):6147-6155.

[43] Zhong M, Liu X.-Y, Shi F.-K, Zhang L.-Q, Wang X.-P, Cheetham A.G, Cui H, Xie X.-M. Self-healable, tough and highly stretchable ionic nanocomposite physical hydrogels. Soft Matter. 2015;11:4235-41.

[44] Li Y, Jiang X. Hysteresis loop and energy dissipation of viscoelastic solid models. Mechanics of Time-Dependent Materials. 2007;11(1):1-14.

[45] Zhu L, Qiu J, Sakai E, Ito K. Rapid recovery double cross-linking hydrogel with stable mechanical properties and high resilience triggered by visible light. ACS Applied Materials & Interfaces. 2017;9(15):13593-601.

[46] Matsuda T, Nakajima T, Gong, J.P. Fabrication of tough and stretchable hybrid double-network elastomers using ionic dissociation of polyelectrolyte in nonaqueous media. Chemistry of Materials. 2019;31(10):3766-76.

[47] Zhu L, Qiu J, Sakai E. A high modulus hydrogel obtained from hydrogen bond reconstruction and its application in vibration damper. RSC Advances. 2017;7(69):43755-63.

[48] Zhou X, Guo B, Zhang L, Hu G.-H. Progress in bio-inspired sacrificial bonds in artificial polymeric materials. Chemical Society Reviews. 2017;46(20):6301-29.

[49] Yan L, Dillard D.A, West R.L, Lower L.D, Gordon G.V. Mullins effect recovery of a nanoparticle-filled polymer. Journal of Polymer Science Part B: Polymer Physics. 2010;48(21):2207-14.

[50] Liang Y, Ye L, Sun X, Lv Q, Liang H. Tough and stretchable dual ionically cross-linked hydrogel with high conductivity and fast-recovery property for high-performance flexible sensors. ACS Applied Materials & Interfaces. 2020;12(1):1577-87.

[51] Haque M.A, Kurokawa T, Gong J.P. Super tough double network hydrogels and their application as biomaterials. Polymer. 2012;53(9):1805-22.

[52] Li J, Liu H, Wang C, Huang G. A facile method to fabricate hybrid hydrogels with mechanical toughness using a novel multifunctional cross-linker. RSC Advances. 2017;7(56):35311-19.

[53] Shanmugam D, Thiruchitrambalam M. Static and dynamic mechanical properties of alkali treated unidirectional continuous palmyra palm leaf stalk fiber/jute fiber reinforced hybrid polyester composites. Materials & Design. 2013;50:533-542.

[54] Ye L, Lv Q, Sun X, Liang Y, Fang P, Yuan X, Li M, Zhang X, Shang X, Liang H. Fully physically cross-linked double network hydrogels with strong mechanical properties, good recovery and self-healing properties. Soft Matter. 2020;16(7):1840-9.

[55] Kumar J.S, Paul P.S, Raghunathan G, Alex D.G. A review of challenges and solutions in the preparation and use of magnetorheological fluids. International Journal of Mechanical and Materials Engineering. 2019;14(1):13.

[56] Ma J, Lee J, Han S.S, Oh K.H, Nam K.T, Sun J.-Y. Highly stretchable and notch-insensitive hydrogel based on polyacrylamide and milk protein. ACS Applied Materials & Interfaces. 2016;8(43):29220-6.

[57] Flauzino Neto W.P, Mariano M, da Silva I.S.V, Silvério H.A, Putaux J.-L, Otaguro H, Pasquini D, Dufresne A. Mechanical properties of natural rubber nanocomposites reinforced with high aspect ratio cellulose nanocrystals isolated from soy hulls. Carbohydrate polymers. 2016;153:143-52.

Chapter 6 Conclusions

In this thesis, Through optimization of the Interaction between polymer chains in hydrogels and the design of stucture of hydrogels. High-performance hydrogels with fast recovery, high resilience,and high toughness has been successful prepared.

In chapter 3, we successfully fabricate high strength PVA-ESO hydrogels through the formation of hydrophobic association, hydrogen bonding, and chain entanglements. The thermal stability and mechanical properties of PVA hydrogels were significantly enhanced and good flexibility was observed, where the ESO acted as the physical entanglement point between the molecular chains and increased the elasticity of the hydrogels. With the increase of ESO content, the tensile strength of the hydrogels increased from 560 kPa to 1.4 MPa. In addition, a porous hydrogel having a certain microscopic morphology could be obtained by controlling the content of ESO. These results indicate that the vegetable oil-based hydrogels will find applications in personal care or health care areas due to its amphipathy, improved mechanical properties and controllability in wet conditions.

In chapter 4, the structure of hydrogel was designed to fabricate a novel hydrogel based on result of chapter 3. A tough, conductive and self-healable double crosslinked PVA/PAA hydrogel (DC-gel) was developed by a facile polymerization triggered by visible light and salt impregnation. The DC-gel exhibits a rubber-like flexible hydrogel network and a homogeneous interconnected phase. The superior interfacial adhesion and low intermolecular repulsive force of the DC-Gel caused by the ionic diffusion of LiCl into PVA/PAA molecular chains can ensure a smooth stress-transfer and recoverable energy dissipation to give the hydrogels with excellent mechanical strength (6.59 ± 1.21 MPa) and toughness (19.27 ± 3.3 MJ/m^3). Moreover, the DC-Gel with proper AA content (PVA: AA=1:5, DC-5) exhibited remarkable recovery properties (resilience > 80% and 95% for successively and intermittently cyclic tensile tests, respectively, and residual strain < 3%). The high strain sensitivity of DC-5 was proved by assembling a capacitance-based strain sensor, and the sensor

could precisely, quickly and continuously distinguish the deformation (0-300%). In general, this work provides a positive exploration in the fabrication of conductive hydrogels and application in wearable electronic sensors.

In chapter 5, we synthesized a composite polyvinyl alcohol (PVA)/poly (acrylic acid) (PAA)/silicone hydrogel (CDN-gel) to futher increase the mechanical properties of the DC-gel based on chapter 4. The VSTO, as a multi-crosslinking point, not only introduces an energy dissipation unit, but also homogenizes the network of DC-gel. The right amount of VSTO can significantly improve the mechanical properties. The tensile strength, fracture elongation, modulus, and toughness of the optimized CDN-gel (VSTO content=0.5%, GEL-0.5) can reach up to ~21 MPa, ~700%, ~3.5 MPa, and ~49 MJ/m^3, respectively. GEL-0.5 exhibited stable mechanical properties in repeated tensile and compression tests thanks to its excellent resilience. The damping test results show that the resilient GEL-0.5 has a good shock absorption property. Moreover, GEL-0.5 exhibits a certain ability to resist crack propagation. Overall, this kind of hydrogel with excellent comprehensive mechanical properties is expected to be used as artificial tissues, such as cartilage and achilles tendon.

Furthermore, hydrogels, as functional materials, have some potential applications in the field of temperature control, sewage treatment, and wearable electronics material. For example, we can add phase change energy storage reagent in hydrogel during the hydrogel preparation process to prepare the automatic temperature control material. In conclusion, with the deep study of hydrogel properties, we believe that hydrogel play an important role in the fields of biomedicine, aerospace, environmental protect, etc.

Publications

Ⅰ. 審査付投稿論文

(1) **Manxi Sun**, Jianhui Qiu*, Shuping Jin, Wendi Liu, Eiichi Sakai, Visible light induced synthesis of high toughness, self-healing ionic hydrogel and its application in strain sensing, Colloids and Surfaces A: Physicochemical and Engineering Aspects, 607(2020) 125438; (IF= 3.990)

(2) **Manxi Sun**, Jianhui Qiu*, Chunyin Lu, Shuping Jin, Guohong Zhang and Eiichi Sakai, Multi-sacrificial bonds enhanced double network hydrogel with high toughness, resilience, damping, and notch-insensitivity, Polymers, 12 (2020) 2263; (IF= 3.426)

(3) **Manxi Sun**, Jianhui Qiu*, Shuping Jin, Hongjian Huang, Wendi Liu, Eiichi Sakai, Ji Lei, High strength and amphiphilic epoxidized soybean oil-modified poly(vinyl alcohol) hydrogels, Polymer Bulletin, Accepted; (IF= 2.014)

(4) **Manxi Sun**, Hongjian Huang*, Xiaowei Wei, Jianhui Qiu, Aggregation of MAO coating and crack formation in the microgrooves on the aluminum surface, International Journal of Electrochemical Science, 15 (2020) 839-844; (IF= 1.573)

(5) Shuping Jin, Jianhui Qiu*, **Manxi Sun**, Hongjian Huang, and Eiichi Sakai, Strain-sensitive performance of a tough and ink-writable polyacrylic acid ionic gel crosslinked by carboxymethyl cellulose, Macromolecular Rapid Communications, 2019, 40, 1900329; (IF= 4.886)

(6) Hongjian Huang, Jianhui Qiu*, **Manxi Sun**, Wendi Liu, Xiaowei Wei, Eiichi Sakai, Kazushi Ito, A hard coating with MAO/AAO double layers prepared on aluminum in etidronic acid by DC oxidation, Surface & Coatings Technology, 360 (2019) 307-317; (IF= 3.784)

(7) Hongjian Huang, Jianhui Qiu*, **Manxi Sun**, Wendi Liu, Xiaowei Wei, Morphological evolution and burning behavior of oxide coating fabricated on aluminum immersed in etidronic acid at high current density, Surface & Coatings

Technology, 374 (2019) 83-94; (IF= 3.784)

(8) Xiaowei Wei, Hongjian Huang*, **Manxi Sun**, Wendi Liu, Jianhui Qiu, Effects of honeycomb pretreatment on MAO coating fabricated on aluminum, Surface & Coatings Technology, 363 (2019) 265-272; (IF= 3.784)

注：博士論文テーマ関連：3 編（(1) ～ (3)），その他：6 編（(4) ～ (8)）

Ⅱ. 国際会議論文・発表

(1) **Manxi Sun**, Jianhui Qiu, Shuping Jin, Hongjian Huang, Wendi Liu, Eiichi Sakai, Influence of Epoxy Soybean Oil on PVA Hydrogel. The 1st International Symposium on Advanced Materials Science and Engineering (AMSE-1), Akita, Japan, August 20-25, 2025

注：博士論文テーマ関連：1 件

Ⅲ. 会議論文・発表

(1) **Manxi Sun**, Jianhui Qiu, Eiichi Sakai, Kazushi Ito, Degradation Characteristics of Straw/Poly (Lactic Acid) Composites in Natural Water Environments, 平成 30 年度化学系学協会東北大会, 2018, 1P084.

Acknowledgements

With a three years' study, I have learnt a lot. I would like to express my sincere thanks. This thesis would not have been possible without the support of the teacher or friends around me. I would like to take this opportunity to extend my sincere gratitude to the following people who have helped me during the thesis-writing.

I owe a deep debt of gratitude in the first stance to my doctoral advisor, Professor Jianhui Qiu. I benefit a lot from his guidance and valuable suggestions. Without his constant encouragement and insightful guidance, I could not have finished this thesis. I feel deeply grateful and fortunate to be his student.

My heartfelt thanks also go to other teachers and professors for their conscientious and illuminating suggestions. I would like to express my gratitude to Prof. Nobuhiro Kanazawa in Department of Management Science and Engineering, Faculty of Systems Science and Technology, Akita Prefectural University; Prof. Teruo Bitoh in Department of Mechanical Engineering, Faculty of Systems Science and Technology, Akita Prefectural University; Prof. Noboru Nakayama in Department of Mechanical Systems Engineering, Faculty of Engineering, Shinshu University; Prof. Qingqing Ni from Department of Mechanical Engineering & Robotics, Shinshu University.

I appreciate the technical support from Prof. Kazushi Ito, Dr. Eiichi Sakai in Akita Prefectural University. In addition, I would like to express my sincere gratitude to my classmates and friends, Prof. Shuping Jin, Ms. Yukiko Takeuchi, Ms. Yui Endo, Dr. Jiao Chen, Dr. Longxiang Zhu, Mr. Haodao Mo, Ms. Rie Nobe, Dr. Wendi Liu, Mr. Hongjian Huang, Mr. Pengpeng Wang, Mr. Qifan Liu, Ms. Chunyin Lu, Mr. Syungo Shimizu, and Mr. Yuto Hiraiwa, for assisting with my research as well as their encouragements and supports during my preparation for this thesis.

Last but not least, I want to thank my family for having provided me with a loving environment and having given me unwavering support.

Manxi Sun

2021.03, Yurihonjo, Japan